Quantifying the effect of woody vegetation on the wave loads on a dike using remote sensing

Large scale physical model tests

C. Çete

TU Delft

Woods versus Waves

Deltares
Enabling Delta Life

Quantifying the effect of woody vegetation on the wave loads on a dike using remote sensing

Large scale physical model tests

By

C. Çete

in partial fulfilment of the requirements for the degree of

Master of Science
in Hydraulic Engineering

at the Delft University of Technology.
to be defended publicly on May 6, 2019.

Student number:	4285883	
Supervisor:	Prof. rd. ir. S.G.J. Aarninkhof	Delft University of Technology
Thesis committee:	Dr. ir. B. Hofland.	Delft University of Technology
	Ir. P. Oosterloo	Delft University of Technology
	Ir. P. van Steegh	Deltares

An electronic version of this thesis is available at http://repository.tudelft.nl/.

Cover Image: Willow trees, with and without leaves, in the Delta flume. Photography by Deltares

Preface

This report presents the results from the thesis research to obtain the Master of Science degree in Hydraulic Engineering at the Delft University of Technology. The research was part of the Woods Versus Waves project initiated by the following three organizations: Delft University of Technology, Deltares and the Royal Netherlands Institute for Sea Research (NIOZ). The experimental research has been conducted in the Delta flume of Deltares in the Netherlands, which is a facility for full scale experiments.

Prior to the actual research, my interest was raised for Building with Nature and coastal protections. From following Building with Nature courses to travelling to Surinam giving advice about the mangroves, has finally led me to the 'Dutch Mangroves', our willow trees. I feel blessed that I got the opportunity to finish my master's degree by researching such an interesting and important subject.

First of all, I would like to express my gratitude towards my committee. Stefan Aarninkhof, I would like to thank you for your advice and insightful questions during the meetings. Bas Hofland, your enthusiasm and critical suggestions have really helped me through this research. Paul van Steegh, it was a pleasure working with you. You taught me many aspects about being a researcher and shared your helpful knowledge regarding wave run-up and overtopping. Patrick Oosterlo, thank you for giving me advice on the analysis of the laser scanner and helping me with my MATLAB scripts. I also want to thank Joost den Bieman of Deltares, for his help with the application of deep learning on the camera footages.

It was an amazing experience being part of such a great research team doing experiments in the large Delta flume. I would like to thank all employees and technicians for their help and patience during the experiments. I also would like to thank my friend Sudarshini Kalloe with whom I spent my thesis period with. Without you the experience, both stressful and fun, would not be the same!

Last but not least, I would like to express my infinite gratitude and love to my parents and sister. Thank you for always supporting and believing in me. Special thanks to Chaimae Derraz for inspiring me to become a Civil Engineer. Finally, my life as a civil engineering student would not have been fun without my friends: Samantha, D'Tasha, Cindy and all others. I wish you all the best for the future. Be patient and stay positive!

ٱلْحَمْدُ لِلَّهِ رَبِّ ٱلْعَٰلَمِينَ

[Quran: 1:2]

Ceylan Çete
Amsterdam, April 2019

Summary

Currently 1.302 km of flood defences do not meet the safety standards. Therefore, it is necessary to strengthen and/or raise the dikes. Due to sea level rise and more intense & longer lasting storms, more dikes must be reinforced. This could cost billions of Euros. A more cost-effective and innovative solution that reduces the required crest height of dikes is therefore preferable. Nature Based Flood Defences are a potential solution for this rising problem. It is already acknowledged that Nature-based Solutions can be used to attenuate waves. However, it is still uncertain to what extent the vegetation can contribute to decreasing the flood risk. So far, mainly small-scale tests have been performed to quantify wave attenuating properties of vegetation. To quantify the effect of vegetation at more extreme wave conditions (high-water levels and wave heights), full scale tests are required. The main objective of the present research is to assess the effectiveness of willow vegetation in reducing wave loads (wave run-up and overtopping) on a dike under storm conditions. This is done by using two types of remote sensing techniques: laser scanning and video imaging.

To reach this objective, large-scale physical model tests with a willow forest of 40 meters in front of a dike, are conducted in the Delta flume of Deltares. Various water depths of 3.0 and 4.5 meters, significant wave heights between 0.5 and 1.5 meters and spectral wave periods between 2.7 and 6.0 seconds are tested. Three different quantitative measuring methods are used:
1. Visual determination of the run-up exceedance levels of each individual wave run-up tongue.
2. A terrestrial laser scanner measures a 2D wave profile along the slope. To determine the wave run-up, a threshold on the reflection intensity and on the water layer thickness is used. The overtopping volumes are determined by integrating the area between the measured water surface and the dry dike slope.
3. Video footage processed by a ‘Machine Learning algorithm’ is used to determine the wave run-up. Image segmentation is used to distinguish the interface between the wave run-up and the dry surface. This algorithm is created by Deltares and applied to the measurements obtained from the experiments.

After processing the data, the probability of exceedance distributions for the wave run-up height are obtained. This is the first time a ‘Machine Learning algorithm’ is used to obtain the wave run-up heights on a dike from video footages. It is also new that the wave overtopping volumes are determined by a laser scanner, without using a wave overtopping tank on the dike or a tank built in the dike slope. This tank was initially used to collect and measure the real overtopping volume.

The most commonly used models for designing a dike are empirical formulas i.e. the TAW (2002) and EurOtop. To compare the wave run-up from the experiments with the empirical formula, the focus is placed on the part behind the willow forest, in front of the dike (neglecting the willows). Comparing the obtained results, show that the determined wave run-up from the experiments are underestimated with an average of 9% by the TAW (2002). This would indicate that using the TAW for the design of the dike in the Delta flume would lead to an underestimation of the crest height. Not only for tests performed in this research, but also previous large-scale experiments have shown larger run-up heights than the TAW. The TAW is an empirical formula, based on a large data set of mainly small-scale experiments. Therefore, the difference between the tests results and the TAW could likely be attributed to scale effects. However, more measurements at full scale are needed to confirm this.

Besides the underestimation, the laser- and camera measurements are found to be 9% and 10% lower than the visual measured run-up heights. This concludes that the laser scanner and camera are an accurate method to measure the wave run-up on a dike slope. The camera measurements also give the variation of the wave run-up over the flume width, with an average of 15 cm. The results show a tendency of higher

run-up heights on one side of the flume for 70% of the analysed tests, which could be attributed to an asymmetry in the construction of the foreshore or dike. Thus, the camera in combination with Machine Learning is an accurate, simple and low-cost technique, to measure the wave run-up on a dike. This technique not only gives the run-up height, but also gives new insights about the variations of the wave run-up over the dike.

Results regarding the virtual overtopping discharges show measured values in the same order of magnitude as calculated using the existing empirical Van der Meer & Bruce formula (2014). However, the results show an overestimation of the overtopping discharges at high water level for higher crest freeboards, making these results less reliable. These overestimations could be due to the splashing of water, caused by waves breaking on the dike. The laser scanner is a simple substitute in measuring the overtopping volumes and discharges, without measuring real overtopped volumes using a tank. So, this is a more cost-efficient measuring technique, applicable in determining the overtopping volumes on more dikes. However, more research and a thorough validation are required to confirm the accuracy of this method.

The effect of the 40 meters willow forest is determined by comparing the experiments with and without willows, eliminating the other effects of wave damping. The 40 meters willow forest shows a range of significant reduction in wave run-up between the 10 and 19%. It also follows that the difference between the reduction in run-up, for willows in summer (with leaves) and winter state (no leaves), are on average only 5%. Even when 50% of the branch density of the willows is removed, a considerable reduction in run-up remains.

A comparison of values obtained from experiments with and without willows, results in an average reduction of the wave-overtopping discharge between 40 and 80%, for water depths of 3 meters. For the higher water levels, a decrease in discharge is calculated between 24 and 66%. The willow forest reduced the overtopping discharges for certain crest levels, so that the discharges do not exceed the tolerable overtopping discharge anymore. This reduction could be beneficial for the erosion of grass covers on a dike.

For both the wave run-up and the wave overtopping, an influence factor is calculated for a pollard willow forest of 40 m. The influence factor, γ_{willow} is valued between 0.8 and 0.9 and valid for the following conditions:

3.0 m	≤	Water depth	≤	4.5 m
0.43 m	≤	Significant wave height	≤	1.47 m
2.7 s	≤	Spectral wave period	≤	6.0 s
15.1 degrees	≤	Dike slope angle	≤	18.3 degrees

From the results obtained by flume experiments can be concluded that remote sensing: laser scanner and video imaging, are accurate methods to measure the run-up on a dike. It can also be concluded that a willow forest of 40 meters causes a significant reduction in the wave run-up and overtopping. Willows are therefore an effective measure to lower the run-up on a dike and further research is needed, so willows can be implemented in a design and the effect can be considered in the assessment of dikes in the Netherlands.

List of contents

List of symbols

Symbol	Description	Units
a	Scaling parameter of the Weibull distribution	-
b	Shape parameter of the Weibull distribution	-
D	Duration	s
g	Gravitational acceleration	m/s^2
h	Water depth at the foreshore	m
H_{m0}	Incoming significant wave height from spectral analysis	m
h_s	Height of the laser perpendicular to the slope	m
$L_{m-1.0}$	Deep water spectral wave length	m
N	Number of incoming waves	-
N_{ow}	Number of overtopping waves	-
N_w	Number of incoming waves	-
P_{ow}	Probability of overtopping per wave	-
P_v	P (v ≥ V) , Probability of the overtopping volume v being larger or equal to V	-
R_c	Crest freeboard of the dike	m
RSSI	The reflection intensity value measured by laser	-
R_u	Run-up height	m
$R_{ux\%}$	Run-up height exceeded by x% of the waves	m
$s_{m-1.0}$	Fictitious wave steepness based on $T_{m-1.0}$	-
s_{op}	Fictitious wave steepness in deep water based on T_p	-
SWL	Still water level	m
t	Time	s

T_m	Average wave period	s
$T_{m-1.0}$	Mean spectral wave period	s
T_p	Peak wave period from spectral analysis	s
V	Overtopping volume	m^3
x	Coordinate in longitudinal direction of the flume with x=0 at the wave board	m
y	Coordinate in transverse direction of the flume, where y=0 is located on the measurement cabin side of the flume	m
z	Coordinate in vertical direction measured from the bottom of the flume	m
α	Slope angle	o
γ	Peak enhancement factor	-
γ_{willow}	Influence factor for the presence of willows	-
γ_b	Influence factor for the presence of a berm	-
γ_β	Influence factor for oblique wave attack	-
γ_v	Influence factor for a vertical wall on the slope	-
γ_f	Influence factor for the permeability and roughness of or on the slope	-
γ^*	Overall influence factor for a storm wall on slope or promenade	-
θ	Scanning angle laser	o
μ_x	Mean of measured parameter x with normal distribution	Unit of x
$\xi_{m-1.0}$	Breaker parameter/ Surf similarity parameter/ Iribarren number	-
σ	Standard deviation of measured parameter x with normal distribution	Unit of x
φ	Slant angle of the laser scanner	o
Γ	Mathematical gamma function	-
Δ_{xy}	Difference between two parameters x and y	Unit of x

1. Introduction

1.1 Background

Every twelve years the Dutch primary flood defences are assessed on their capability of resisting loads during storm conditions (i.e. high water levels and wave loads). Currently 1.302 km of flood defences do not meet the safety standards (Deltaprogramma, 2018). For this it is necessary to strengthen and/or raise the dikes. Due to sea level rise and more intense & longer lasting storms, more dikes must be reinforced, however this will cost billions of Euros (Verhaege et al., 2008; Deltaprogramma, 2018).

Therefore, a more cost-effective and innovative solution that reduces the required crest height is preferable. Nature-based Flood Defences are a potential cost-effective solution to this rising problem. Vegetated foreshores not only enhance flood safety by reducing the storm surge and wave impact, but also provide many ecosystem services such as biodiversity (Borsje et al., 2011). Examples of vegetated foreshores are salt marches, intertidal flats and mangroves in tropical countries. The incoming waves are attenuated due to depth-induced wave breaking, bottom friction and wave attenuation by the vegetation, as wave forces are acting on the stem, leaves and branches (Vuik et al., 2019). Hydraulic wave conditions result in run- up and overtopping on the dike. The wave run-up and overtopping on a dike are influenced by the characteristics of the foreshore. Overtopping discharge can result in erosion of the inner slope of the dike and can even lead to a breach of the dike resulting in inundation of the land behind the dike. For design and assessment of a dike, a reliable estimate of the overtopping discharge is needed.

1.2 Problem description

It is already acknowledged that Nature-based Solutions can be used to attenuate waves, however it is still uncertain to what extent the vegetation can contribute to decreasing the flood risk. Hence, the wave damping effect is not yet considered in the safety assessment of the dikes in the Netherlands. Therefore, it is necessary to research the reliability of the wave damping effect of vegetation, so it can be implemented in the assessment of the flood defences.
Due to the stochastic nature of wave breaking and wave run-up and the relevance of many parameters, it is very challenging to develop theoretical or numerical approaches to describe these processes (e.g. wave run-up and wave overtopping). Physical modelling is often used to predict wave run-up and overtopping by fitting an empirical formula through the obtained data. In the past different laboratory and field measurements have been conducted with moderate wave conditions and low water depths. However, field measurements of vegetation attenuating waves under more extreme storm conditions (i.e. higher wave heights and water levels) are lacking. Due to the scaling effects of the biophysical processes involved in wave attenuation of the vegetation, the upscaling of small-scale flume models results in major uncertainties. Therefore, quantifying the wave attenuating properties of vegetation is required, at full scale under more extreme wave conditions.

Furthermore, wave run-up and wave overtopping are two of the main failure mechanisms, thus more applicable and innovative measuring techniques are needed. Currently the wave overtopping is determined by a wave overtopping tank, which collects and measures the volume of water overtopping the crest of the dike. However, placing an overtopping tank at the crest or implementing a tank in the slope of the dike is not applicable for every dike. Therefore, new techniques which measure the overtopping without using a tank are a necessity. There is also room for improvement of determining the wave run-up using more innovative measuring tools.

1.3 Research objective

The main objective of this research reads:

To assess the effectiveness of willow vegetation in reducing wave loads on a dike, specifically wave run-up and wave-overtopping, under storm conditions, using remote sensing (Laser scanning and video imaging).

1.4 Research questions

In order to achieve the main objective, the following sub-questions are defined:

1. To what extent is terrestrial laser scanning applicable to quantify the run-up and overtopping processes on a dike?
2. To what extent is video imaging applicable to quantify the run-up processes on a dike?
3. What is the effect of willow vegetation on the wave run-up height?
4. What is the effect of willow vegetation on the wave-overtopping?

1.5 Research approach and scope

To research the effectiveness of willow vegetation as a Nature-based Solution, for the first time, large-scale physical model tests with real willows in front of a dike are conducted. The experiments were executed in June and July 2018 in the Delta flume of Deltares. To assess the effect of vegetation on the processes on a dike, three different quantitative measuring methods will be used: visual measurements, terrestrial laser scanning and video imaging. This is the first time a 'Machine Learning algorithm' created by Deltares, is used to obtain the wave run-up heights on a dike from video footages. It is also new that the wave overtopping volumes are determined by a laser scanner, without using a wave overtopping tank on the dike or a tank built in the dike slope. This tank was initially used to collect and measure the real overtopping volume.

The set-up of the experiment and the placement of the laser scanner were already specified by Deltares. My major responsibility during the experiments concerned the collection of data from the visual-, camera- and laser measurements regarding the wave run-up on the dike. For the equipment I had to set up a suitable resolution, scanning range and frequency for the laser scanner. Also, I had to make sure that the video camera was placed so that the full range of the wave run-up was recorded. Subsequently, the data is processed, analysed and the findings of the different methods will be compared. The results show how applicable the remote sensing techniques are in measuring the wave run-up and overtopping. The errors and limitations of the measurement techniques will be brought to light and so these can be minimized.

In Figure 1 an overview of the approach is given. The two processes that will be investigated in this research are the wave run-up and the wave overtopping on the dike. The influence of the wave impact on the dike is not considered in this study, because insufficient data about the wave impact is gathered from the used measurement devices. The velocities are also not included in the scope of this thesis report.

1.6 Relevance of study

The following knowledge gaps will be focused on in this report:

- The applicability of camera and laser equipment to measure the wave run-up on a dike. (Research question 1 & 2)

- The applicability of a laser scanner to measure the wave overtopping discharges. Using a laser scanner will make it possible to determine the overtopping volumes for every virtual crest height on every dike. (Research question 1)
- The unknown variation of the wave run-up over the width of the flume. As it is, a laser scanner only measures a 2D profile along the slope, so the effect over the width is absent. (Research question 2)
- The analysis of video imaging using a 'Machine Learning algorithm' to measure the wave run-up. (Research question 2)
- The uncertainty in the quantitative effect of willows on the wave run-up and wave-overtopping under storm conditions. (Research question 3 & 4)

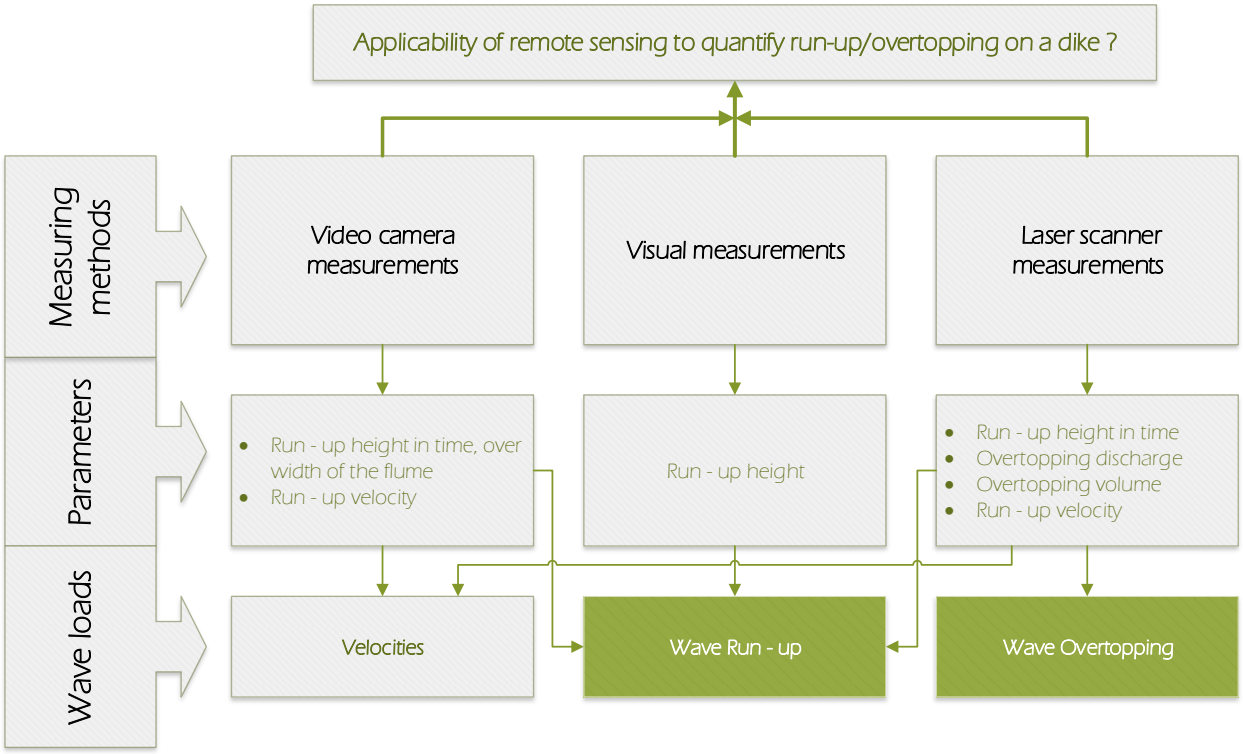

Figure 1 Scheme of the approach followed in this report, only the wave run-up and the wave overtopping are focused on in this report

1.7 Report outline

This report is structured as follows. In Chapter 2 a review is given of previous literature regarding the run-up and overtopping on a dike. It also refers to past researches conducted with vegetation or using remote sensing techniques. Subsequently, in Chapter 3 the set-up of the large-scale experiments and the used measurement equipment are given. In Chapter 4, the used method to obtain and process the data from the three different sources are elaborated. The results of the experiments are given in Chapter 5 and these results are discussed in Chapter 6. Finally, in Chapter 7 the conclusions regarding this research are drawn answering the research questions. This chapter also contains recommendations for further research.

2. Literature review

2.1 Wave run-up

For the design of a dike, three wave-structure interaction processes can be distinguished: the wave impact, the run-up/run-down and the wave overtopping. The processes are shown in Figure 2.

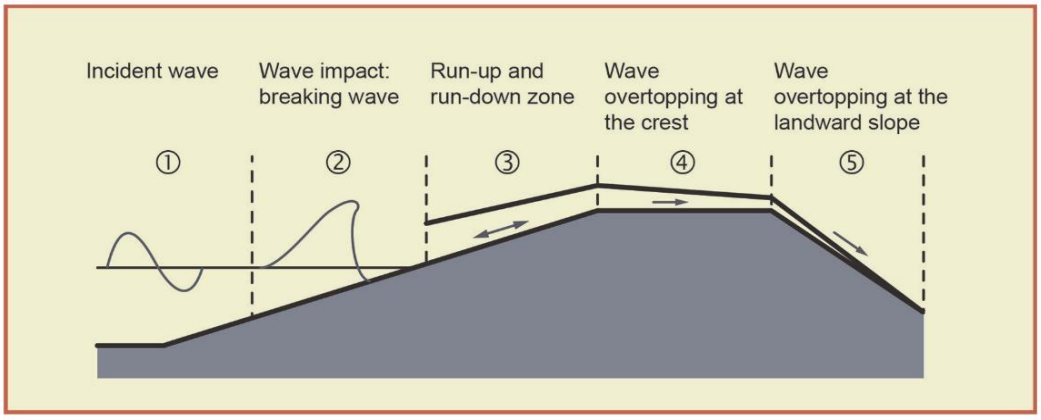

Figure 2 Main wave-structure interaction processes on a dike (Schüttrumpf, 2001; EurOtop, 2018)

In the **wave impact zone,** the waves break and exert large pressures on the dike. Dependent on the slope of the dike, the wave period and the wave height, the type of wave breaking on the dike will be different (see Figure 3). The type of wave breaking can be characterised by the surf similarity parameter, breaker parameter or Irribaren number (Battjes, 1974):

$$\xi_{m-1.0} = \frac{tan(\alpha)}{\sqrt{s_{m-1.0}}}, \text{ where } s_{m-1.0} = \frac{H_{m0}}{L_{m-1.0}} \text{ and } L_{m-1.0} = \frac{gT_{m-1.0}^2}{2\pi}$$

Where α is the slope angle of the structure, $s_{m-1.0}$ the fictitious wave steepness, H_{m0} the wave height at the toe of the dike and $L_{m-1.0}$ the wave length at deep water based on the spectral wave period ($T_{m-1,0}$) at the toe of the dike.

For a steep slope and/or waves with low steepness, the breaker parameter is large. For a fully developed storm sea (swell waves), the wave steepness is around 0.025 (Holman, 1986) and for normal wind sea waves the steepness is between 0.04 and 0.06 (EurOtop, 2018).

After breaking, the wave tongue runs up the slope until a certain level. For the design of a dike **the run-up height**, $R_{u2\%}$ (shown in Figure 4), is defined as the vertical distance above SWL, which is exceeded by 2% of the total incident waves at the toe of the dike (not of the number of run ups) (Van der Meer, 2002). The distance from the still water level to the crest of the dike is called the crest freeboard, R_c (see Figure 4). The run-up height can be estimated using Formula 2.1, which is based on a large dataset of both small- and large-scale tests including roughness, berms, oblique wave attack etcetera. (Van der Meer, 2002).

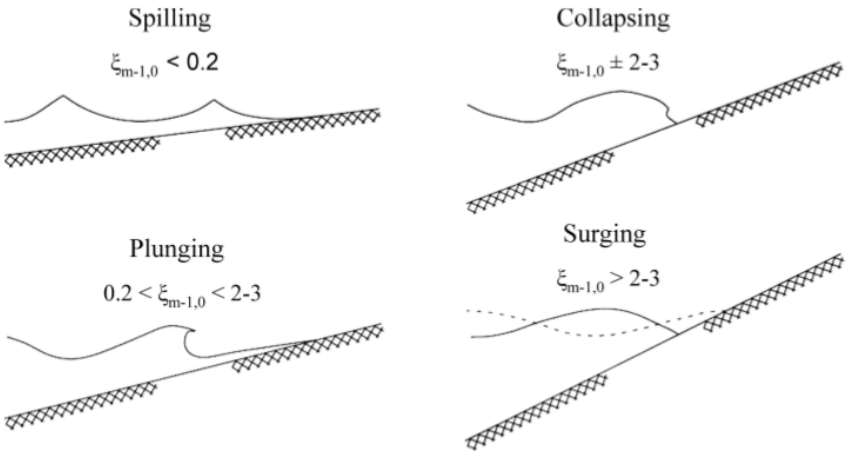

Figure 3 Different types of wave breaking on the slope of the dike (Battjes, 1974; Schüttrumpf et al., 2009)

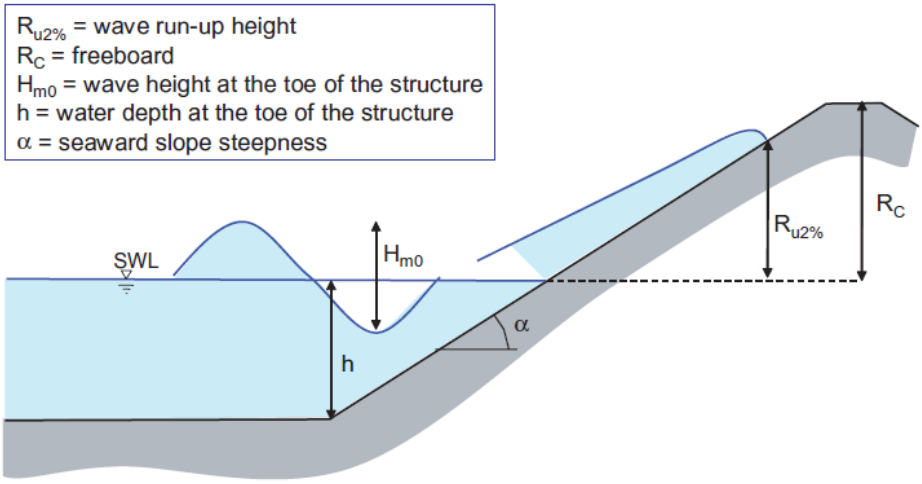

Figure 4 Definition of the different relevant parameters on a dike (Schüttrumpf et al., 2009)

$$\frac{R_{u2\%}}{H_{m0}} = min\left[a \cdot \gamma_b \cdot \gamma_f \cdot \gamma_\beta \cdot \xi_{m-1.0}\,;\; b \cdot \gamma_f \cdot \gamma_\beta \cdot \left(4.0 - \frac{1.5}{\sqrt{\gamma_b \cdot \xi_{m-1.0}}}\right)\right] \qquad (2.1)$$

γ_f, γ_b and γ_β are influence factors for respectively the roughness, the presence of a berm and the angle of incidence of the waves. The parameters a and b can be considered as stochastic normal distributed variables with a mean (μ) and standard deviation (σ). Where: μ_a=1.65, σ_a =0.10, μ_b=1.0 and σ_b =0.07 (Van der Meer, 2002).

2.2 Wave overtopping

If the freeboard R_c of the dike is smaller than the maximum run-up level R_{max}, **wave overtopping** will take place. Nowadays, dikes are designed using the wave overtopping discharge, which makes this one of the most important parameters. Overtopping on a dike is defined as the average discharge per meter of width (q). Based on a large amount of field and physical model studies, an empirical formula (shown in Formula 2.2, Weibull type function) describing the average overtopping discharge is fitted through the experimental data (Van der Meer et al., 2014 or EurOtop, 2018).

$$\frac{q}{\sqrt{g \cdot H_{m0}^3}} =$$

$$\min\left(\frac{c}{\sqrt{tan(\alpha)}}\gamma_b \cdot \xi_{m-1.0} \cdot exp\left[-\left(d\frac{R_c}{\xi_{m-1.0}\cdot H_{m0}\cdot \gamma_b\cdot \gamma_f\cdot\gamma_\beta\cdot\gamma_v}\right)^{1.3}\right]; e \cdot exp\left[-\left(f\frac{R_c}{H_{m0}\cdot \gamma_f\cdot\gamma_\beta\cdot\gamma^*}\right)^{1.3}\right]\right) \quad (2.2)$$

Where c, d, e and f are stochastic parameters with a mean: $\mu_c = 0.023$, $\mu_d = 2.7$, $\mu_e = 0.09$ and $\mu_f = 1.5$ and standard deviation: $\sigma_c = 0.003$, $\sigma_d = 0.20$, $\sigma_e = 0.0135$ and $\sigma_f = 0.15$. The standard deviation is a measure for the reliability of the equation. γ_v is an influence factor for a wall at the end of the slope and γ^* an influence factor for the presence of non-breaking waves in front of a storm wall or promenade (Van der Meer et al., 2014).

In deep water the wave height is well described by a Rayleigh distribution. When waves reach shallow water, waves break and the distribution of the wave height changes from a Rayleigh distribution to a composite Weibull distribution. This means, processes related to shallow water waves and wave overtopping, follow a Weibull distribution and show a deviation from the straight Rayleigh distributed curve (Battjes et al., 2000).

The probability of overtopping for a single wave can be calculated with Formula 2.3, assuming the run-up height to be Rayleigh distributed (TAW, 2002):

$$P_{ow} = \frac{N_{ow}}{N_w} = \exp\left[-\left(\sqrt{-\ln 0.02}\,\frac{R_c}{R_{u2\%}}\right)^2\right] \quad (2.3)$$

With N_{ow} the number of overtopping waves and N_w the number of incoming waves. The individual overtopping wave volumes are represented by a Weibull distribution and can be calculated for different probability of exceedances (P_v) as follows:

$$V = a\,[-\ln(1-P_v)]^b\,, \quad (2.4)$$

$$\text{with } a = \left(\frac{1}{\Gamma\left(1+\frac{1}{b}\right)}\right)\frac{T_m q}{P_{ow}} \quad (2.5)$$

Where b is a shape parameter and a is the scaling parameter, with Γ the mathematical gamma function. The shape factor b has a large influence on the prediction of the overtopping wave volumes and can be estimated for smooth structures with Formula 2.6 (Zanuttigh et al., 2013):

$$b = 0.73 + 55\left(\frac{q}{gH_{m0}T_{m-1,0}}\right)^{0.8} \quad (2.6)$$

For relative discharges $\frac{q}{gH_{m0}T_{m-1,0}}$ <10^{-4}, b is around 0.75. However, a significant increase in the relative discharge results in gentler distributions of the individual wave volume.

2.3 Remote sensing

In the past years, more alternative methods are searched to measure the water surface providing higher spatial resolution. One of these methods which is more often used, is remote sensing. Examples of remote sensing are LIDAR (Laser Imaging Detection And Ranging) and video imaging. A LIDAR instrument transmits pulses which are reflected back by the surface to the instrument. The laser determines the distance to the surface by measuring e.g. the travel time of the transmitted pulse. Another technique is video imaging, which has low costs and can result in high spatial and temporal resolution. However, the accuracy of the information obtained from video data, is affected by the subjective judgement of the operator. Also, the applicability of video technique during storms is very low, especially during the run-down. The run-down is not always clearly visible, particularly when water drains into the soil (Holman et al., 1984).

Different experiments in the field and in the lab have been performed using remote sensing techniques.

- Field measurements for the run-up on the beach have been measured with both wire sensors and photo imaging techniques. From these measurements was observed that the mean horizontal excursion of the video data is 3 cm higher and the variance is 83% higher than the measured run-up with wire sensors (Holman & Guza, 1984).

- The free- surface in a wave flume has been measured with both a SICK laser scanner and four wave probes. The measurements showed that the RMS differences were less than 2% of the wave height. It was also observed that the laser underestimated the upstream measurements and overestimated the downstream measurements (Blenkinsopp et al., 2012).

- Also, large scale experiments simulating a swash zone have been conducted using both 2D laser scanner and video imaging. Compared with an ultrasonic measuring device, it was observed that the 2D laser scanner was underestimating the measured surface elevation, but the differences were quite small. Combining the data obtained from the scanner and the video imaging, improved the accuracy of the information by more than one order of magnitude. Furthermore, the video imaging data added extra information to the laser scanner data (Vousdoukas et al., 2014).

- The hydrodynamics and morphology in the swash zone of a gravel beach have been measured using a SICK laser scanner. The 2D laser had a vertical accuracy of approximately 1.5 cm. (Almeida et al., 2015)

- Furthermore, the wave run-up heights, virtual wave overtopping volumes and virtual mean overtopping discharge were measured with a 2D laser scanner (frequency of 32 Hz) during a large-scale flume experiment. For the determination of the run-up heights the reflection intensity value was used, which improved the accuracy of the run-up measurements by approximately 20 cm, compared to visual measurements. The remaining bias between the laser and visual measurements were at maximum 10 cm. The measured overtopping results were compared with the existing formula of Van der Meer & Bruce (2014) and most of the results were within the 90% confidence band. The results for low crest heights were out of the 90% confidence band and were underestimated. (Hofland et al., 2015)

2.4 Vegetation

In recent years, the effectiveness of applying willow trees as Nature based Solution has been studied. The first field measurements with willows were conducted at the tidal river Noord near Dordrecht in 2015 (Stam, 2018). Two willow plots of each 7x7 m where placed on the side of the river. One plot consisted of 3-year-old willows and one contained 1-year old willows. The water depth in the river varied between 0.8 m and 2 m above the crate in which the willows were placed. The main source of waves in the river were ship waves with a height between 0.05 and 0.20 m. In Appendix A, the set-up of the willows in the river are shown. In each plot five pressure transducers were placed in one line through the middle of the plot. The transducers measured the wave height, from which the reduction in wave height through the willow plot is determined. From the measurements in the field was observed that the highest waves showed the largest wave damping of on average 4.1% per m of willows. It was also seen that the amount of wave attenuation decreases when the water level increases and the willows become more submerged. However, due to the small measurement area and the distortion of the flow caused by the elevation of the willows above the surface, the accuracy of the measurements is low. Also, the measured wave conditions are not representative for storm conditions.

Besides the field measurements a sensitivity analysis has been performed. A SWAN model was made for a dike section near the Heesseltsche Uiterwaarden with a willow forest of 60 meters on the floodplain. From the model simulations has been found that the wave overtopping discharge is largely influenced by the ratio between water depth and vegetation height. The second important influence factor is the drag coefficient, which has a large variation and gives a large standard deviation to the overtopping discharge. After the drag coefficient, the overtopping discharge is very sensitive to the density and width of the forest (Stam, 2018).

Another study has been performed by Vuik et al. (2016) on two different vegetated foreshores in the Netherlands. Namely, a foreshore with cordgrass and one covered with grassweed. A numerical model describing the wave propagation over a vegetated foreshore was set up. The model is validated and calibrated by field measurements, conducted during severe storms at the Western Scheldt estuary in the Netherlands. A maximum wave height of 0.7 and a maximum water depth of 2.5 m were measured during the storm. Results showed a significant reduction on the wave height between the 25 and 50% compared to a foreshore without vegetation. The dissipation by vegetation is found more effective for smaller water depths with higher biomass density. Even when the vegetation is in winter state and more inundated, still a considerable reduction remains (Vuik et al., 2016).

In another research conducted by Deltares (2016), a part of the dike system from Tiel – Waardenburg has been modelled in SWAN to determine the effect of different vegetation on the wave height. The maximum wave height was given a value of 1.2 m. For pollard willow trees (Griend), with a length of 3 m and a density of 0.55 stems per m^2, the average effect of a 20 m and 60 m vegetation belt are found to be respectively 9% and 17% in relation to the reference case without vegetation. The maximum measured effect amounts respectively 18% and 31%. Using different vegetation types with different densities showed that low effective vegetation densities (lower than 0.1 branches·m/m^2), and a vegetation width of only 20 m do not give significant reduction in wave height (Smale et al., 2016).

3. Experimental set-up

In this chapter the experimental set-up in the Delta flume is explained and the data collection using the different measuring techniques are further elaborated.

3.1 Model facility

The experiments were conducted in the Delta flume of Deltares. The model facility has a length of 300 m, a width of 5 m and a depth of 9.5 m. With a wave board of 10 m high, a wave field with a significant wave height of 2.0 m (irregular waves) can be generated. The wave board is equipped with an Active Reflection Compensation to minimize the re-reflection of waves from the wave board (Hofland et al., 2013). The dimensions of the flume and the available wave conditions create a good opportunity to perform large-scale physical model tests.

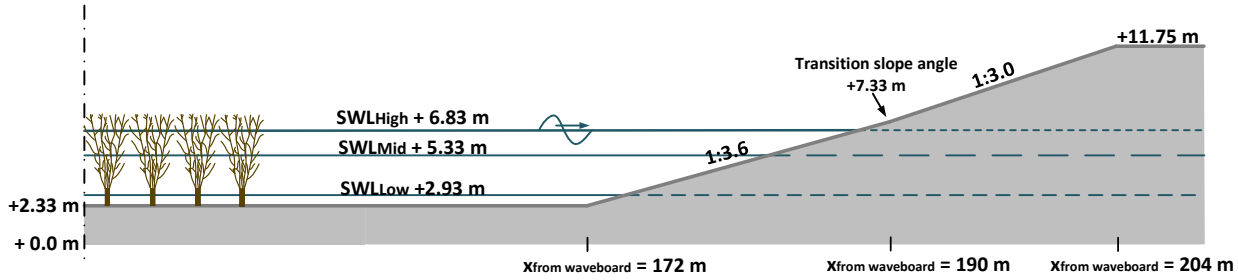

Figure 5 Schematization of the slope of the dike in the flume with the different water levels and coordinates, with SWL the different tested still water levels in the flume

The experimental set-up is schematized in Figure 5. A dike with a foreshore is constructed in the flume. The dike was made of concrete with an extended part of plywood. The dike was composed of two parts: the lower part had a 1:3.6 slope and the upper part a 1:3 slope. The dike had a total height of 11.75 m and the toe of the dike was situated at 172 m from the wave board. In the flume a platform, with a length of 85 m, representing the foreshore was constructed. The foreshore, situated at 2.33 m above the flume bottom, was covered with a layer of concrete to prevent the willows from rooting up due to the extreme wave conditions (for more details see Measurement report Deltares (Wolters et al., 2018)).

On the foreshore a willow forest of 40 m was constructed. The forest contained 32 willows of which 30 of the specie Salix Alba and 2 of the specie Salix Viminalis. The willows had an average branch density of 15 branches per m^2 (counted at the knot of the willow). The characteristics of the willow trees are shown in Table 1. The willows were placed in two rows with a centre to centre distance of 2.5 m in x - direction of the flume. To obtain an even biomass density along the flume, the willows are staggered on tree height in both x - and y - direction. Also, the distance between the willows and the wall was chosen so that the biomass was equally distributed in y - direction. In Figure 6 the position of the willows in the delta flume with their tree height are shown. In Appendix C the biomass distribution of an average tree is given.

Table 1 The characteristics of the willow trees in [cm]. The number of branches is measured at the knot of the tree (Wolters et al., 2018) & (Kalloe, 2019).

	Trunk diameter	Trunk height	Total height	Width canopy	Branch diameter	Number branches/tree
Min	16	87	427	160	0.35	54 branches
Max	28	116	657	250	8.40	158 branches
Average	22	102	540	199	4.38	90 branches

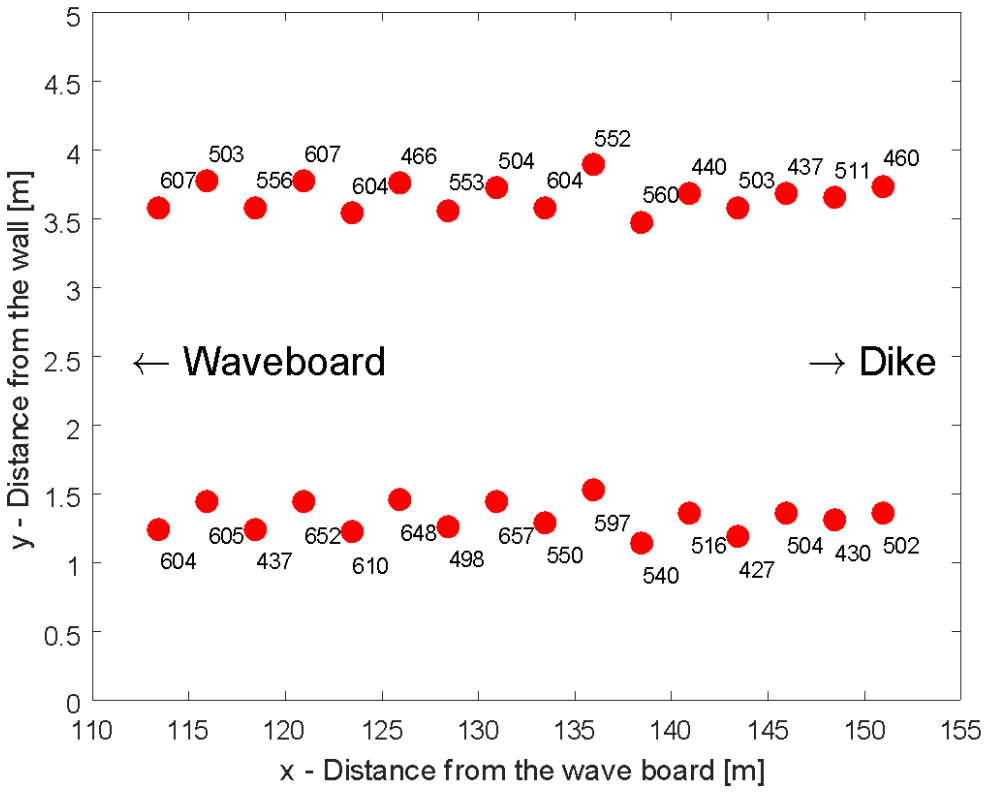

Figure 6 Position of the centre points of the willows in the flume and the height [cm] of the willows

3.2 Test program

In total 42 tests were performed. The varying parameters during the experiments were the hydraulic conditions and the configuration of the willow trees in the flume. Four different configurations are tested:

- Willows with leaves
- Willows without leaves
- Willows without leaves and only 50% branch density
- Reference test, without willows

In Appendix B, an overview is shown of the four different willow configurations. For every configuration different tests with varying wave height, water depth and wave steepness were carried out. The significant wave height varied between H_{m0} = 0.2 m and H_{m0} = 1.5 m. The water level at the foreshore varied between h = 0.6 m and h = 4.5 m, and the wave steepness was set between s_{op} = 0.02 and s_{op} = 0.05. For each test

a set of around 550 irregular waves following a JONSWAP spectrum, with a peak enhancement factor of γ = 3.3, was generated. During the tests the Active Reflection Compensator at the wave board was used. The full test program is given in Table 2. Test T041 and T042 are repetitions (same steering file) of T037 and T038. The tests with the same steering file, which can be compared are given in Appendix E.

Table 2 Test program based on measured incident values at the wave board (WHM 1-3) Source: (Wolters et al., 2018)

Test-ID	Configuration willows	h (m)	H_{m0} (m)	T_p (s)	$T_{m-1.0}$ (s)	s_{op} (-)	N (-)	Duration (s)
T001	Leaves	0.6	0.17	1.8	1.7	0.03	515	821
T002	Leaves	0.6	0.19	2.5	2.3	0.02	560	1109
T003	Leaves	0.7	0.21	2.0	1.9	0.03	539	911
T004	Leaves	0.7	0.23	2.8	2.6	0.02	565	1327
T005	Leaves	3.0	0.44	2.8	2.6	0.04	514	1265
T006	Leaves	3.0	0.97	3.9	3.7	0.04	539	1750
T007	Leaves	3.0	0.45	3.9	3.7	0.02	551	1750
T008	Leaves	3.0	0.97	5.6	5.1	0.02	559	2446
T009	Leaves	4.5	0.43	2.8	2.7	0.03	520	1266
T010	Leaves	4.5	0.91	3.9	3.7	0.04	533	1750
T011	Leaves	4.5	0.44	3.9	3.7	0.02	553	1750
T012	Leaves	4.5	0.91	5.6	5.2	0.02	552	2444
T013	Without leaves	3.0	0.44	2.8	2.6	0.04	518	1263
T014	Without leaves	3.0	0.95	3.6	3.4	0.05	517	1611
T015	Without leaves	3.0	0.45	3.9	3.7	0.02	554	1748
T016	Without leaves	3.0	0.97	5.6	5.1	0.02	561	2445
T017	Without leaves	4.5	0.43	2.8	2.7	0.03	517	1264
T018	Without leaves	4.5	0.91	3.9	3.7	0.04	537	1749
T019	Without leaves	4.5	0.44	3.9	3.7	0.02	551	1762
T020	Without leaves	4.5	0.91	5.6	5.2	0.02	563	2466
T021	Without leaves	4.5	1.40	4.8	4.6	0.04	553	2188
T022	Without leaves	4.5	1.41	6.8	6.3	0.02	557	2956
T023	Without leaves, 50 % branch density	3.0	0.43	2.8	2.6	0.03	522	1265
T024	Without leaves, 50 % branch density	3.0	0.93	3.6	3.4	0.05	526	1611
T025	Without leaves, 50 % branch density	3.0	0.43	3.9	3.7	0.02	543	1749
T026	Without leaves, 50 % branch density	3.0	0.97	5.6	5.1	0.02	560	2443
T027	Without leaves, 50 % branch density	4.5	0.88	3.9	3.7	0.04	539	1749
T028	Without leaves, 50 % branch density	4.5	0.94	5.6	5.2	0.02	561	2444
T029	Without leaves, 50 % branch density	4.5	1.40	4.8	4.5	0.04	569	2188
T030	Without leaves, 50 % branch density	4.5	1.44	6.8	6.3	0.02	556	2957
T031	Reference, without willows	0.6	0.17	1.8	1.7	0.03	526	812
T032	Reference, without willows	0.6	0.19	2.5	2.3	0.02	549	1129
T033	Reference, without willows	3.0	0.44	2.8	2.6	0.03	527	1264
T034	Reference, without willows	3.0	0.94	3.9	3.7	0.04	542	1747
T035	Reference, without willows	3.0	0.46	3.9	3.7	0.02	562	1748
T036	Reference, without willows	3.0	0.96	5.6	5.1	0.02	565	2443
T037	Reference, without willows	4.5	1.40	4.8	4.5	0.04	563	2187
T038	Reference, without willows	4.5	1.43	6.8	6.3	0.02	565	2956
T039	Reference, without willows	0.7	0.21	2.0	1.9	0.03	520	910
T040	Reference, without willows	0.7	0.23	2.8	2.6	0.02	540	1267
T041	Reference, without willows*	4.5	1.36	4.8	4.6	0.04	559	2187
T042	Reference, without willows*	4.5	1.37	6.8	6.3	0.02	568	2956

3.3 Data collection

As mentioned before, three different measuring methods will be analysed by their data, to quantify the effect of woody vegetation on the wave run-up and overtopping on the dike. The techniques are: measurements by laser scanning, video imaging and visual determination of the run-up exceedance levels. Furthermore, wave gauges of the resistance type and radar are used to measure the wave conditions in front of the foreshore and in front of the dike. In Figure 7 an overview is given of the used measuring equipment in the flume. The coordinates of the different equipment are given in Appendix F. The different measuring methods are further elaborated in this section.

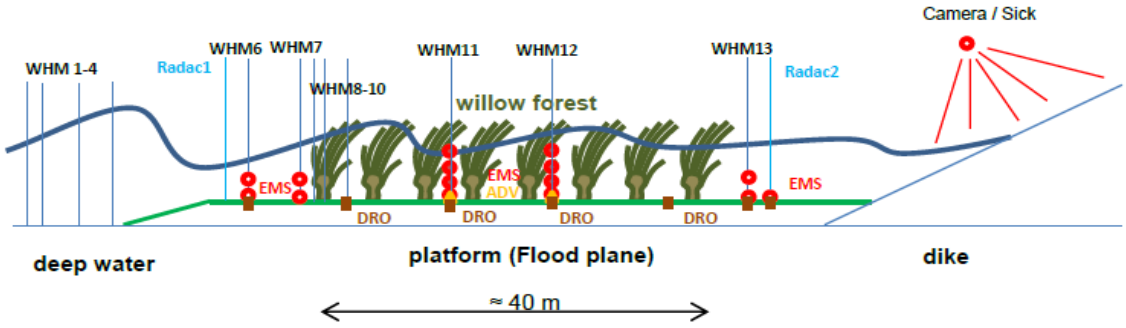

Figure 7 Experimental set-up in the flume with the most important measuring equipment: WHM = Wave gauge (resistant type). RADAC = radar wave gauge. DRO = pressure sensor. EMS = electromagnetic velocity sensor, SICK = laser scanner, Camera = video camera (Wolters et al., 2018).

3.3.1 Visual determination of run-up exceedance levels

The exceedance levels of the individual wave run-up tongues can be visually determined. On the slope of the dike parallel lines with a width of 2.5 m were drawn, which are used as indicators during the visual observations. The lines had a distance of 0.5 m to each other and were numbered from 0 to 65 (see Figure 10). The measured coordinates of the lines are given in Appendix D. To exclude the possible wall effect, the measurements are only focussed over the 2.5 m width of the line. For each individual wave run-up, the exceedance level was marked. If the wave run-up tongue exceeds approximately 70% of the width of a line, the wave is counted as run-up of that corresponding line (See Figure 8). To obtain more reliable data, the visual measurements are executed by three individuals (see Figure 9). After having determined the exceedance levels for each individual wave, the probability of exceedance for each run-up height can be obtained from which the R_{u2}% for each test can be derived.

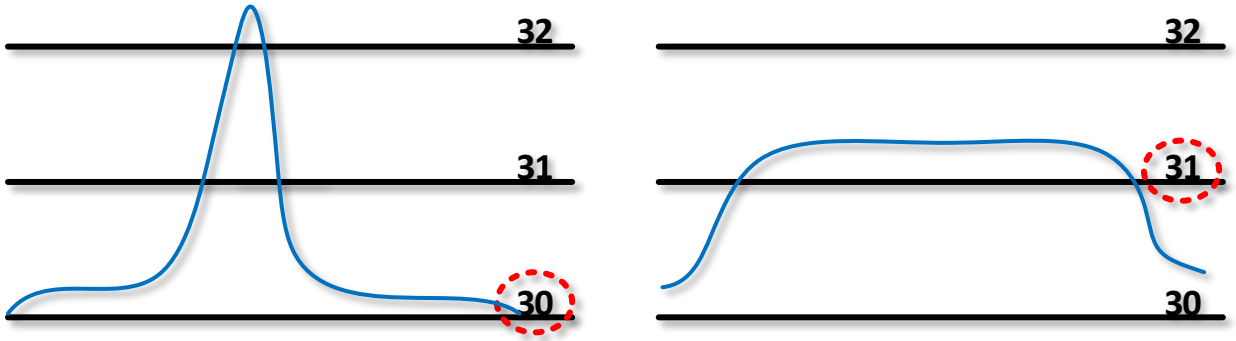

Figure 8 The method of visually determining the run-up exceedance levels. Exceedance level is reached when the wave exceeds approximately 70% of the length of the line.

Figure 9 Three students determining the wave run-up exceedance levels (Deltares, 2018)

Figure 10 The upper part of the dike with the drawn lines (Deltares, 2018)

3.3.2 Laser scanner

During the test a 2D terrestrial laser scanner (TLS) model type SICK LMS511-PRO was mounted above the slope of the dike, to measure the instantaneous water surface. The laser scanner transmits a laser beam along a plane, which is reflected, transmitted or absorbed by the surface. The distance is determined by the Time of Flight principle, which measures the time between the emitted signal and received signal. The receiver measures both the distance to the surface and the Received Signal Intensity Strength Indicator (RSSI) of the reflected laser ray. The RSSI value has an 8-bit resolution, with integer values between 1 and 255 (SICK, 2015). Where 1 is the weakest possible signal and 255 the strongest signal that could be measured. For a dry surface the reflection is high, which gives a high RSSI value. During wave run-up the reflection decreases, and the reflection intensity drops to lower values. By combining the measured distance and the RSSI value, the wave run-up heights can be determined with a higher accuracy (Hofland et al., 2015). Besides the wave run-up, the virtual wave overtopping volumes and virtual overtopping discharges can be determined by the laser scanner.

The laser was placed at a height of 5 m in a line perpendicular to the slope, with local coordinates x = 193 m, y = 0.3 m and z = 13.3 m, see Figure 11. Figure 12 shows the placement of the laser on the wall of the flume.

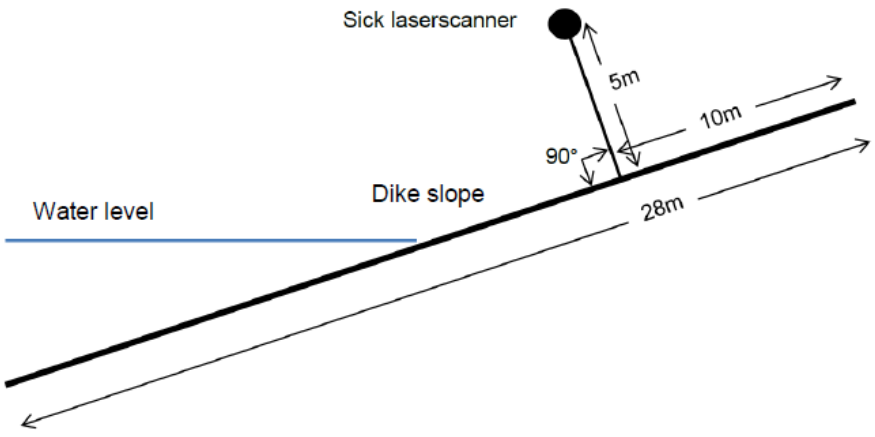

Figure 11 Position of SICK laser on dike slope (Deltares, 2018)

Figure 12 Positioning of the laser scanner on the wall of the flume (Çete, 2018).

The laser has a range of 190°, but the scope was set from 5° to 150° (Field of View = 145°), so the data set will only contain points in the area of interest. The scanner is set to a frequency of 33 Hz and a resolution of 0.33°. This resolution is chosen so that the run up at the lower water levels are also measured. For recording the measurements, the SOPAS software interface was used.

3.3.3 Video camera

During the tests a video camera was focused on the slope of the dike recording the wave run-up, see Figure 13. The camera was positioned at the walking bridge above the mid of the flume. The camera was situated at a height of approximately 8.5 m above the foreshore. The distance of the camera to the dike was not fixed and was dependent on the wave conditions and the expected wave run-up for each test. So, for each test the Field of View of the camera recordings are different. The wave run-up over the total width of the flume in time, can be extracted and analysed from the camera observations.

Figure 13 The video camera positioned on the walking bridge pointing to the slope of the dike (Çete, 2018)

3.3.4 Wave measurements

To measure the wave conditions at different locations 2 radar wave gauges (RADAC Wave Guide5) and 13 wave gauges of the resistant type are placed in the flume, their positions are shown in Figure 7. The wave gauges had a frequency of 60 Hz and the radar gauges a frequency of 10 Hz. Also, pressure sensors are applied within the forest, which will not be used as part of the analysis. During the tests the variables: H_{m0}, $T_{m-1.0}$ and T_p are measured. The deep-water wave conditions are determined using the measurements of the three resistance type wave gauges at deep water (WHM1-3). The incident wave conditions behind the forest are obtained from radar wave gauge 2 (see Figure 14). The results obtained from WHM6 and RADAC 2 are given in Appendix G.

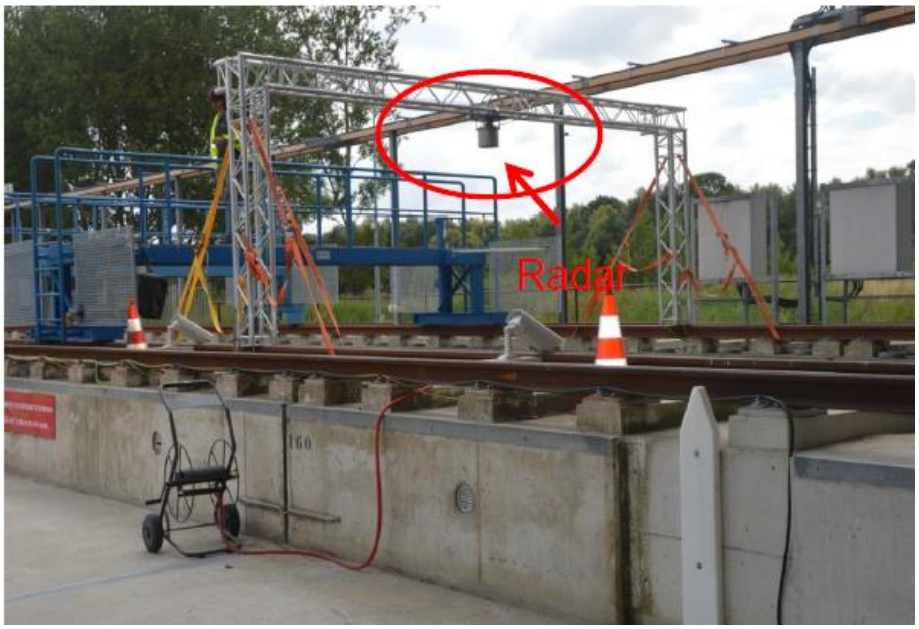

Figure 14 Radar wave gauge behind the forest (Deltares, 2018).

4. Data processing

This section explains how the data obtained from the laser scanner and video camera will be processed in order to reach the aim of this research.

4.1 Laser scanner

The main aim of the laser scanner is to measure the water surface elevation in time. The laser data was used in determining the run-up heights and the overtopping volumes on the dike. In this section it is explained how the laser data is pre- processed and how the run-up/overtopping are determined.

4.1.1 Pre-processing

An overview of the pre-processing of the data is given in Figure 15.

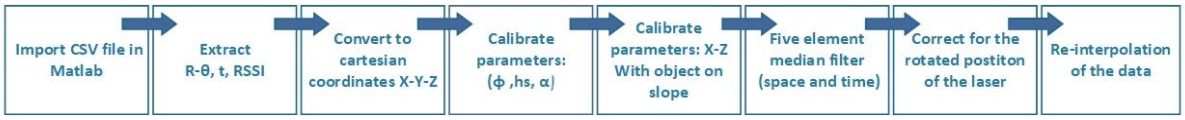

Figure 15 Pre-processing of the data obtained by the laser scanner

With a MATLAB script the CSV files are loaded into MATLAB and the following parameters are extracted:

- t: The time step corresponding to each measured profile, measured in milliseconds.
- R-Θ: The distance (R) measured for each pulse belonging to a certain angle (Θ in degrees) and time step, measured in mm.
- RSSI: The measured intensity of the received reflected signal.

The measurements are in polar coordinates (R, Θ) and need to be converted into Cartesian coordinates (x, z). The slope of the dike consists of two different angles, so the conversion is done by introducing a cartesian coordinate system, which is shown in Figure 16.

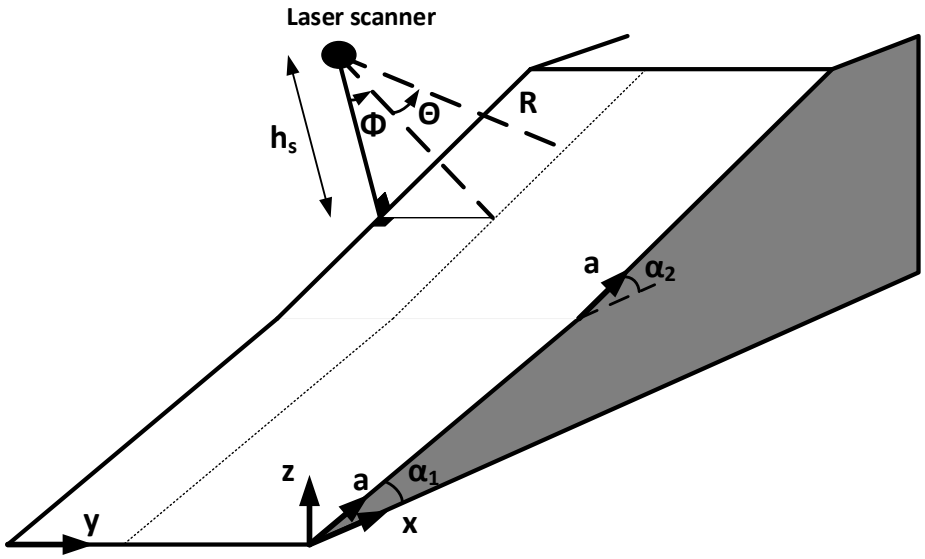

Figure 16 Setup of the laser on the slope, with the used coordinate system

Subsequently, the measured data is calibrated in two steps. The slant angle of the laser (φ), the height of the laser perpendicular to the slope (h_s) and the slope angle (α_1 and α_2) are calibrated so that the measured slope and the theoretical slope have the least deviation. The difficult accessibility of the mounting position of the laser caused a slight deviation from the design. The line along which the laser scans, has been determined during the calibration measurement and is shown in Figure 17 (and Appendix H). Apparently, the Field of View of the laser was not parallel but oblique to the slope, caused by the difficult placement of the laser. The measured line deviates from the normal with 4.4 degrees at the lower and 3.3 degrees at the upper slope. This obliqueness is corrected during the processing of the data. The measured profile still ranges between the selected 2.5 m part in the centre of the flume, so the possible wall effects are excluded.

The slant angle is the angle between the scanning line of the laser and the line perpendicular to the slope, see Figure 16**.** The slant angle has been calculated to be around 23 degrees. However, knowing that the position of the laser on the wall is not certain, the slant angle can vary between approximately 22 and 24 degrees. The used slant angle is greater than the recommended minimum of 5 to 15 degrees. This prevents direct reflection of the laser pulses which could lead to erroneous measurements (Hofland et al., 2015).

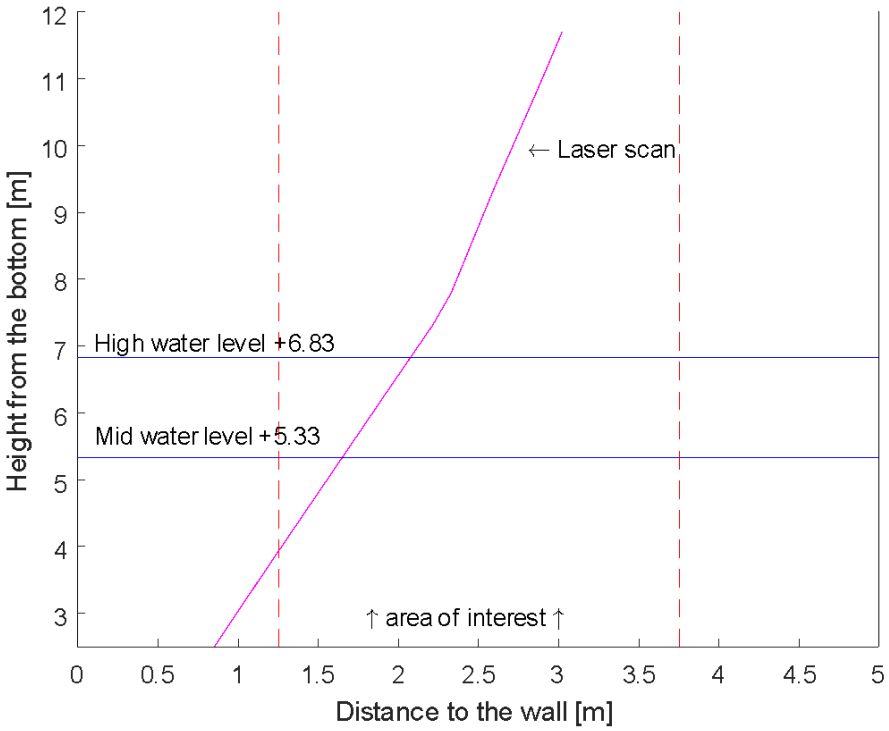

Figure 17 Line along which the laser scans the slope, with the water levels indicated

Secondly, the measured dike slope is calibrated by placing a wooden block with known dimensions (38x15.5x5.7 cm) on several lines on the slope. The initial coordinates of the lines measured by the laser scanner are compared to the coordinates measured by hand, the difference is given in Table 3. Apparently, the laser underestimates the coordinates, with a larger deviation at the upper slope. The data has been calibrated by adding a factor of 1.0035 in x-direction and 1.0155 in z-direction. These calibration factors give the smallest deviation to the hand measurements (see Table 3). It must be noted that the measurements by hand can also contain a measurement error.

Table 3 Deviation between coordinates measured by hand and by laser scanner, before and after calibration

[cm]	Δx before calibration	Δz before calibration	Δx after calibration	Δz after calibration
Lower slope	10.6	13.2	3.4	2.2
Upper slope	12.6	15.9	4.1	3.6

The still present deviations are small compared to the coordinates of the dike (31.4 m wide and 9.4 m high), which is a deviation of less than 0.4%. The layer thickness of the wave run-up is not affected by this deviation, as both the water surface and the dry slope are measured with the same deviation Δz. However, the still water level and the wave run-up both contain an error in z-direction:

$$Ru_{2\%} = (z_{Run-up} + \Delta z_{Run-up}) - (z_{SWL} + \Delta z_{SWL})$$

Having $\Delta z_{SWL\,Low} \approx 1.6\,cm$ and $\Delta z_{SWL\,High} \approx 2.1\,cm$ (from the error of the measured lines) results in a deviation on the run-up height of approximately 5 cm. After calibration, a five-element median filter is applied on the z-coordinates and the RSSI values in both time and space. This filter removes the outliers in the data.

During the analysis of the data, it is noticed that the measured dike profile has rotated in time. In Figure 18 it is shown how the dike profile has subsided at the top and uplifted at the lower part, with a maximum value of 4 cm. The point around which the dike slope has rotated coincides with the central axis of the laser. So, the conclusion that can be drawn is that the laser itself has rotated around its axis. This can be due to how the laser is positioned. The mounting of the laser is made from wood, therefore aspects such as humidity and temperature could have caused shrinkage or creep of the wood. Also, the effect of wind in combination with a weak support could have caused rotation of the camera around its own axis.

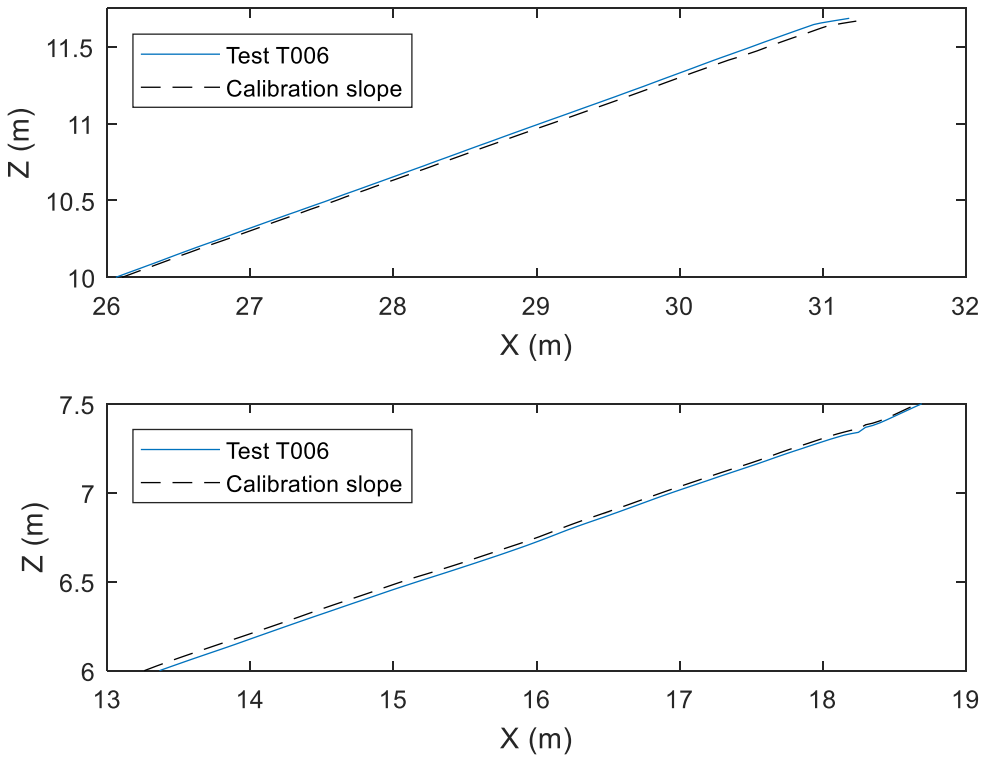

Figure 18 Plot of the slope measured by laser of test T006 and the calibration, for both the upper and lower part of the dike

To compare the individual tests, a correction must be applied to the measured coordinates. For each individual test the measured points are rotated around the central axis of the laser, using the rotation matrix, so that the deviation with the calibration test is minimal. Afterwards, the maximum bias measured between the slope during calibration and the test amounts 0.9 cm. Figure 19 shows the bias before and after applying the correction for test T006.

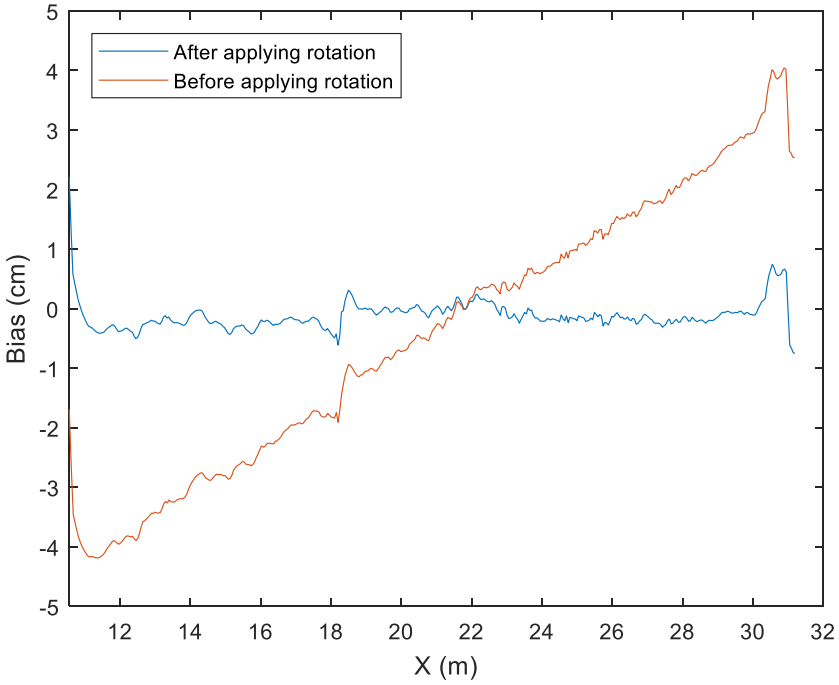

Figure 19 Bias between the slope of test T006 w.r.t the slope of the calibration, before and after applying an extra rotation

The scanned dike profile has a varying point density which is given in Table 4. To obtain a dike profile with equally distributed points, re-interpolation of each point is applied. Weighing the calculation time and the obtained bias ($Ru_{2\%\_laser}$ - $Ru_{2\%\_visual}$) resulted in the selection of a point distance of five times the former minimum point distance (see Figure 21).

Table 4 Point distance in x and z direction of the measured profile

Position	Point distance X-direction	Point distance Z-direction
Low	51 cm	14 cm
Middle	1 cm	-
High	12 cm	4 cm

4.1.2 Determining the run-up

In this section it is explained how the wave run-up is determined using two different methods. In Figure 20 an overview is shown of the steps taken to obtain the probability of exceedance distribution of the run-up height.

Figure 20 Overview of the steps taken to obtain the wave run-up height distribution

In the analysis the dry reference slope is taken as the average of the first 60 seconds of each individual test. The wave run-up height will be calculated using two different methods:

1. Run-up based on a threshold on the water layer thickness.
2. Run-up based on a threshold on the RSSI value.

1. Run-up: Layer thickness threshold

In this report the layer thickness is defined as the vertical distance between the measured water surface and the dry reference slope. The wave run-up is determined using a maximum threshold on the water layer thickness, meaning that, at this minimum layer thickness the wave run-up is determined. Different threshold values between 0 and 5 cm have been considered. In Figure 21 the bias for the run-up with respect to the visual observed run-up heights are given for different thresholds and interpolation distances. Thresholds lower than 1 cm resulted in unrealistic run-up heights. This can be explained by the small displacements of the laser scanner which cause small deviations in the measurement of the slope. Therefore, for further analysis a layer thickness threshold of $Z_{Water} - Z_{Slope} > 1$ cm is used, where Z_{Water} is the measured coordinate of the water surface and Z_{Slope} the measured coordinate of the dry slope.

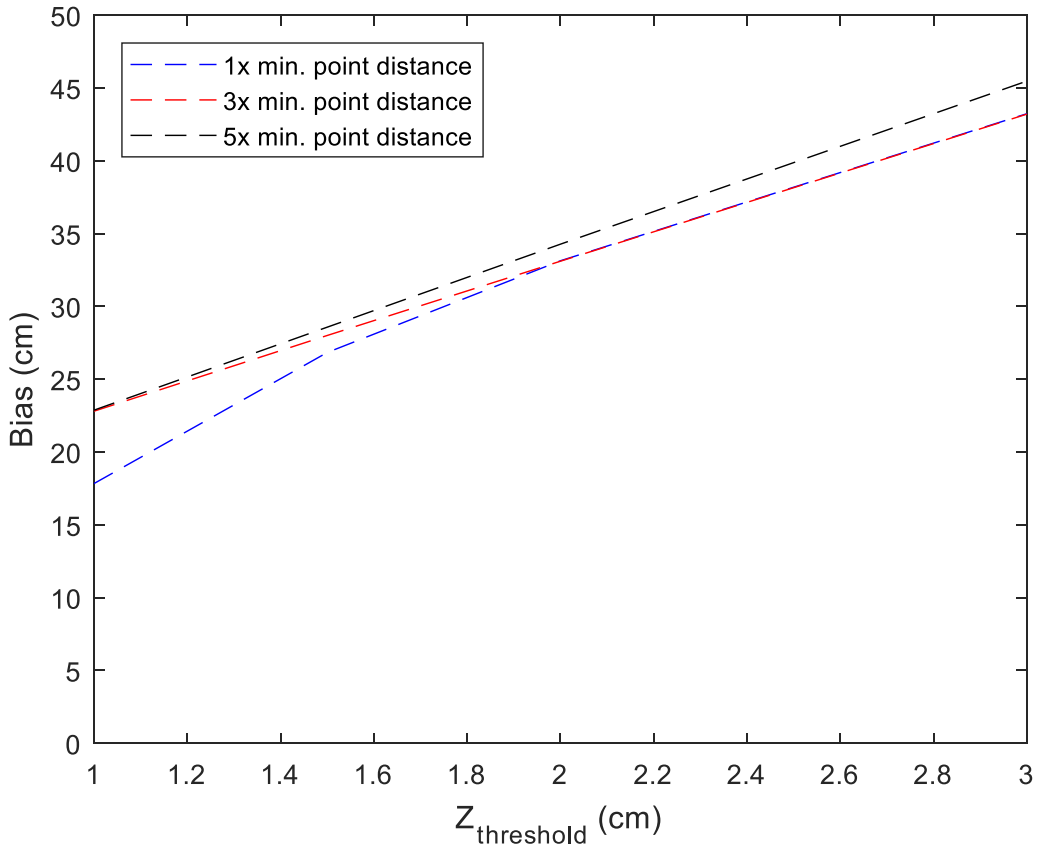

Figure 21 Bias of the measured run-up height w.r.t the visual observations for three different interpolation distances, for test T012, see Appendix J for the determined $R_{u2\%}$ values.

2. Run-up: RSSI threshold

The second method to calculate the run-up height is based on the signal intensity of the reflected pulse (RSSI value). This value varies between 0 and 255 [-]. A dry slope results in a high reflection which corresponds to a high RSSI value. As the water runs up the slope, the reflection becomes less, resulting in a decrease in the signal intensity. In previous research the use of the RSSI value in determining the run-up height, has shown to improve the accuracy of the results. The run-up heights determined with a layer thickness threshold, were underestimated with 0.1 to 0.3 m with respect to the visual measurements. While the run-up heights obtained using the RSSI values were only underestimated by 10 cm (Hofland et al., 2015).

In Figure 22 the wave run-up and the RSSI value for test T012 are shown. From this can be observed that the RSSI value at the upper part of the slope does not return to the initial dry slope value. Due to wave run-up, the slope becomes wet resulting in less reflection and lower RSSI values than before. An extra threshold in time is used to distinguish the “dry” slope and the real decrease in reflection intensity caused by the wave run-up. The following threshold values are used to determine the wave run-up height measured by the laser, where the run-up height is the maximum location on the slope where the following thresholds apply:

- $RSSI_{test}$ - $RSSI_{dry\ slope}$ > 5 [-]
- $RSSI_{t=i}$ – $RSSI_{t=i+5}$ > 16 [-]

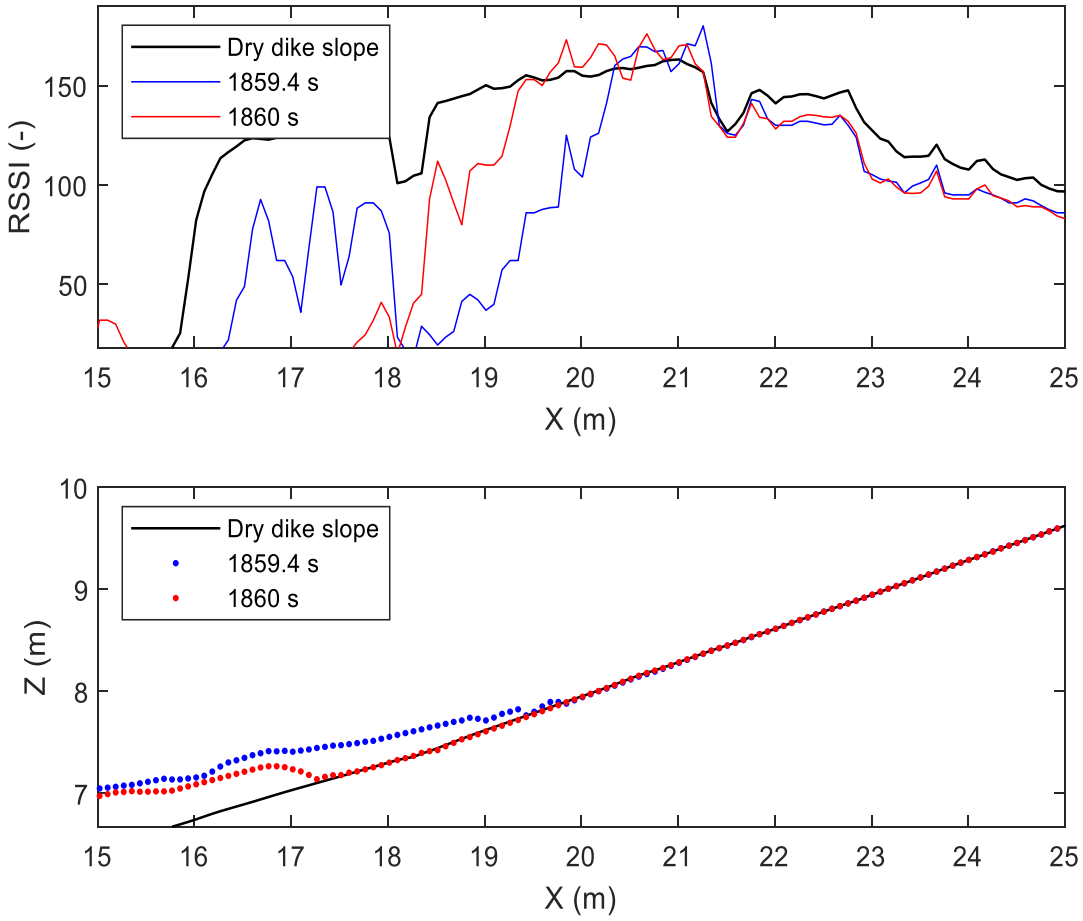

Figure 22 Wave run-up and RSSI values of two different time instances for test T012

3. Synchronization

The laser is synchronised with the rest of the measurement devices by a pulse received from the measurement system. The wave board is activated one minute after the pulse is given and the measurement of the test starts two minutes after activation of the wave board, so that the wave pattern has fully evolved. The pulse can be found back in the data file, which indicates the start time of the measurement, see Figure 23**.** The duration and end time of each test are written down, so these are known as well.

A	B	C	D	E	F	G	H	I	J	K	L
ms since start	Recording time	LMS5xx	LMS5	LMS5xx_F	LMS5xx_F	LMS5xx_F	LMS5xx_F	LMS5xx_F	LMS5xx_F	LMS5xx_Fie	LMS5xx_F
267774	2018-06-27 11:33:11.470 CEST(+0200)	0	1	13020104	0x0000	10911	11253	3,4E+09	3,4E+09	0x0000	0x3f00
267805	2018-06-27 11:33:11.501 CEST(+0200)	0	1	13020104	0x0000	10913	11255	3,4E+09	3,4E+09	0x0000	0x3f00
267837	2018-06-27 11:33:11.533 CEST(+0200)	0	1	13020104	0x0000	10914	11256	3,4E+09	3,4E+09	0x0000	0x3f00
267868	2018-06-27 11:33:11.564 CEST(+0200)	0	1	13020104	0x0000	10916	11258	3,4E+09	3,4E+09	0x0800	0x3f00
267899	2018-06-27 11:33:11.595 CEST(+0200)	0	1	13020104	0x0000	10917	11259	3,4E+09	3,4E+09	0x0800	0x3f00
267930	2018-06-27 11:33:11.626 CEST(+0200)	0	1	13020104	0x0000	10919	11261	3,4E+09	3,4E+09	0x0800	0x3f00
267961	2018-06-27 11:33:11.657 CEST(+0200)	0	1	13020104	0x0000	10920	11262	3,4E+09	3,4E+09	0x0800	0x3f00
267993	2018-06-27 11:33:11.689 CEST(+0200)	0	1	13020104	0x0000	10922	11264	3,4E+09	3,4E+09	0x0800	0x3f00
268024	2018-06-27 11:33:11.720 CEST(+0200)	0	1	13020104	0x0000	10923	11265	3,4E+09	3,4E+09	0x0800	0x3f00
268055	2018-06-27 11:33:11.751 CEST(+0200)	0	1	13020104	0x0000	10925	11267	3,4E+09	3,4E+09	0x0800	0x3f00
268086	2018-06-27 11:33:11.782 CEST(+0200)	0	1	13020104	0x0000	10927	11269	3,4E+09	3,4E+09	0x0800	0x3f00

Pulse

T_{start}

Figure 23 Pulse in the CSV file obtained by the laser scanner

4. Filtering noise from data

After determining the run-up heights using both methods, noise is observed in the data (see Figure 24 and 25). The noise indicates measured layer thicknesses larger than 1 cm at locations where no water has reached. These large layer thicknesses are likely to be attributed to small displacements of the laser scanner. Apparently, the irregularities occur especially at the kink of the dike and the transition between concrete and the wooden slope. The already present small height difference of the transitions, together with the small displacement of the laser scanner result in layer thicknesses larger than 1 cm.

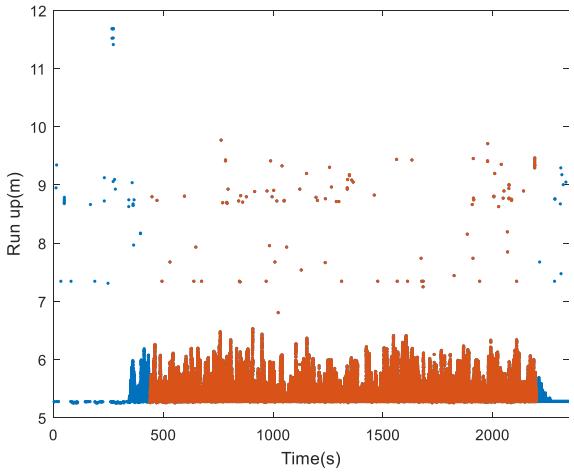

Figure 24 The wave run-up height for T007 with noise

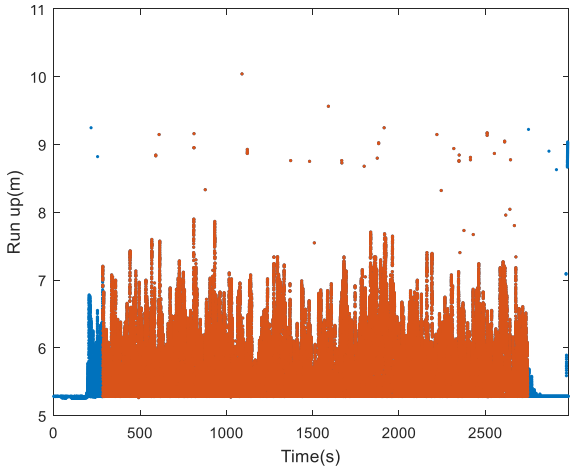

Figure 25 The wave run-up height for T008 with noise

An instantaneous change in wave run-up of 0.5 m in a time interval of 31 ms is unrealistic and is caused by noise in the data. The noise is eliminated from the run-up data using the following filter:

$$R_{u\,t=i} - R_{u\,t=i+1} > 0.5\ m.$$

After filtering the data, the peaks are obtained. A Peak Over Threshold analysis is used to determine the probability of exceedance distribution of the wave run-up. In obtaining the peaks, a minimum peak distance and a minimum peak prominence are specified. The minimum peak distance is specified as the spectral wave period, and the peak prominence is chosen so that both low and high peaks are identified counting each run-up only once. As the number of incoming waves are known the number of calculated peaks can be estimated beforehand. From the visual observations is noted that the observed run-ups are on average 86% of the incoming waves. In Figure 26 an overview is given of the steps taken to obtain the wave run-up distributions.

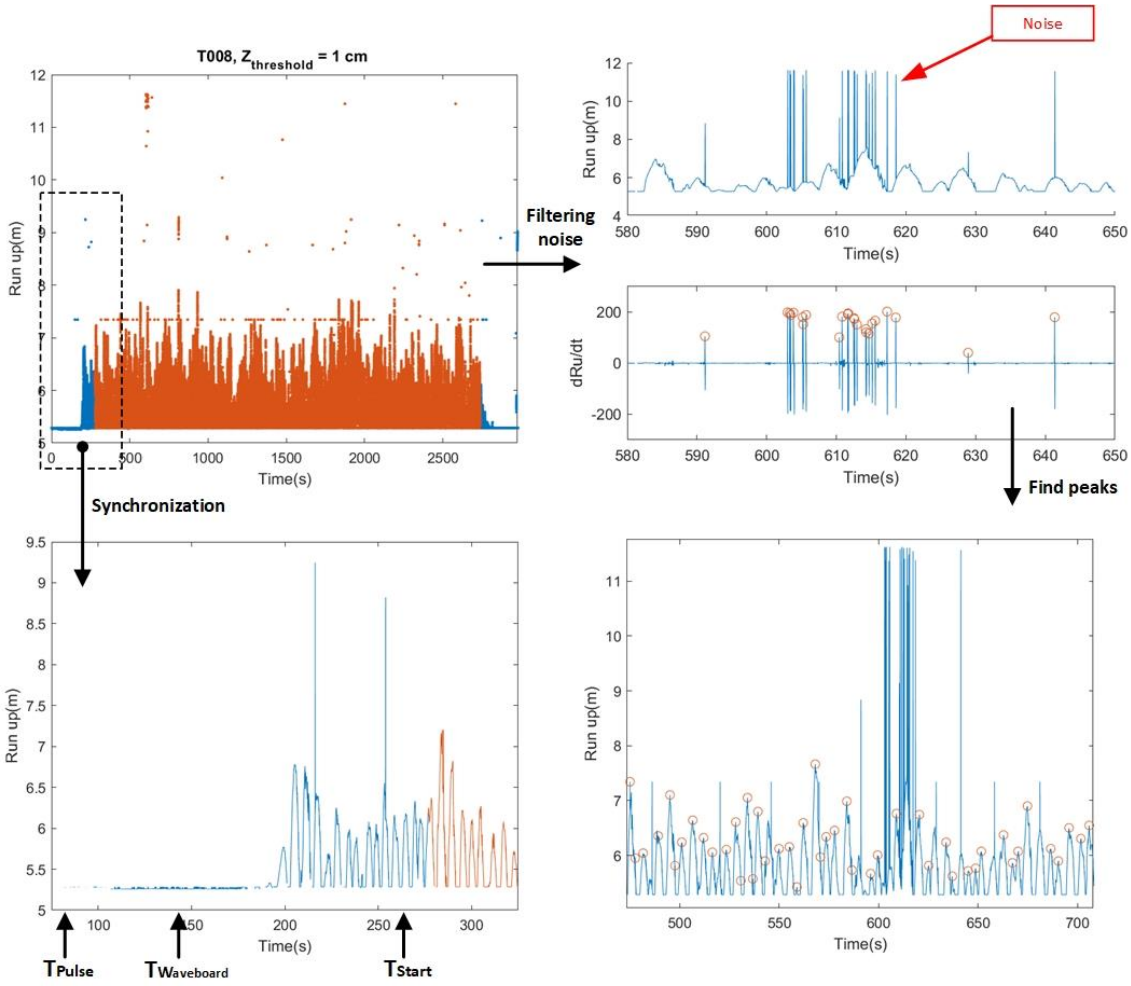

Figure 26 Filtering, synchronization and finding the peaks of the wave run-up height

4.1.3 Determining virtual overtopping

The wave overtopping discharge is the volume of water that flows over the crest of the dike in a certain time. This section explains how the overtopping volumes and discharges are determined from the laser scanner. With this laser method, there was no overtopping tank or a tank build in the dike slope to measure any real volumes. For each arbitrary virtual crest elevation, the virtual overtopping volume can be determined. The volumes are obtained by integrating the area between the dry slope and the water surface above a certain virtual crest level. This area is indicated in Figure 27. Calculating this area for each individual time instance results in a time signal of the volumes. In Figure 28 the obtained overtopping volumes in time are plotted for test T033, with a crest height of 0.41 m. Water layer thicknesses smaller than 0.5 cm are close to the error margin of the laser and are therefore neglected in the determination of the volumes.

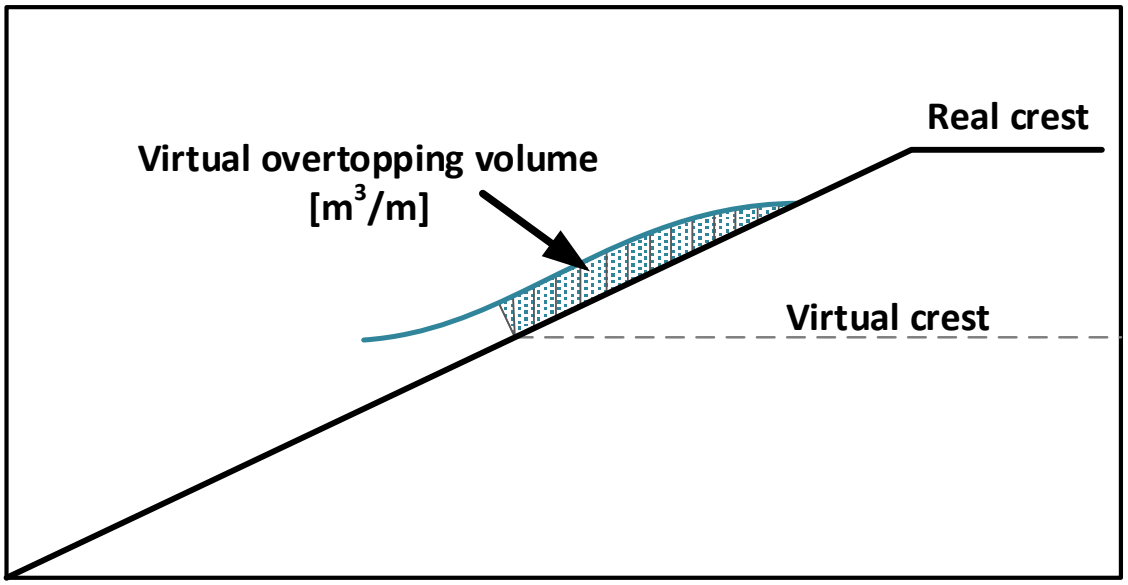

Figure 27 Schematization of the determination of the virtual overtopping volumes by laser scanner

From the time signal, the virtual overtopping volumes for each individual wave run-up can be determined taking the maximum volume during each wave cycle, which is represented by the peaks in Figure 29. Here the hypothesis is made that the volume overtopping a certain crest level during one individual wave run-up, equals the maximum calculated area exceeding this virtual crest level. The virtual mean overtopping discharge for each test can be calculated summing up all the individual overtopping volumes above a certain virtual crest height, using Formula 4.1.

$$q = \frac{\sum V_i}{D} \tag{4.1}$$

Where V_i is the virtual overtopping volume for a single event and D the duration of the test. It must be noted that no real overtopping has occurred, except for test: 22, 30, 37, 38, 41 and 42. In the aforementioned tests less than 2% of the waves overtopped the real crest of the dike. This means that the same volume of water that runs-up the slope also runs down, for the majority of the tests.

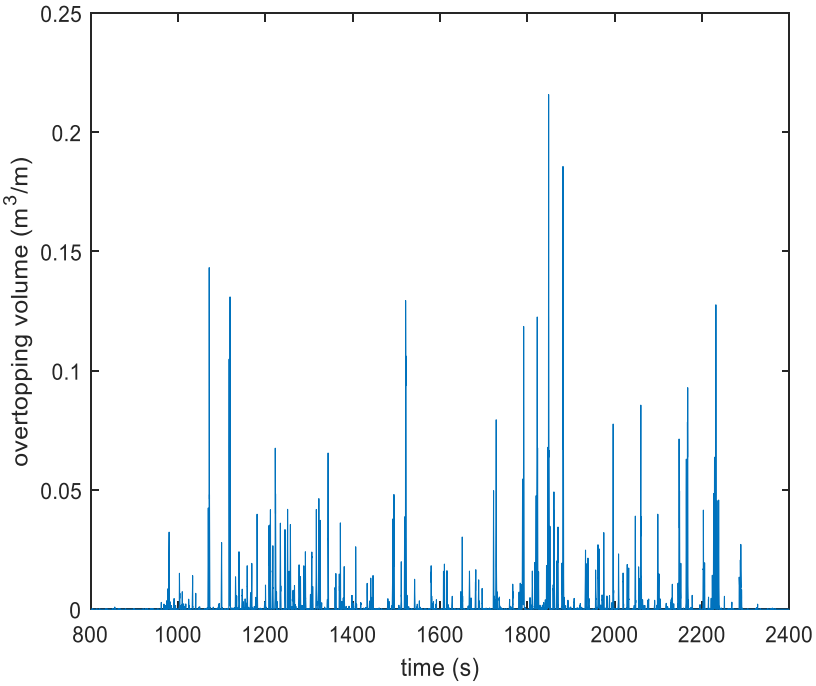

Figure 28 Determined virtual overtopping volumes for test T033, with R_c = 0.4139 m and wave conditions in front of the dike: h = 3.0, H_{m0} = 0.40 , $T_{m-1.0}$ = 2.71

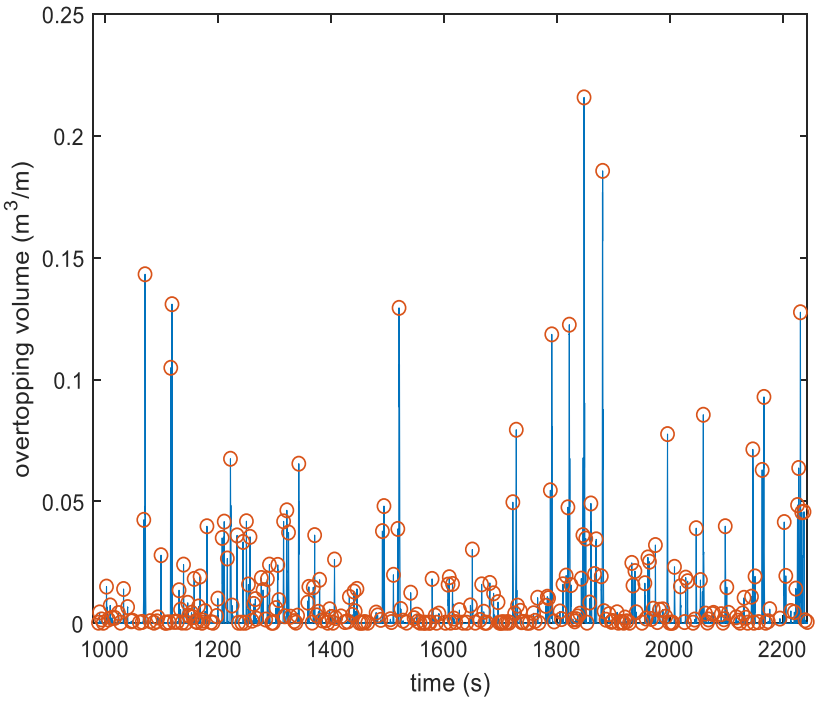

Figure 29 The determined Peaks of the individual overtopping volumes for test T033, with R_c = 0.4139 m and wave conditions in front of the dike: h = 3.0, H_{m0} = 0.40, $T_{m-1.0}$ = 2.71

4.2 Video camera

The camera is used to determine the wave run-up along the full width of the flume, while the laser scanner only measures along one transect of the slope. The camera was synchronised with the other measuring equipment using a red LED light (see Figure 30). The LED lights up when a synchronization pulse is received from the measuring system. This is the same pulse sent at the same time to all other measuring devices. As the start- and end time of the tests are known, the results can be compared with the other measuring methods.

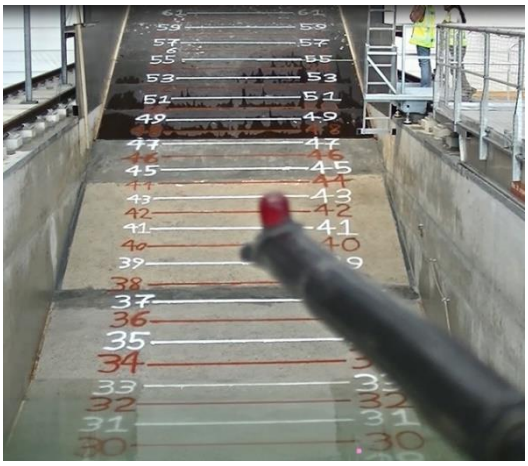

Figure 30 Synchronization LED light (Çete, 2018)

To obtain the wave run-up from the camera measurements, a Machine Learning algorithm created by Deltares is used (J. den Bieman, personal communication, February 19, 2019). The algorithm contains a Convolutional Neural Network (CNN) with a SegNet architecture, which was initially designed for pixel-wise segmentation of road and indoor scene (Badrinarayanan et al., 2016). In this research, image segmentation is used to distinguish the two different classes: wave run-up and dry dike slope. Figure 31 shows a schematization of the steps taken to obtain the run-up heights from camera footage. The CNN is made out of a series of convolutional layers for encoding and decoding, followed by a pixel-wise classification layer. In each convolutional layer, matrix multiplications are executed by different matrices moving over the input images. This results in smaller and more detailed matrices highlighting the important lines (e.g. vertical and horizontal). After applying the different convolutions, the small detailed matrices with main features are transformed back to the original image. This transformation also consists of numerous steps and layers.

First the obtained video footages are divided into a large number of time stacks, corresponding to one-pixel row in time, which will be the input for the CNN. The time stacks are RGB images represented by a 250x1080x3 array of pixels formed by the three-color components: red, blue and green. Before using the algorithm, the CNN must be trained. Approximately 80 time stacks on which the transition of water and dry slope are marked by hand are used to train the network. The CNN recognizes the marked features, finds the importance of each filter to detect these features and assigns a weighing factor to each filter. After training, a trial with around 20 time stacks will be executed to see if the program functions. If the outcome shows large deviations, the program needs to be tuned until it shows valuable outcomes.

Subsequently, time stacks of the full test are inserted into the CNN. The outcome contains marked time stacks, which can be combined back to a video. The video shows markers distributed over the width of the flume, following the water surface in time. The markers move in vertical pixel direction of the video image and not in vertical direction along the slope. Hence, re-interpolation along the width of the flume is applied. The camera captures the slope with a certain perspective, where the footage of the flume becomes narrower as the distance from the slope to the camera increases. This perspective is

eliminated in the analysis by specifying a line of 2.5 m at both the upper and lower part in the video image. The pixel coordinates are converted back to real y- and z-coordinates using the known positions of the lines on the slope. This gives the run-up height over the width of the flume for each time instance. Finally, the probability of exceedance distribution of the run-up height can be determined by using a Peak Over Threshold analysis.

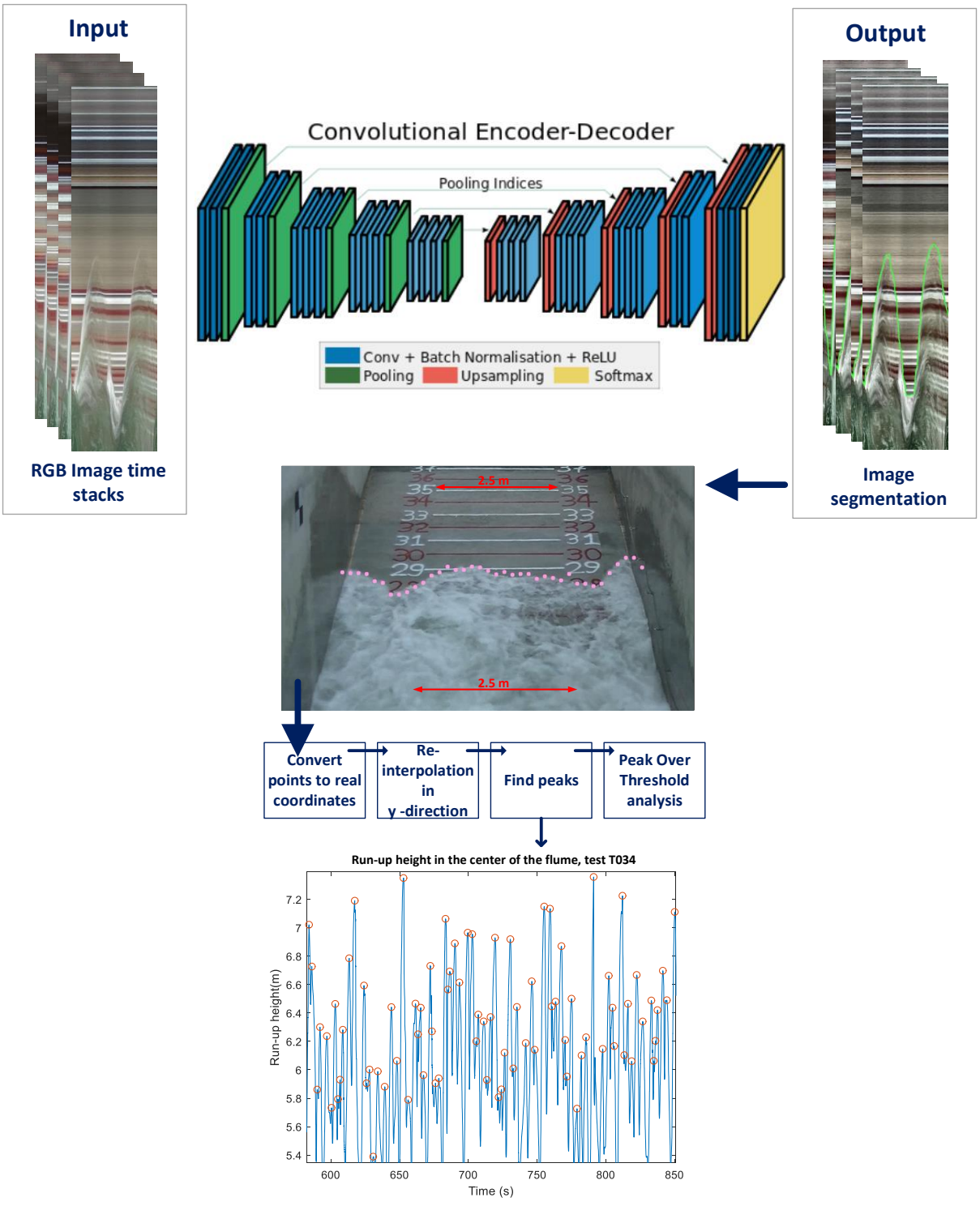

Figure 31 Schematization of the processing of the camera measurements by the Machine Learning algorithm (Badrinarayanan et al., 2016). Input are RGB time stacks with as output segmented images with the detected water surface.

5. Results

In this chapter, the results based on the analysis of the visual-, camera- and laser measurements, are presented. The tests with water levels of 0.6 and 0.7 m (test T001 until T004, T031, T032, T039 and T040) are not analysed in this report, because they gave a small number of run-up levels and the measured run-up is close to the error margin of the used measurement equipment. In Chapter 6, the obtained results and findings will be discussed.

5.1 Visual determination of run-up exceedance levels

Before presenting the results, based on the analysis of the visual determination of the run-up distribution, the reliability of the method is shown. Two sets of reference tests (T037-T041 and T038-T042) have been executed with each having the same incoming wave conditions (same steering file). These extra tests were used to check the influence of the protection nets on the wave gauges (see Figure 32).

Figure 32 Protection nets in the flume (Deltares, 2018)

The results of the four tests are presented in Figure 33, which shows that the two run-up height distributions fall in the same 8% interval. This means that the same wave run-up is measured for the same hydraulic conditions. From which can be concluded, that the method of determining the run-up distribution by visual observation, produces reliable data. This also indicates that the nets do not affect the run-up height, since the dimensions of the nets are very small with respect to the wave height and wave period.

As expected, it is shown in Figure 34 that the run-up height is linearly dependent on the wave height. It is also observed that a longer period or a higher wave height results in a higher wave run-up.

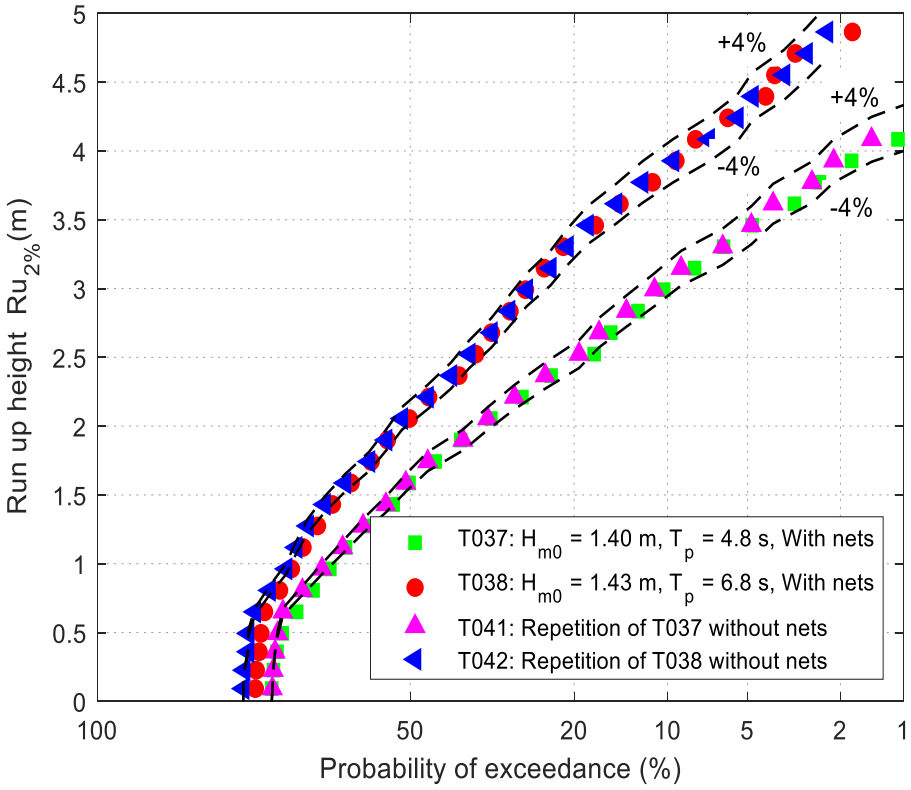

Figure 33 Reliability of the visual measurements by comparing tests with and without nets with the same incoming wave conditions at the wave board (same steering file).

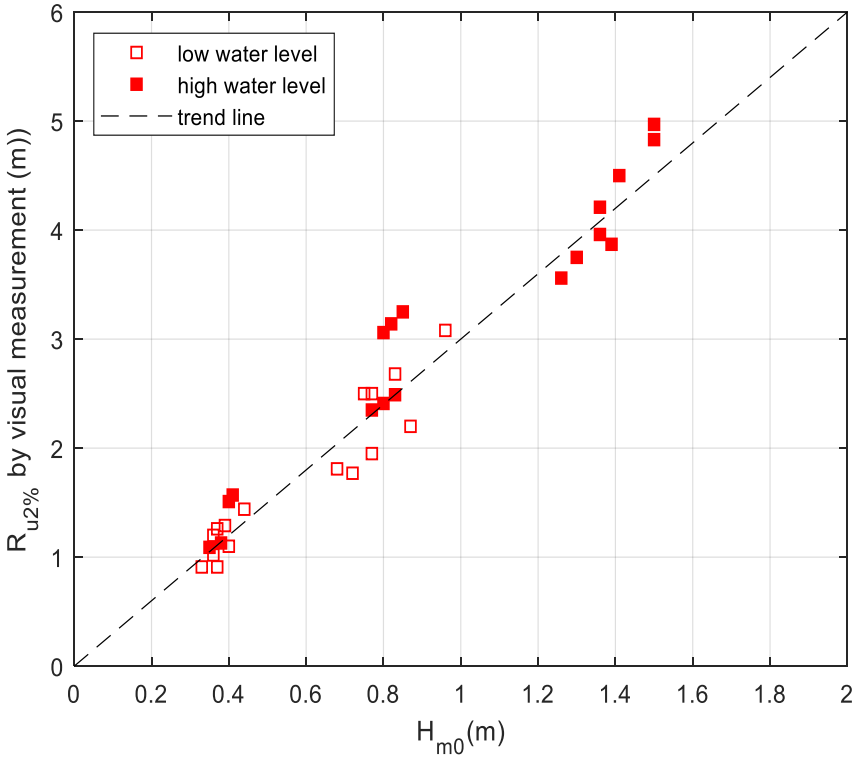

Figure 34 The visual measured run-up with respect to the wave height measured in front of the dike

In Figure 35, the effect of the water depth on the wave run-up is shown (more graphs can be found in Appendix K). The wave run-up that occurs at mid water level seems to be lower than the wave run-up at high water, under the same wave conditions. For the different willow configurations, the following reductions with respect to high water level are found: willows with leaves between 17 and 26%, willows without leaves between 18 and 22% and willows with 50% density around 20%.

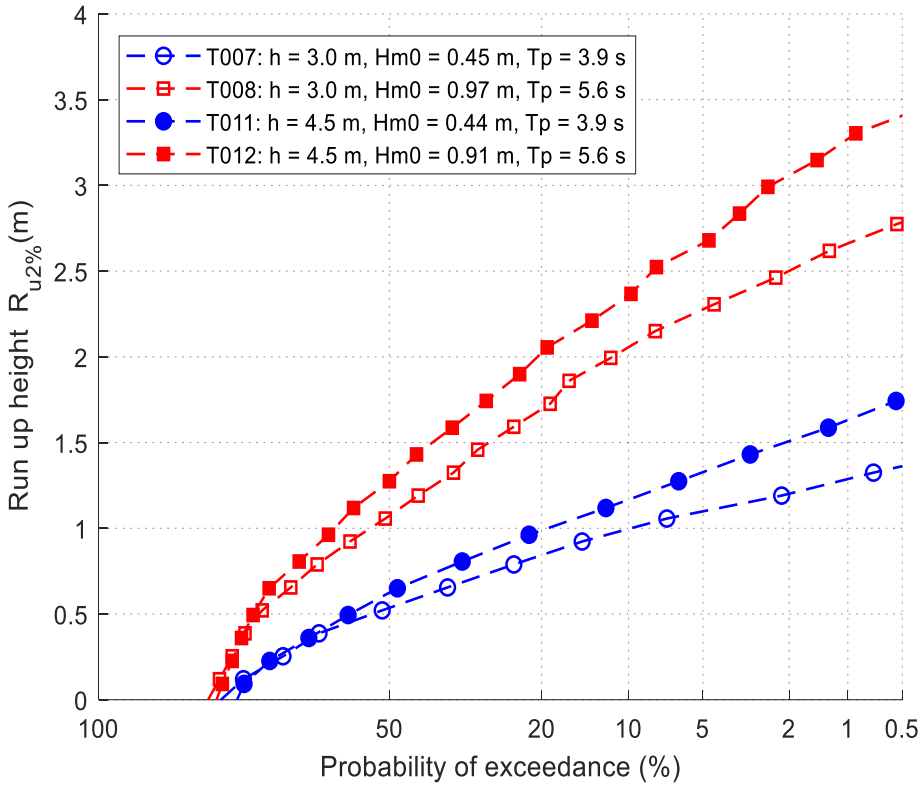

Figure 35 Comparison run-up height for different tests. The given wave conditions are incoming conditions at the wave board and all tests containing willows with leaves

In Figure 36 the probability of exceedance distributions for tests with the same incoming wave conditions are shown, referring to Appendix K for the distributions of the other tests. The results of the tests are compared to the empirical TAW (2002). For these tests the influence factors all reduce to 1: no berm (γ_b = 1), perpendicular wave attack (γ_β = 1), no vertical wall on top of the dike (γ_v = 1) and the slope of the dike can be considered as smooth and impermeable (γ_f = 1). The distributions are close to or well within the 90% confidence band of the TAW (2002), except for comparison 8 (T011 and T019) and comparison 9 (T012, T020 and T028) which are totally outside this error band.

Comparing the tests with willows to the reference tests without willows, for the same wave conditions, makes it possible to determine the effect of willows on the wave run-up. The effect of the foreshore is present in both run-up heights and is therefore eliminated (see Figure 37). The effect of the foreshore is calculated by comparing the wave height at WHM1-3 with RADAC 1. This resulted in a maximum damping of 4.4% and maximum shoaling of 9.5%. For the different tests, the run-up height which is exceeded by two percent of the incoming waves and the corresponding reduction in wave run-up, is given in Table 5. The given percentages are with respect to the reference case, where there are no willows present.

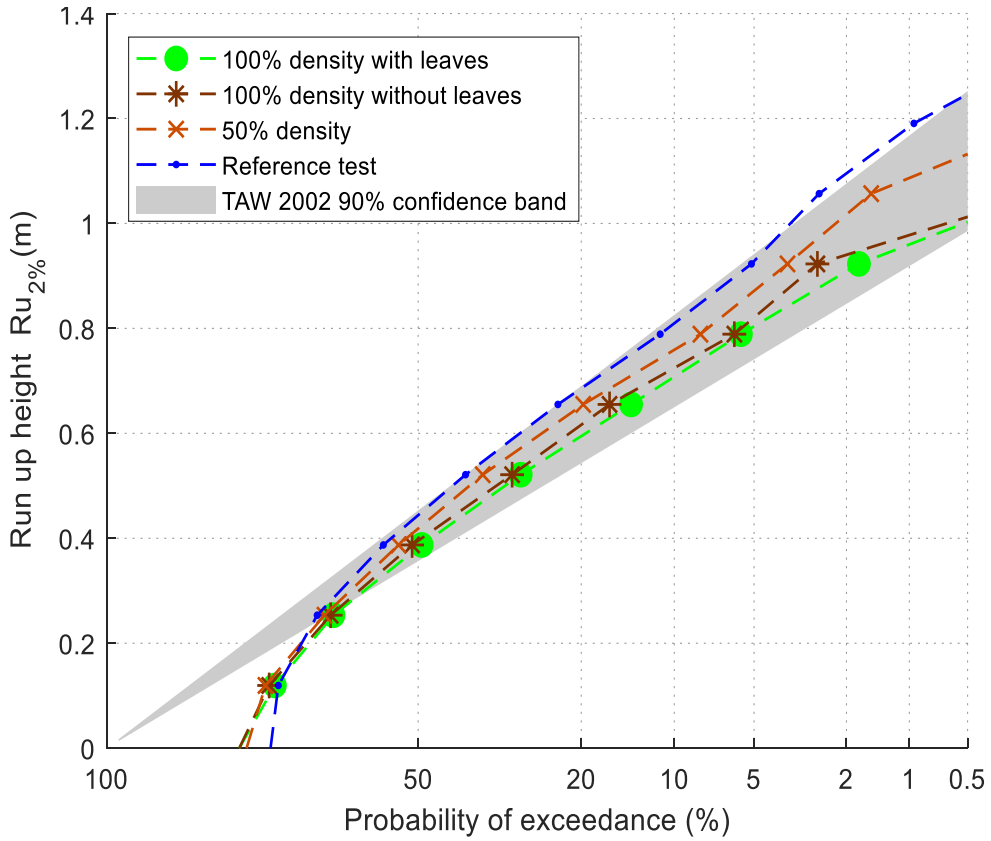

Figure 36 Probability of exceedance distribution for comparison test 1: T005 - T013 - T023 - T033, having the same incoming wave conditions at the wave board: h = 3.0 m, H_{m0} = 0.48 m, $T_{m-1,0}$ = 2.75 s

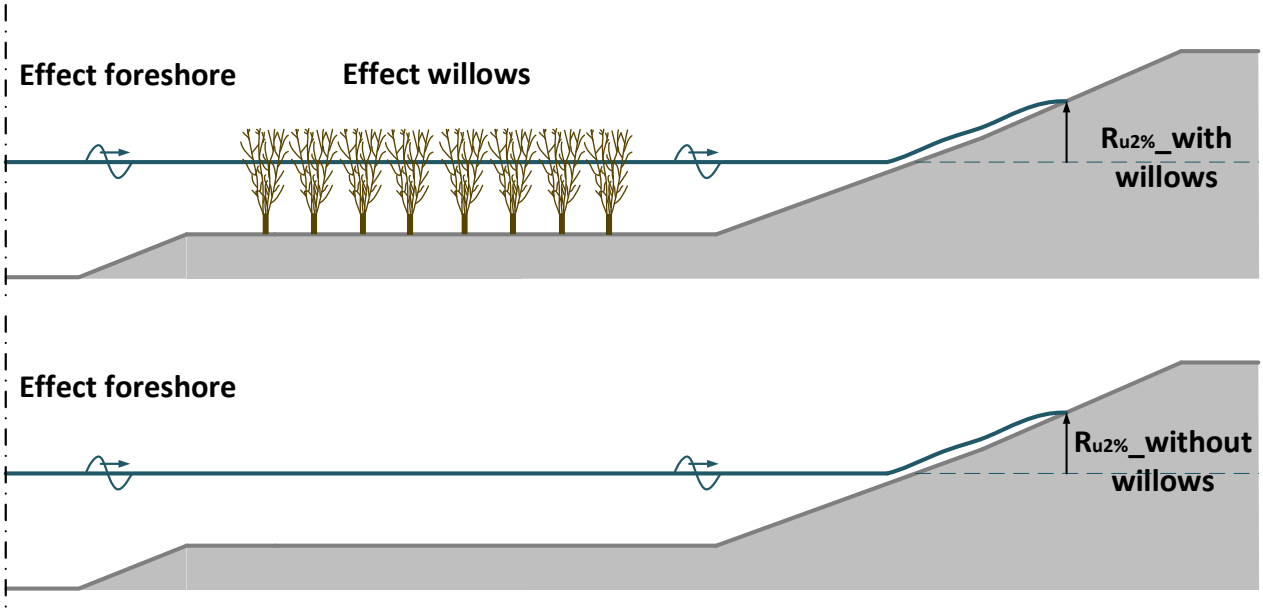

Figure 37 Schematization of the method used to calculate the reduction in run-up height caused by the willow forest (not to scale).

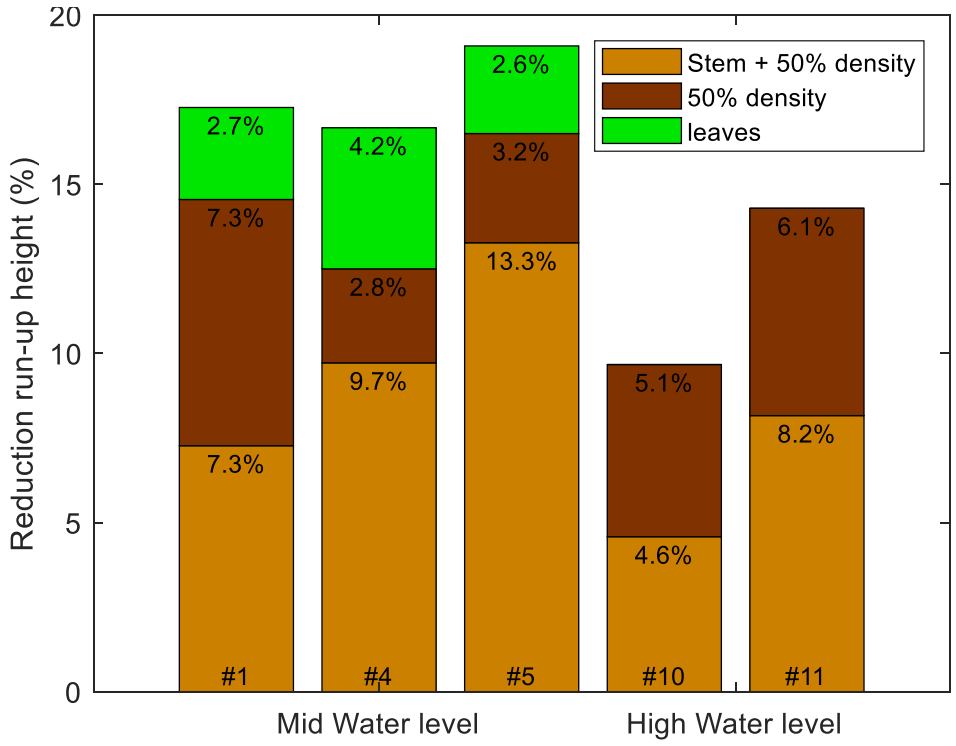

Figure 38 Contribution of the different willow configurations to the wave run-up, numbers giving the reduction in run-up height with respect to the reference test. The reduction is determined by comparing the tests with and without willows.

Table 5 The 2% exceeded run-up height determined by visual measurements for tests with the same steering file and different configurations (with/without willows) are given. The reductions are with respect to the reference case without willows. The given wave conditions are measured at the wave board.

	Wave conditions				Willows with leaves			Willows without leaves		
Comparison #	**h (m)**	**H_{m0} (m)**	**$T_{m-1.0}$ (s)**	***s_{op} (-)***	**Test-ID**	**$R_{u2\%}$ (m)**	**Reduction (%)**	**Test-ID**	**$R_{u2\%}$ (m)**	**Reduction (%)**
#1	3.0	0.44	2.6	0.04	T005	0.91	17.3	T013	0.94	14.6
#2	3.0	0.97	3.9	0.04	T006	1.81	17.7			
#4	3.0	0.45	3.9	0.02	T007	1.20	16.7	T015	1.26	12.5
#5	3.0	0.97	5.6	0.02	T008	2.50	19.1	T016	2.58	16.5
#10	4.5	1.40	4.8	0.04				T021	3.55	9.7
#11	4.5	1.41	6.8	0.02				T022	4.2	14.3
	Wave conditions				**Willows 50% density**			**No willows (reference test)**		
Comparison #	**h (m)**	**H_{m0} (m)**	**$T_{m-1.0}$ (s)**	***s_{op} (-)***	**Test-ID**	**$R_{u2\%}$ (m)**	**Reduction (%)**	**Test- ID**	**$R_{u2\%}$ (m)**	
#1	3.0	0.44	2.6	0.04	T023	1.02	7.3	T033	1.10	
#2	3.0	0.97	3.9	0.04				T034	2.20	
#4	3.0	0.45	3.9	0.02	T025	1.30	9.7	T035	1.44	
#5	3.0	0.97	5.6	0.02	T026	2.68	13.3	T036	3.09	
#10	4.5	1.40	4.8	0.04	T029	3.75	4.6	T037	3.93	
#11	4.5	1.41	6.8	0.02	T030	4.50	8.2	T038	4.90	

In Figure 38, the contribution of the different parts of the willows to the reduction in run-up height, are shown in a bar plot, for both mid and high-water level. The results show an effect of the leaves of around 3-4 %. It can clearly be seen that the 50% willow density contributes to around 3-7%, to the total reduction in run-up height. It is remarkable that the contribution of the 50% density is in the same order as the contribution of the still left branches and stem, for three of the fife test cases. For two of the given wave conditions, there is almost a factor 4 between the contribution of the 50% density and the rest of the willow branches and stems. From the results, it can also be indicated that for most tests, a longer period or a higher wave height result in a larger reduction in run-up.

It is also observed, that reducing the canopy density gave a larger difference in run-up height reduction, compared to removal of only the leaves. Reducing the canopy density with 50%, gave a run-up which is around 3 to 9% higher with respect to full canopy density. Removal of the leaves from the willows, resulted in a 2 to 7% higher run- up relative to willows with leaves.

In Table 6 the reductions for the different willow configurations are summarized. At first sight, it is apparent that the strongest wave damping of approximately 19% is reached at mid water level. Here the water depth is at around halve the canopy height with incoming wave conditions: H_{m0} = 0.96 m and $T_{m-1,0}$ = 5.6 s. At this level, the surface area is the largest and decreases as the canopy height increases. In Appendix C, the surface area distribution of an average tree is shown. From the results it cannot be concluded, whether s = 0.04 or s = 0.05 gave the highest reduction in wave run-up.

Table 6 Reduction in Ru2% of the different water levels and configurations with respect to the reference test

	With leaves	Without leaves	Reduced canopy density
Low water level	12-18%		
Mid water level	17-19%	13-17 %	7-13%
High water level		10-14%	5-8%

From the measured run-up heights, a range for an influence factor can be derived, where the influence factor is defined as follows:

$$\gamma_{willow} = \frac{Ru_{2\%;\,willows}}{Ru_{2\%;\,reference}}$$

This results in the following:

- Mid water level with leaves: $\gamma_{willow} \approx 0.81 - 0.83$
- Mid water level without leaves: $\gamma_{willow} \approx 0.81 - 0.88$
- High water level with leaves: $\gamma_{willow} \approx 0.85 - 0.90$

To compare the determined wave run-up with the empirical TAW (2002) formula, the focus is placed on the part behind the willow forest, shown in Figure 39. The wave conditions in front of the dike and the corresponding run-up height are taken.

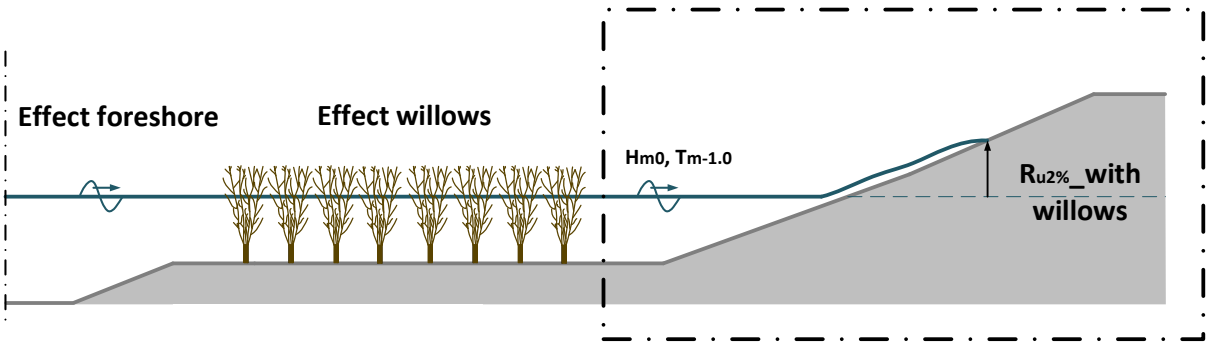

Figure 39 Focus area for comparing the run-up determined by visual measurement with the empirical TAW (2002).

In Figure 40**,** the visual measurements are shown together with the TAW (2002) formula, from which can be observed that almost 50% of the measurements are outside the 90% error band of the TAW. It is noticed that a majority of these points are found around the 5% upper limit of the TAW. However, it is also remarkable to see that a group of five data points have a large deviation to the TAW. Further analysis shows that these data points belong to two sets of tests (T012, T020, T028 and T011, T019). These test sets each have the same wave conditions containing high water levels and a wave steepness smaller than 0.02. In Figure 41 the relative error to the TAW is plotted against the wave steepness. Here it can clearly be seen that these set of tests are the only ones having a wave steepness lower than 0.02, at high water level. The rest of the tests at high water level, all have an error to the TAW between the 0 – 14%, while the outlying tests have an error of around 28%. Also, for the lower water level, the error is valued between the 0-14% regardless of the wave steepness of the test.

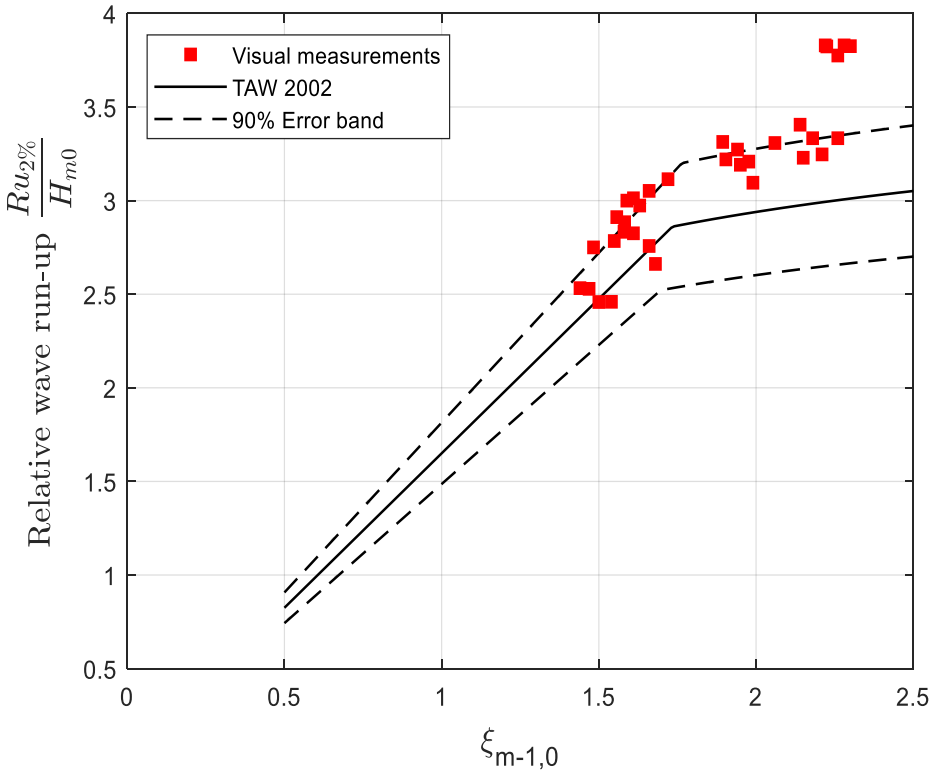

Figure 40 Plot of the visual measured run-up compared to the TAW (2002), with wave conditions in front of the dike

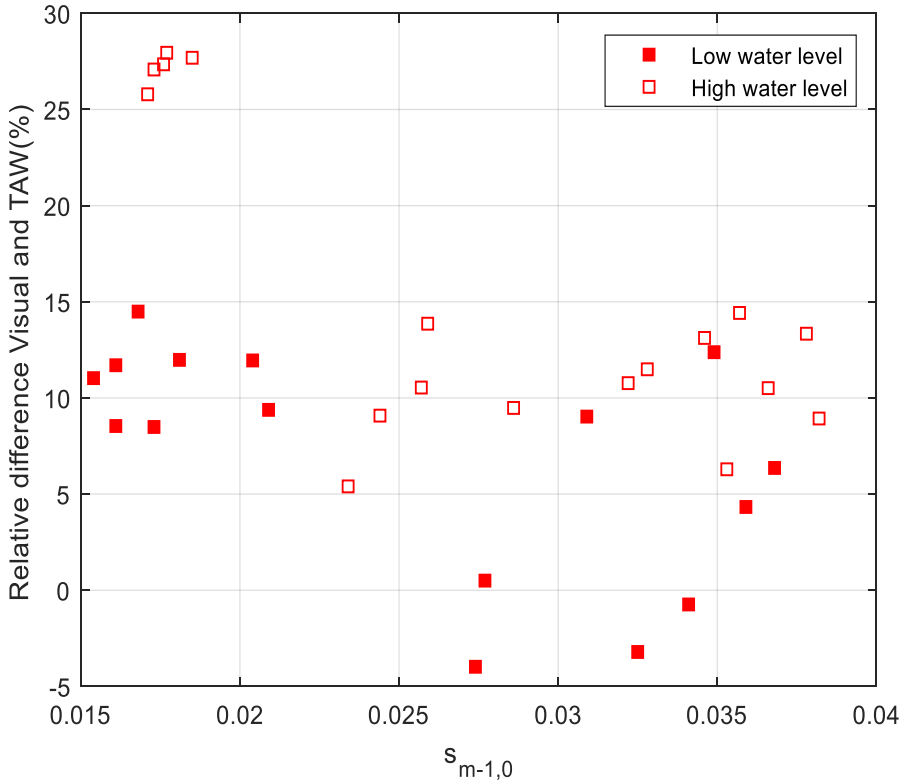

Figure 41 The relative difference of the visual measurements with respect to the TAW formula (2002) plotted against the wave steepness determined in front of the dike.

During the tests not only the run-up exceedance levels, but also the highest line at which the flotsam has reached on the dike have been listed (see Appendix L for more details). It is remarkable how well the highest observed run-up and the observed flotsam lines correspond. Only 25% of the flotsam is found to be around 0.3 m lower than the maximum reached water level. However, it is clearly seen that the highest wave run-up by a single wave, is not sufficient to take debris along the slope. The debris needs force from more than one wave run-up to take the debris to the highest levels.

5.2 Video camera

The data obtained from the video camera have been processed using a Machine Learning algorithm created by Deltares. This is the first time this processing technique is applied to determine the wave run-up on a dike. Different tests with and without willows are analysed. However, in this section the focus is only on the area behind the forest (see Figure 39), with the incoming wave conditions determined in front of the dike. The following tests will be analysed: T007 - T012, T023, T034, T036, T037 and T042. The run-up is evaluated for different locations along the flume. To compare the camera measurements with the other measuring methods, the R_{u2}% is taken as the average run-up height over the 2.5 m in the centre of the flume. The determined run-up heights are given in Table 7. Figure 42 illustrates the run-up results obtained by camera measurements, plotted against the surf similarity parameter. The results are compared to the empirical TAW (2002) formula and the visually determined run-up heights. The results from the camera are very close to the results of the visual measurements with a maximum deviation of around 9.8%. Here it is also seen that the data points are more located at the outer edge of the 90% error band of the TAW.

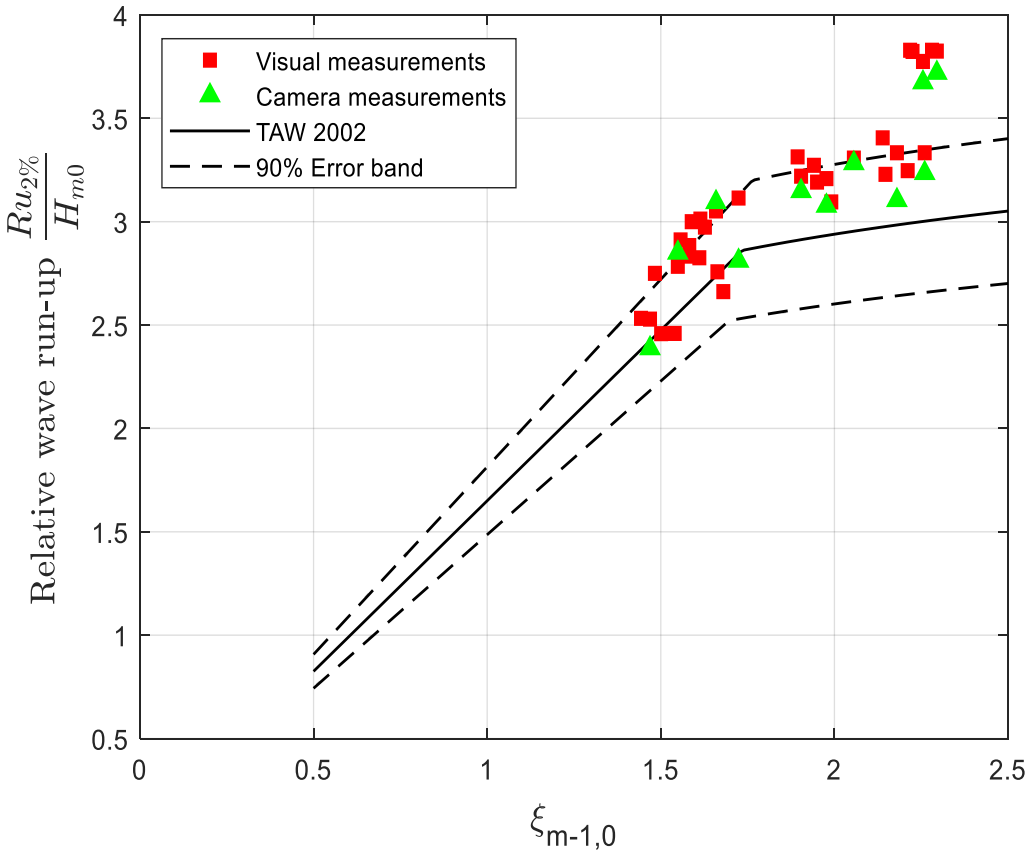

Figure 42 The relative run-up height of the camera measurements, laser measurements (RSSI) and the TAW formula (2002), with the wave conditions taken in front of the dike.

Figure 43 and Figure 44 both give a time plot and probability of exceedance curves of the run-up, at three different locations on the dike slope (for other tests see Appendix M). It is interesting to see that not only the run-up signals, but also the probability of exceedance distributions deviate for different positions in the flume.

Many measuring techniques (e.g. Laser scanner) only measure the run-up along one line on the dike slope. However, a camera measures the run-up over the full width of the flume, giving new insights in the variations of the wave run-up over the width. The variation of the 2% exceeded run-up heights over the flume width are calculated and given in Table 7. Results show a significant variation of the $R_{u2\%}$ of on average 15 cm, over the 2.5 m width in the flume. For test T036 the variation in $R_{u2\%}$ is shown in Figure 45 (see Appendix M for more tests). In Figure 46 the variation over the width is plotted against the run-up height. Apparently, the results show a trend of increasing variation for higher run-up heights, with test T042 as outlying point. Another remarkable observation shows relatively higher $R_{u2\%}$ at the left part of the flume compared to the right part, for 7 out of the 10 tests that have been analysed (see Appendix M).

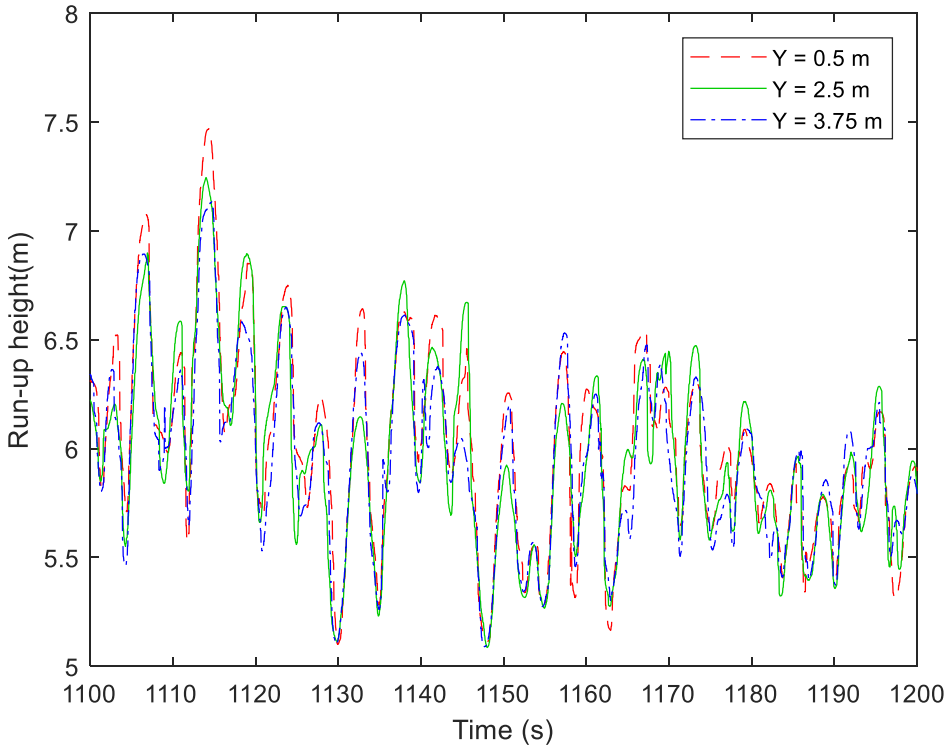

Figure 43 Wave run-up in time, at three positions on the slope of the dike, for test T008. With wave conditions in front of the dike: h =3.0 m, H_{m0} = 0.75 m, $T_{m-1.0}$ = 5.59 s

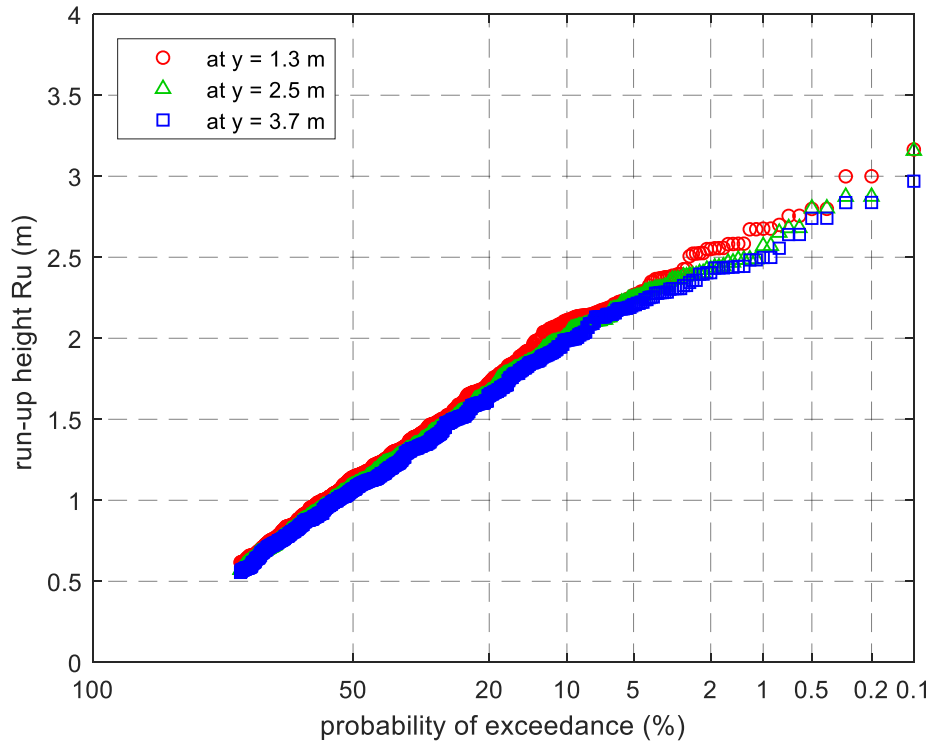

Figure 44 Probability of exceedance curves of the run-up height at three different locations on the slope, for test T008. With wave conditions in front of the dike: h =3.0 m, H_{m0} = 0.75 m, $T_{m-1.0}$ = 5.59 s

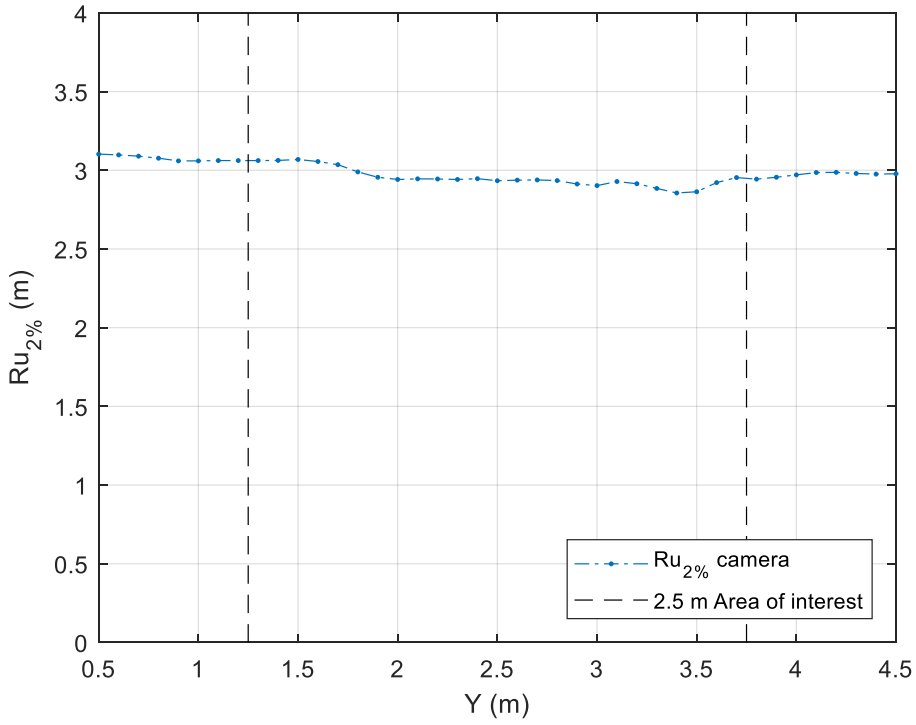

Figure 45 $R_{u2\%}$ over the flume width for test T036, with the wave conditions in front of the dike: h = 3.0 m, H_{m0} = 0.96 m, $T_{m-1.0}$ = 5.43 s

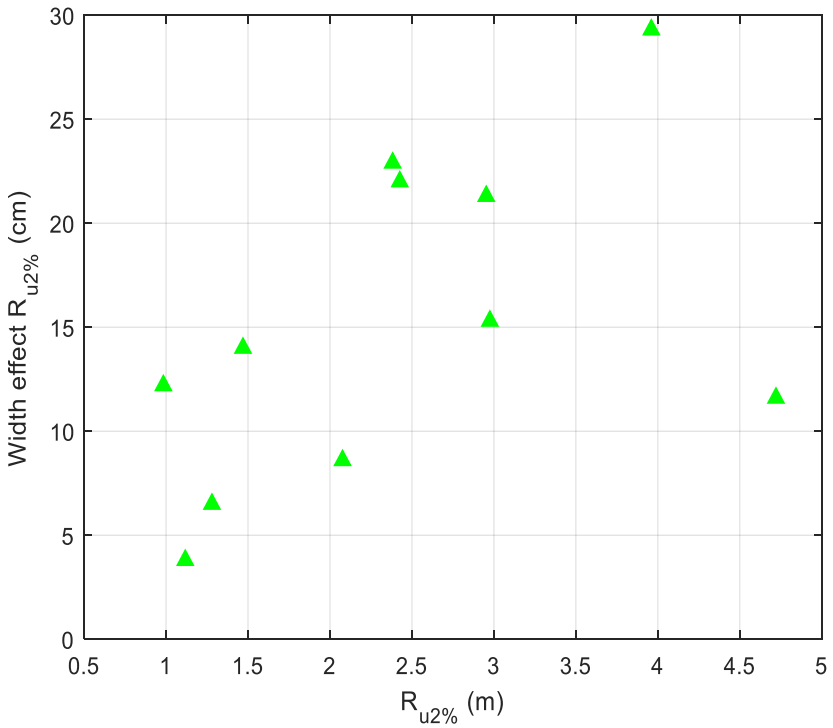

Figure 46 Variation of the wave run-up height over the 2.5 m width in the centre of the flume for different tests

Table 7 Results of the camera measurements. $R_{u2\%}$ and variation of the $R_{u2\%}$ over the width of the flume

Test - ID	h (m)	H_{m0} (m)	T_p (s)	$T_{m-1,0}$ (s)	$R_{u2\%\_camera}$ (m)	Deviation $R_{u2\%}$ over 2.5 m (m)	Deviation $R_{u2\%}$ over 4 m (m)
T007	3.00	0.36	4.18	3.79	1.12	0.04	-
T008	3.00	0.75	5.95	5.59	2.43	0.22	-
T009	4.50	0.35	2.79	2.80	0.98	0.12	-
T010	4.50	0.77	4.18	3.88	2.38	0.23	-
T011	4.50	0.40	4.18	3.87	1.47	0.14	-
T012	4.50	0.80	5.76	5.44	2.98	0.15	-
T025	3.00	0.39	4.17	3.71	1.28	0.07	-
T034	3.00	0.87	4.20	3.94	2.08	0.09	0.15
T036	3.00	0.96	5.88	5.43	2.95	0.21	0.25
T037	4.50	1.39	4.45	4.83	3.96	0.29	
T042	4.50	1.50	6.14	6.12	4.72	0.12	0.28
					Average	0.15	0.23

5.3 Laser scanner

The laser scanner measurements have been processed. The run-up heights, overtopping volumes and discharges are determined, which are given in the following sections.

5.3.1 Run-up

The run-up has been determined using two methods: based on the water layer thickness threshold and based on a threshold on the RSSI (reflection intensity) value. The obtained results from the laser scanner together with the results of the camera- and visual measurements are given in Table 8. The deviation of the results with respect to the visual measurements are also given in this table. The results are visualised in Figure 47, where the wave run-up $R_{u2\%}$ of the laser and the camera are plotted against the visual measured $R_{u2\%}$. The relative bias between the different measuring techniques and the visual measurements are shown in Figure 48. Results indicate that the laser scanner (based on RSSI) on average deviates with 3.0% and the camera measurements deviate with 3.5%, compared to the visual measurements. Comparison of the two laser methods shows that the run-up height calculated based on the RSSI threshold, gives a smaller deviation (0 - 0.2 m/ average 3%) from the visual measured run-up, than the one calculated by the layer thickness threshold (0.1 - 0.6 m/ average 14%). This is in line with the findings of earlier research (Hofland et al., 2015). From Figure 48, it is remarkable to see that the bias seems to decrease for higher wave run-up values. This can be explained by a higher resolution at the higher parts of the slope.

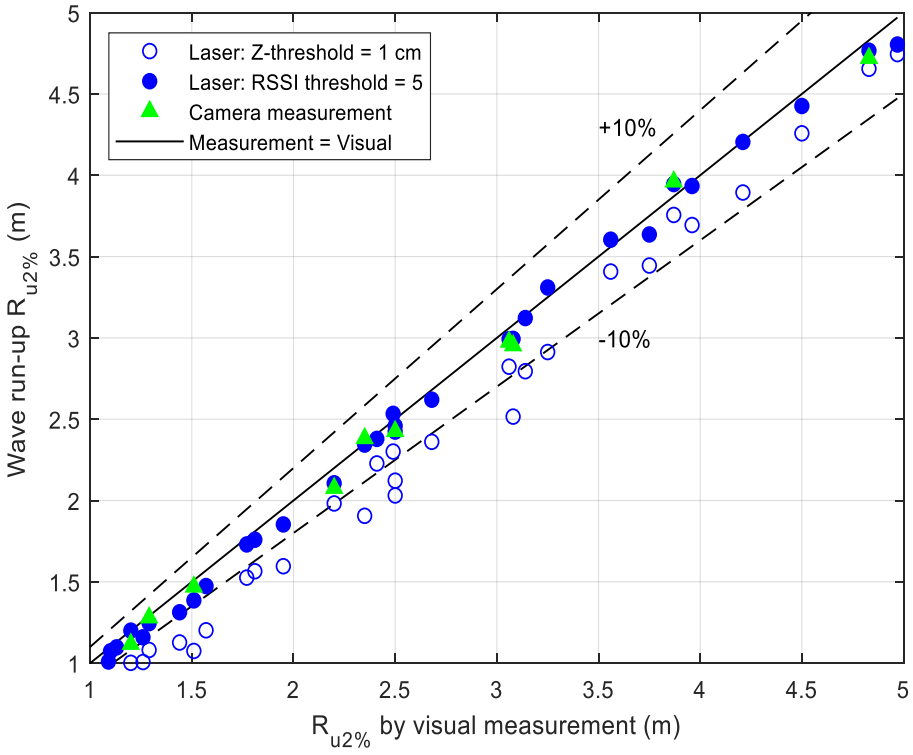

Figure 47 Wave run-up measurements with respect to the visual measurements

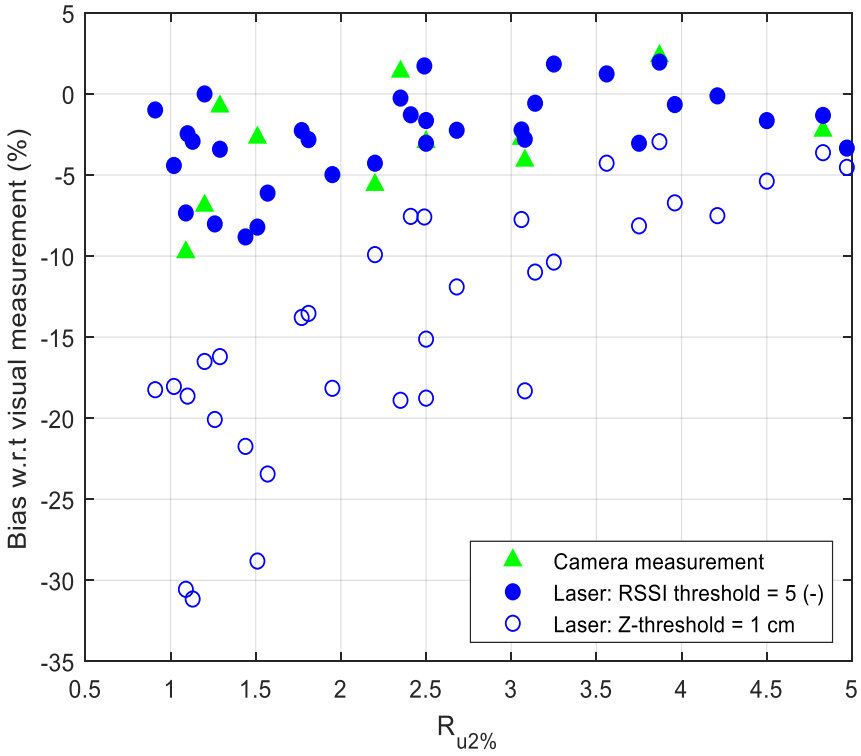

Figure 48 relative bias of the determined wave run-up with respect to the visual measurements

Table 8 Results of the run-up height with the three different measurement techniques, with deviation given w.r.t visual measurements, with incoming wave conditions at the wave board: WHM1-3

	Wave conditions			Run-up $R_{u2\%}$				Δ Deviation with visual measurement			
Test-ID	h (m)	H_{m0} (m)	T_p (s)	$R_{u2\%}$_Visual (m)	$R_{u2\%}$_Z threshold (m)	$R_{u2\%}$_RSSI threshold (m)	$R_{u2\%}$_Cam (m)	$R_{u2\%}$_RSSI vs. visual (m)	$R_{u2\%}$_RSSI vs. visual (%)	$R_{u2\%}$_Cam vs. visual (m)	$R_{u2\%}$_Cam vs. visual (%)
T005	*3.0*	*0.44*	*2.8*	*0,91*	-	-		-	-		
T006	*3.0*	*0.97*	*3.9*	*1,81*	*1.57*	*1.76*		*-0.05*	*-2.8*		
T007	*3.0*	*0.45*	*3.9*	*1,20*	*1.00*	*1.20*	*1.12*	*0.00*	*0.0*	*-0.08*	*-6.9*
T008	*3.0*	*0.97*	*5.6*	*2,50*	*2.03*	*2.42*	*2.43*	*-0.08*	*-3.0*	*-0.07*	*-3.0*
T009	*4.5*	*0.43*	*2.8*	*1,09*	*0.76*	*1.01*	*0.98*	*-0.08*	*-7.3*	*-0.11*	*-9.8*
T010	*4.5*	*0.91*	*3.9*	*2,35*	*1.91*	*2.34*	*2.38*	*-0.01*	*-0.3*	*0.03*	*1.4*
T011	*4.5*	*0.44*	*3.9*	*1,51*	*1.08*	*1.39*	*1.47*	*-0.12*	*-8.2*	*-0.04*	*-2.7*
T012	*4.5*	*0.91*	*5.6*	*3,06*	*2.82*	*2.99*	*2.98*	*-0.07*	*-2.2*	*-0.08*	*-2.8*
T013	*3.0*	*0.44*	*2.8*	*0,91*	*0.74*	*0.90*		*-0.01*	*-1.0*		
T014	*3.0*	*0.95*	*3.6*	*1,77*	*1.53*	*1.73*		*-0.04*	*-2.3*		
T015	*3.0*	*0.45*	*3.9*	*1,26*	*1.01*	*1.16*		*-0.10*	*-8.0*		
T016	*3.0*	*0.97*	*5.6*	*2,50*	*2.12*	*2.46*		*-0.04*	*-1.6*		
T017	*4.5*	*0.43*	*2.8*	*1,13*	*0.78*	*1.10*		*-0.03*	*-2.9*		
T018	*4.5*	*0.91*	*3.9*	*2,41*	*2.23*	*2.38*		*-0.03*	*-1.3*		
T019	*4.5*	*0.44*	*3.9*	*1,57*	*1.20*	*1.47*		*-0.10*	*-6.1*		
T020	*4.5*	*0.91*	*5.6*	*3,14*	*2.80*	*3.12*		*-0.02*	*-0.6*		
T021	*4.5*	*1.40*	*4.8*	*3,56*	*3.41*	*3.60*		*0.04*	*1.2*		
T022	*4.5*	*1.41*	*6.8*	*4,21*	*3.89*	*4.21*		*0.00*	*-0.1*		
T023	*3.0*	*0.43*	*2.8*	*1,02*	*0.84*	*0.98*		*-0.05*	*-4.4*		
T024	*3.0*	*0.93*	*3.6*	*1,95*	*1.60*	*1.85*		*-0.10*	*-5.0*		
T025	*3.0*	*0.43*	*3.9*	*1,29*	*1.08*	*1.25*	*1.28*	*-0.04*	*-3.4*	*-0.01*	*-0.8*
T026	*3.0*	*0.97*	*5.6*	*2,68*	*2.36*	*2.62*		*-0.06*	*-2.2*		
T027	*4.5*	*0.88*	*3.9*	*2,49*	*2.30*	*2.53*		*0.04*	*1.7*		
T028	*4.5*	*0.94*	*5.6*	*3,25*	*2.91*	*3.31*		*0.06*	*1.8*		
T029	*4.5*	*1.40*	*4.8*	*3,75*	*3.45*	*3.64*		*-0.11*	*-3.0*		
T030	*4.5*	*1.44*	*6.8*	*4,50*	*4.26*	*4.43*		*-0.07*	*-1.6*		
T033	*3.0*	*0.44*	*2.8*	*1,10*	*0.90*	*1.07*		*-0.03*	*-2.5*		
T034	*3.0*	*0.94*	*3.9*	*2,20*	*1.98*	*2.11*		*-0.09*	*-4.3*		
T035	*3.0*	*0.46*	*3.9*	*1,44*	*1.13*	*1.31*		*-0.13*	*-8.8*		
T036	*3.0*	*0.96*	*5.6*	*3,08*	*2.52*	*2.99*		*-0.09*	*-2.8*		
T037	*4.5*	*1.40*	*4.8*	*3,87*	*3.76*	*3.95*	*3.96*	*0.08*	*2.0*	*0.09*	*2.3*
T038	*4.5*	*1.43*	*6.8*	*4,97*	*4.75*	*4.80*		*-0.17*	*-3.3*		
T041	*4.5*	*1.36*	*4.8*	*3,96*	*3.69*	*3.93*		*-0.03*	*-0.7*		
T042	*4.5*	*1.37*	*6.8*	*4,83*	*4.66*	*4.77*	*4.72*	*-0.06*	*-1.3*	*-0.11*	*-2.3*
							Average |Δ|:	*0.06*	*3.0*	*0.07*	*3.5*
							Min |Δ|:	*0.00*	*0.0*	*0.01*	*0.8*
							Max |Δ|:	*0.17*	*8.8*	*0.11*	*9.8*

In Figure 49 the normalised wave run-up is plotted against the surf similarity parameter and compared with the TAW (2002). The wave run-up is normalised with the incoming wave height behind the forest, measured at RADAC 2. So far, it seems that almost one third of the measured run-ups is found to be outside the 90% error band of the TAW (2002). Here it is also seen, that there is a group of outliers with a large deviation from the TAW. However, the group of outliers only consists of three test results (T012, T020 and T028). The remaining two tests (T011 and T019) are still outside the 90% band of the TAW, however the deviation is smaller compared to the visual measured run-up. In Appendix N, data from all three measuring methods are plotted with the TAW (2002).

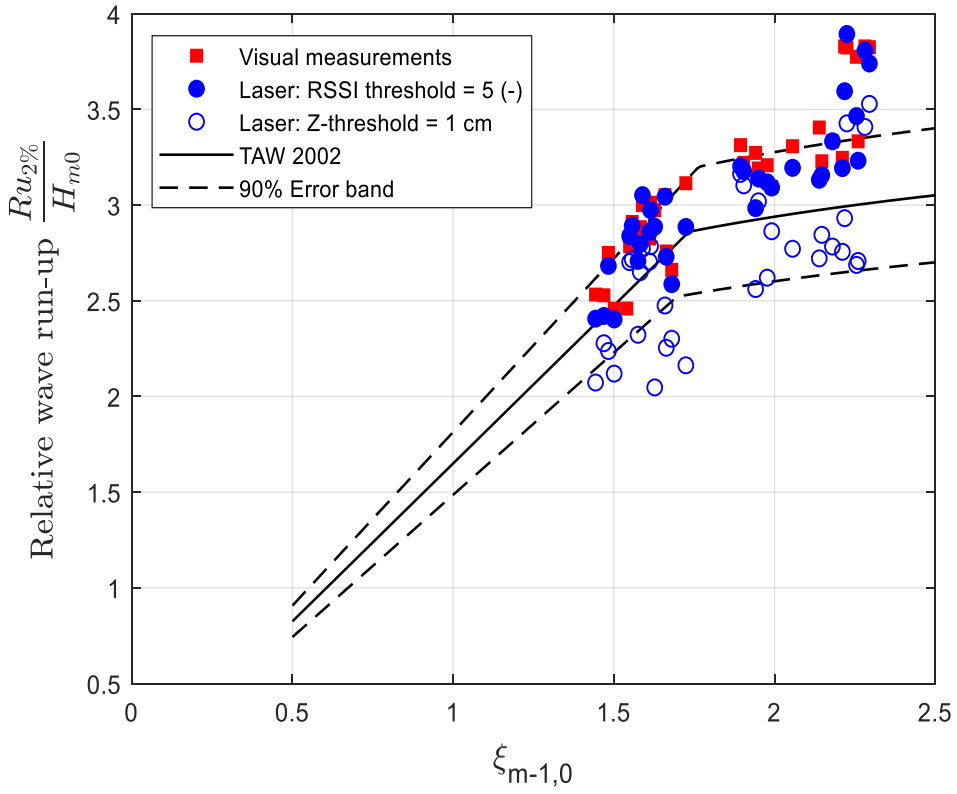

Figure 49 The run-up height by visual- and laser measurements compared to the TAW (2002), with the wave conditions in front of the dike.

5.3.2 Overtopping discharge

The virtual overtopping discharges have been calculated from the laser data, by integrating the area between the measured water surface and the dry dike slope. The normalised overtopping discharges of the reference tests at mid water level are plotted in Figure 50. The plot shows that the tests with a surf similarity parameter lower than 2, nicely fit into the 90% error band of the Van der Meer & Bruce formula (2014). However, the tests with a value larger than 2 are found outside this interval band. This is because of the fact that the overtopping formula changes around a value of 2, where the waves go from plunging to surging, see section 2.2.

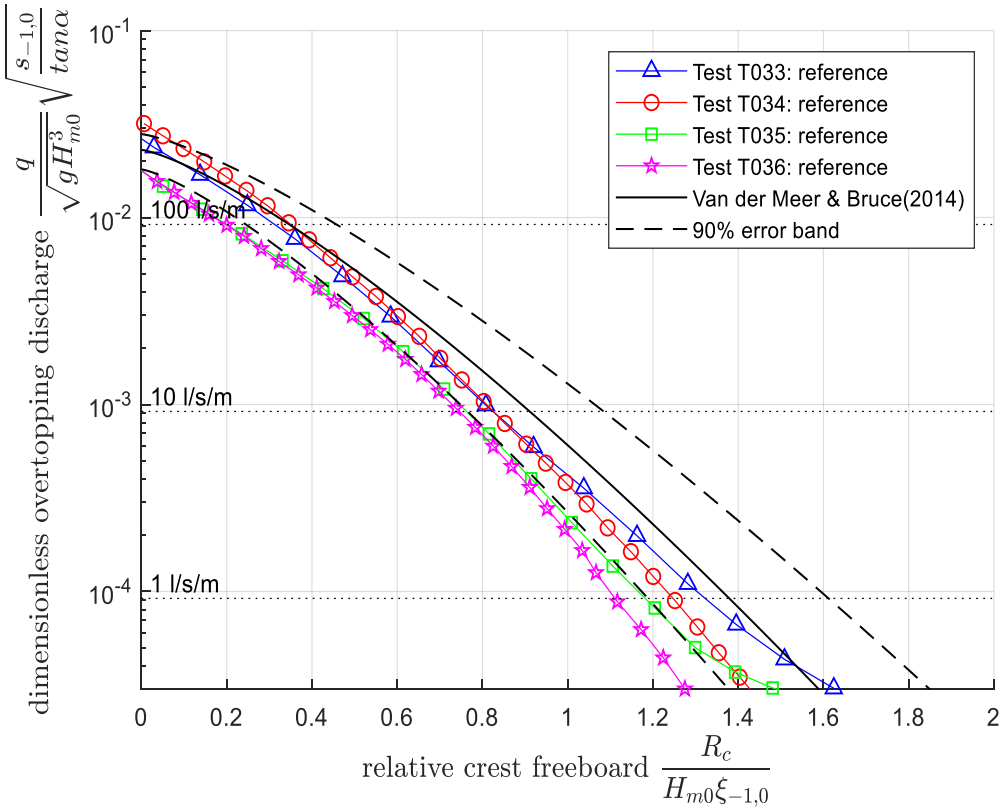

Figure 50 Dimensionless overtopping discharge for the reference tests/no willows at mid water level h=3.0 m

In Figure 51 and 52 the dimensionless overtopping discharges are plotted for the reference tests at high water. Comparing tests with the same incoming wave conditions, T038 with T042 and T037 with T041, show a good agreement in overtopping discharges, for crest levels lower than 2.0 m. Although these tests have the same incoming wave conditions (same steering file), a clear difference is observed between the two measured discharges, for crest freeboards higher than 2.0 m. The overtopping discharge is around 25% larger for T042 compared to T038. For T037 the overtopping discharge even becomes 200% greater compared to T041. Although these large differences, the results fit nicely into the 90% error band of the Van der Meer & Bruce formula, except for T041 which gets an odd shape for the higher crest levels.

In Figure 53 the tests with willows of 100% density, willows of 50% density and the reference test are plotted. As expected, a smaller overtopping discharge is found when a willow forest is present, where the overtopping discharge decreases for increasing density of the forest. This is observed for all analysed tests (for more plots see Appendix O), except for tests in comparison 10 (see Figure 54 and 55).

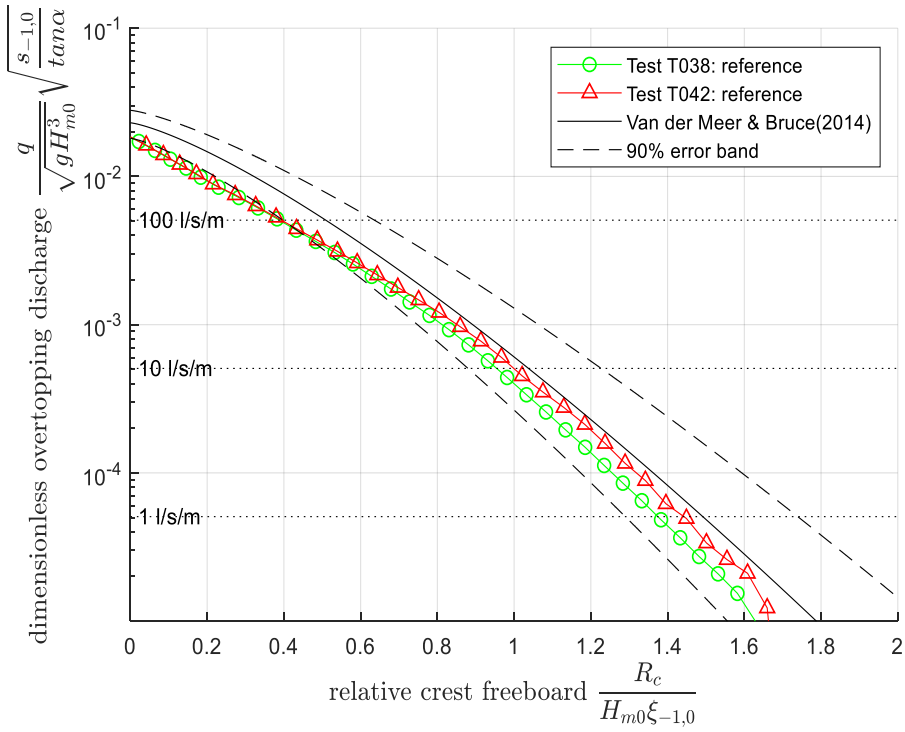

Figure 51 Dimensionless overtopping discharge of test T038 and T042, having the same steering file. Wave conditions at the wave board: h = 4.5 m, H_{m0} = 1.43 m, $T_{m-1.0}$ = 6.3 m

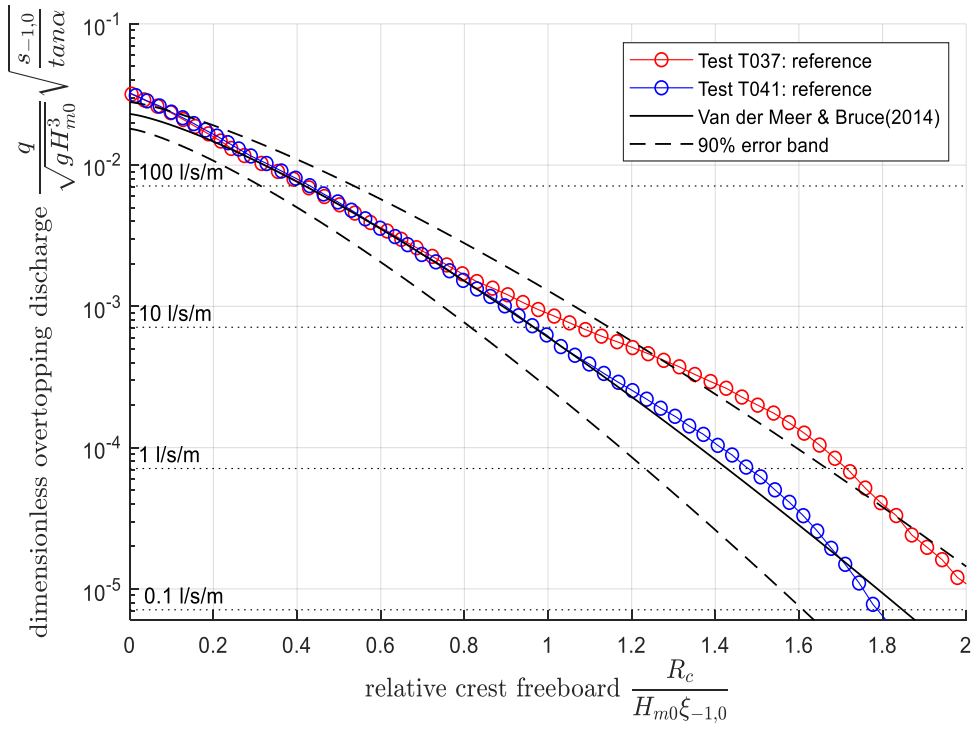

Figure 52 Dimensionless overtopping discharge of test T037 and T041, having the same steering file. Wave conditions at the wave board: h = 4.5 m, H_{m0} = 1.40 m, $T_{m-1.0}$ = 4.5 m

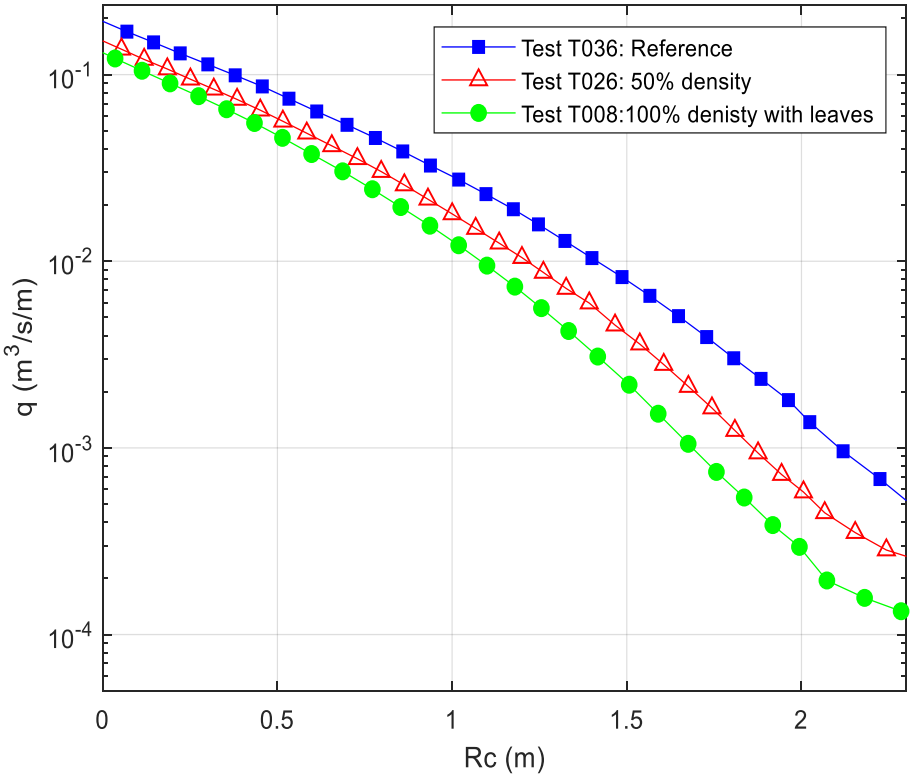

Figure 53 Dimensionless overtopping discharge for tests with and without willows in the flume

In Figure 54 and 55, the reference tests are plotted together with the experiments with willows in the flume. It is remarkable to see that the willows with only 50% density, show less overtopping discharge than the test containing willows with 100% density, for higher crest levels. The test without willows (T041), even shows a lower discharge than the tests with willows. These results go against expectations and strongly deviate from the other findings. The results for these wave conditions (comparison number 10) are therefore considered as not reliable.

In Table 9 the overtopping discharges at different virtual crest heights for several tests are given. In Appendix O the discharge with respect to the crest height, are plotted for the different tests with and without willow trees. From the determined discharges in Table 9, the effect of the willows has been calculated, resulting in a decrease in discharge between the 40 and 80%, for low water depths with R_c = 0.5 - 2.0 m. For the higher water level, the decrease in discharge is calculated between 24 and 66% for R_c = 1 - 3 m. From the measured discharges the following influence factor is derived:

$$\gamma_{q;willow} = \frac{\ln(q_{reference})}{\ln(q_{willows})}$$

With the following range of values:

- Mid water level: $\gamma_{q;willow} \approx$ 0.77 - 0.93
- High water level: $\gamma_{q;willow} \approx$ 0.82 - 0.89

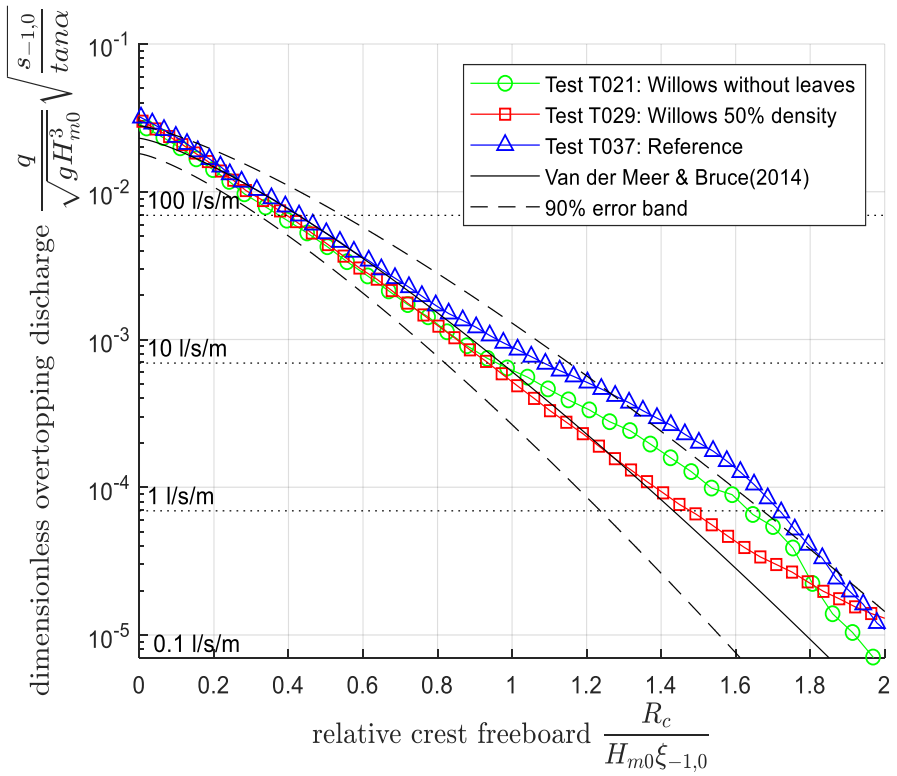

Figure 54 Dimensionless overtopping discharge for tests with the same incoming wave conditions

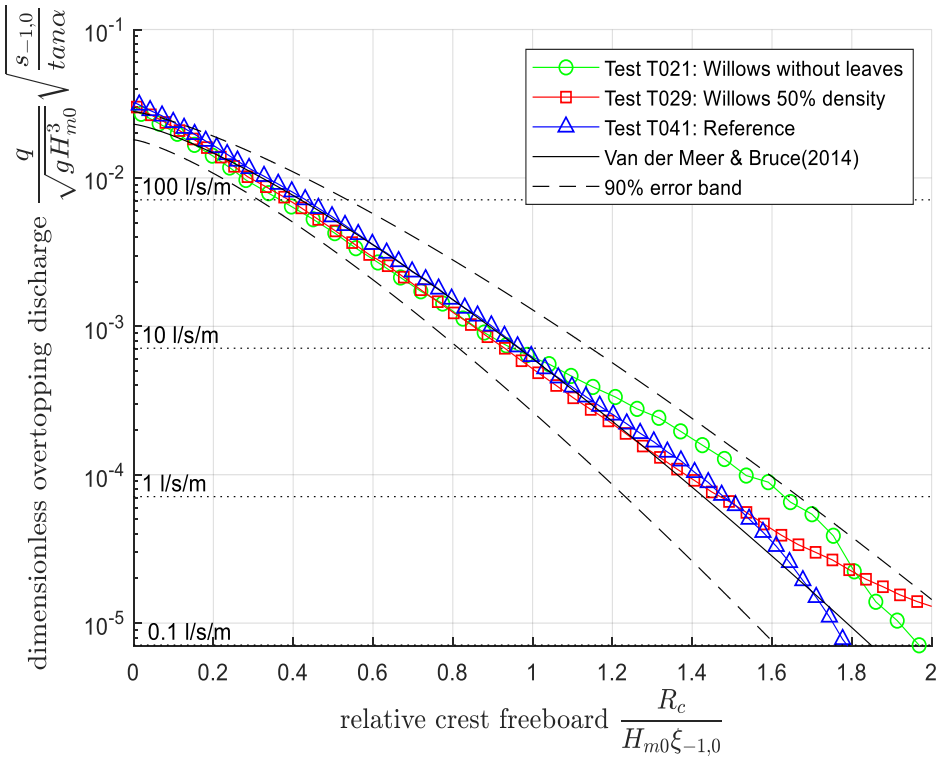

Figure 55 Dimensionless overtopping discharge for tests with the same incoming wave conditions

Table 9 Overtopping discharges determined from the laser measurements for different crest heights, with the wave conditions given at the wave board.

Test ID	h (m)	H_{m0} (m)	T_p (s)	$q_{Rc = 0.5\ m}$ ($m^3/s/m$)	$q_{Rc = 1m}$ ($m^3/s/m$)	$q_{Rc = 1.5\ m}$ ($m^3/s/m$)	$q_{Rc = 2\ m}$ ($m^3/s/m$)	$q_{Rc = 3\ m}$ ($m^3/s/m$)
Willows with leaves								
T006	*3.0*	*0.97*	*3.9*	$2.7 \cdot 10^{-2}$	$2.8 \cdot 10^{-3}$	$1.3 \cdot 10^{-4}$	-	-
T007	*3.0*	*0.45*	*3.9*	$3.9 \cdot 10^{-3}$	$1.1 \cdot 10^{-4}$	$4.0 \cdot 10^{-5}$	-	-
T008	*3.0*	*0.97*	*5.6*	$4.7 \cdot 10^{-2}$	$1.3 \cdot 10^{-2}$	$2.2 \cdot 10^{-3}$	$2.9 \cdot 10^{-4}$	-
Willows without leaves								
T013	*3.0*	*0.44*	*2.8*	$7.6 \cdot 10^{-4}$	-	-	-	
T021	*4.5*	*1.40*	*4.8*	-	$5.8 \cdot 10^{-2}$	-	$8.4 \cdot 10^{-3}$	$1.7 \cdot 10^{-3}$
T022	*4.5*	*1.41*	*6.8*	-	$8.4 \cdot 10^{-2}$	-	$1.9 \cdot 10^{-2}$	$2.6 \cdot 10^{-3}$
Reference tests								
T033	*3.0*	*0.44*	*2.8*	$1.9 \cdot 10^{-3}$	$5.7 \cdot 10^{-5}$	-	-	-
T034	*3.0*	*0.94*	*3.9*	$5.4 \cdot 10^{-2}$	$8.2 \cdot 10^{-3}$	$1.0 \cdot 10^{-3}$	-	-
T035	*3.0*	*0.46*	*3.9*	$7.3 \cdot 10^{-3}$	$3.3 \cdot 10^{-4}$	$8.1 \cdot 10^{-5}$	-	-
T036	*3.0*	*0.96*	*5.6*	$7.9 \cdot 10^{-2}$	$2.9 \cdot 10^{-2}$	$7.9 \cdot 10^{-3}$	$1.5 \cdot 10^{-3}$	-
T037	*4.5*	*1.40*	*4.8*	-	$8.7 \cdot 10^{-2}$	-	$1.6 \cdot 10^{-2}$	$4.2 \cdot 10^{-3}$
T038	*4.5*	*1.43*	*6.8*	-	$1.1 \cdot 10^{-1}$	-	$3.4 \cdot 10^{-2}$	$7.6 \cdot 10^{-3}$
T041	*4.5*	*1.36*	*4.8*	-	$8.5 \cdot 10^{-2}$	-	$1.1 \cdot 10^{-2}$	$1.4 \cdot 10^{-3}$
T042	*4.5*	*1.37*	*6.8*	-	$1.1 \cdot 10^{-1}$	-	$3.2 \cdot 10^{-2}$	$6.1 \cdot 10^{-3}$

5.3.3 Wave measurements

From the wave height measurements executed with the radar behind the forest (RADAC 2) and the wave gauges (WHM 1-3) in front of the forest, the following is observed (Wolters et al., 2018):

- Almost full wave damping occurs in the first half of the willow forest.
- A higher wave height shows more wave damping. This effect is less clear with higher wave steepness, due to more waves breaking on the platform.
- Wave attenuation increases with higher wave height and larger period, with a maximum of approximately 22%.
- The strongest wave damping is observed around mid-water level, where the surface area is at maximum.

The last three findings from the wave measurements correspond well with the results found from the wave run-up measurements.

6. Discussion

In this section the results presented in chapter 5 are discussed.

6.1 Measurements & data processing

The wave data used in the calculations are especially from the WHM1-3 and the RADAC 2. For all wave run-up calculations, the wave conditions behind the forest are used (from RADAC 2). However, the waves still need to travel 15 m before reaching the toe of the dike. Meaning that the wave conditions at the toe can slightly be different, but this effect will be minimum as the foreshore does not fluctuate in this part of the flume.

For each test around 550 incoming waves are generated, making sure that the R_{u2}% can be determined with a relatively high confidence. For the Peak Over Threshold analysis the number of incoming waves at the wave board are taken. However, depth-induced wave breaking at the foreshore, bottom friction and wave attenuation by the vegetation, could have caused this number to decrease. Thus, the probabilities of exceedance are somewhat higher than calculated, resulting in higher $R_{u2\%}$. Nevertheless, decreasing the number of incoming waves with 10%, increases the $R_{u2\%}$ only with less than 1%, so this effect is very small and does not affect the results.

For a couple of tests, overtopping has taken place over the real crest of the dike. The number of waves that overtops the real crest of the dike in the flume, are less than 2% of the number of incoming waves. Thus, this does not impede the determination of the R_{u2}%.

For the processing of the camera measurements deep learning is used, however results show that the trained Convolutional Neural Network was not sufficient to predict the run-up for all tests. At certain time instances during the experiment, it is noticed that the water level is not captured for the full width of the flume (see Figure M.22). Approximately 14% of the points stay behind and do not follow the wave run-up. Therefore, these tests are not analysed any further. These missing wave run-ups for test T005 could likely be attributed to the overexposure of light at the lower part of the flume, which is different than the light in the eighty trained images. So far, this caused that the algorithm cannot detect the clear difference between the wave run-up and the dry slope and therefore catches a wave run-up of zero. In all other analysed tests, the light at the video image was more or less the same as of the trained video images (T012) giving sufficient results. To apply deep learning on the video footage it is therefore necessary to know whether the light changes in time. If so, to tune the Convolutional Neural Network with more time stacks, containing more representative samples of the video footage.

Although the visual measurements are dependent on human interpretation, the probability of exceedance by the visual measurements have been measured quite accurately. To prevent mistakes and different interpretations, the measurements have been executed by three different persons. The results show more or less the same distributions, meaning that the number of exceeded waves is well counted. With this, the probability of exceedance distributions have been determined with the accuracy of the lines on the slope, which is estimated around 2 cm.

6.2 Comparison results with the TAW

The most commonly used models for designing a dike are empirical formulas i.e. the TAW and EurOtop. However, comparing the obtained results with the TAW (2002), show that the determined wave run-up from the Delta Flume experiments are underestimated with an average of 9% and a maximum of 30% by the TAW. This would indicate that using the TAW (2002) for the design of the dike in the delta flume would lead to an underestimation of the crest height. It is therefore of importance to further analyse and possibly adjust the TAW formula.

The TAW is an empirical formula based on a large set of experiments. The scale on which the experiments are conducted can entail scaling effects caused by for example wind, large wave conditions and resistance. One of the main advantages of the new Delta flume is that the experiments can be performed on prototype scale, where the scale effects are minimum. In Figure 56 the TAW formula with data points are shown. The data points are from small-scale experiments by De Waal & Van der Meer (1998) and from large scale results, which are considered reliable by Van Gent (1999). The test results have shown that a majority of the measurements are found around the upper 5% exceedance limit of the TAW (2002). This trend is also observed for some data points from tests conducted in the old Delta flume with a 1:3 dike slope (M1795), these data points are encircled in Figure 56. Just like the used New Delta Flume, the old Delta Flume is a full-scale test facility only having a smaller length and height (LxBxH = 233x5x7 m). The majority of the data points from small-scale experiments, are closer to the TAW than the points obtained by large-scale experiments. Therefore, the difference between the tests results and the TAW could likely be attributed to scale effects, related to for example roughness of the dike slope and the effect of wind. However, more wave run-up measurements at full scale are needed to confirm this for both high and low run-up values.

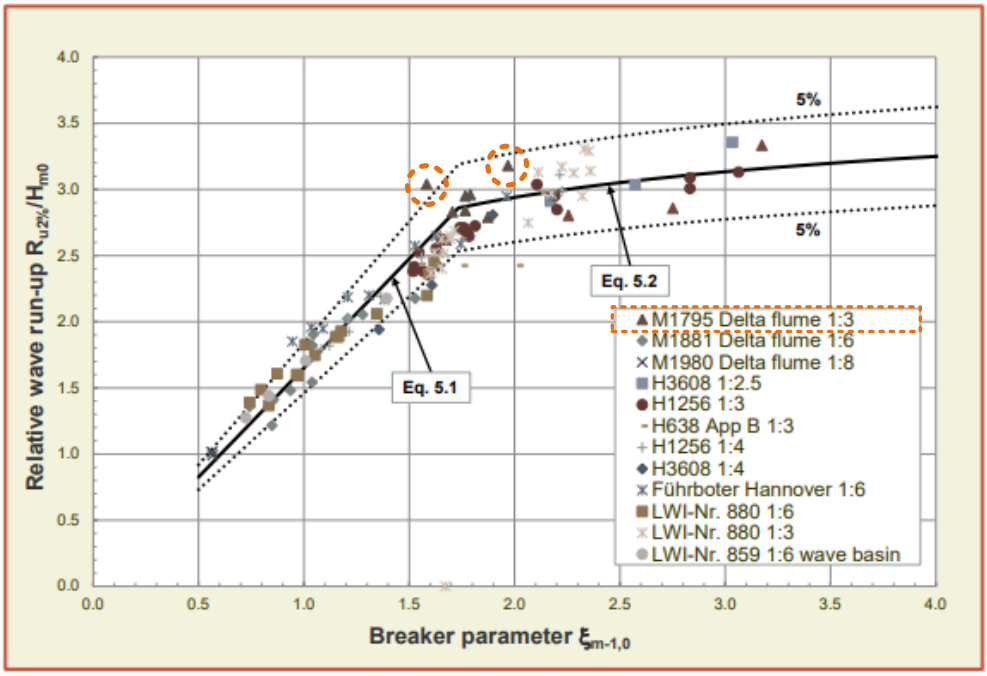

Figure 56 Wave run-up for different conducted flume tests with a smooth straight slope in relatively deep water with perpendicular wave attack. (EurOtop, 2018).

The five outlying data points above the 5% exceedance limit are remarkable, with a difference of 28% relative to the TAW formula. Analysis of the three different measuring techniques shows the same trend of outlying data points, also the tests have not been conducted right after each other. From which can be

concluded that this large difference is not caused by the measuring techniques, environmental conditions or processing of the run-up. Nevertheless, it was remarkable that the data points result from two sets in which the same incoming wave conditions hold. Another noticeable aspect is that these tests all contain the lowest wave steepness, smaller than 0.02, with a water depth of 4.5 m (see Figure 57). The very low wave steepness indicates relative low waves with a large wave period.

The ratio h/H_{m0} indicates whether the waves are in deep or shallow water. For the two test series giving the outliers, the ratio h/H_{m0} is larger than 4. This means the waves are still in deep water and wave breaking has not taken place yet. Long waves containing a lot of wave energy therefore result in high wave run-up heights. However, the results do not show any outliers for tests with the same incoming wave conditions, but only having a different water level. In Figure 58, the bias to the TAW for data points with a wave steepness smaller than 0.02 are plotted, for both low- and high-water level. Here it is clearly shown that the ratio h/H_{m0} for low water levels is lower, compared to high water conditions, even resulting in shallow water conditions for one of the datasets. So, for the lower water levels, the long waves are closer to or even, in shallow water, meaning that wave breaking will occur. The reduction of the energy of the high waves, will give a lower wave run-up and with this a smaller difference to the TAW.

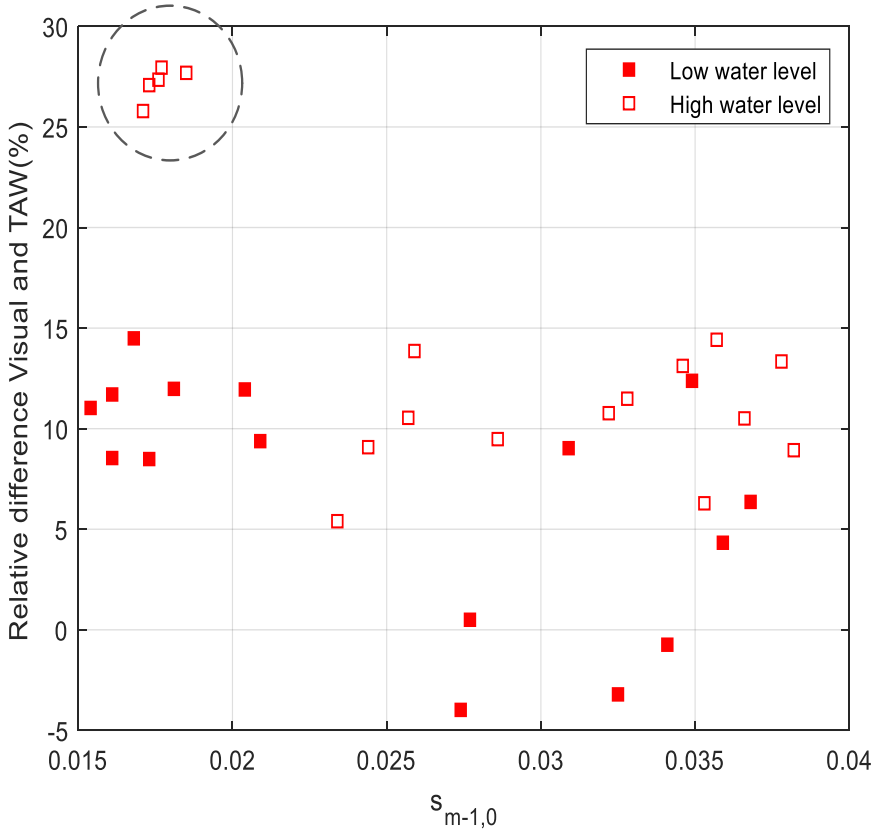

Figure 57 The relative difference of the visual measurements with respect to the TAW formula, with emphasis on the outlying points

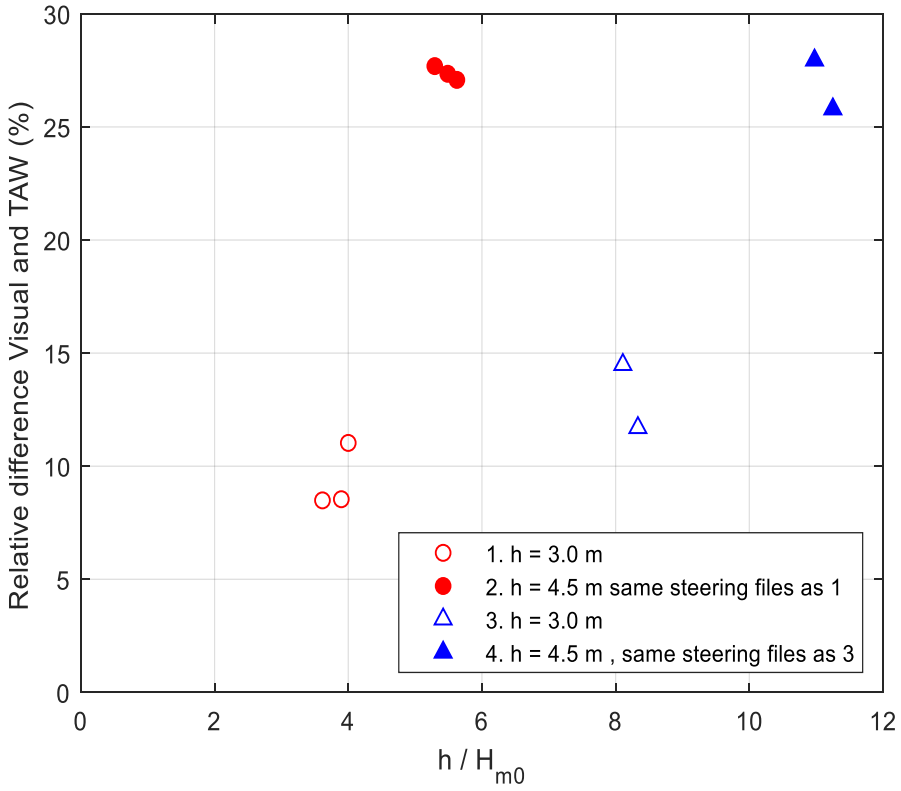

Figure 58 The relative difference of the visual measurements with respect to the TAW for the data points having a wave steepness smaller than 0.02.

6.3 Comparison Laser and Camera results

The bias of the run-up height determined by camera, laser-RSSI and laser-Z-threshold, to the visual observed run-up were respectively 3.5%, 3% and 14% (on average). It can be said that the laser- RSSI and camera both have results with almost the same accuracy in relation to the visual measurements. It also shows that the method of the laser based on the RSSI is more accurate than the method based on a layer thickness of 1 cm, which is as expected and in line with findings from previous research (Hofland et al., 2015). With the RSSI, the water surface is detected up till a much thinner layer thickness than 1 cm.

In previous research (Hofland et al., 2015) the bias with respect to the visual measurements for the laser-RSSI and laser-Z-threshold, were on average 4% and 13% respectively. Although a threshold on the water layer thickness of 1 cm instead of 3 cm was taken in the present research, the biases are still almost the same. Using a layer thickness of 3 cm instead of 1 cm shows a difference in run-up of around 20 cm, which would raise the expectation for a more accurate result. The difference between the set-up of both experiments is mainly in the run-up range, which is now almost twice as large as in the previous research. A greater range causes a smaller point density when further away from the laser, meaning a lower accuracy at these locations. However, using a smaller layer thickness threshold, has resulted in a lower bias with respect to the visual measurements, which is in the same order as in the previous research.

The difference between the laser and visual measurement is likely to be attributed to the scanning of a 2D line on the slope, while during the visual measurement, the observer has a 3D overview of the wave run-up. From the camera measurements the variation of the run-up over the 2.5 m width in the flume, has been

valued at an average of 15 cm. This variation could have caused the maximum bias of 17 cm between the laser measurements and the visual measurements. Another aspect that caused the deviation is the calibration of the laser. After calibration still a deviation on the run-up height of approximately 5 cm was left. The results also show a trend of decreasing bias for larger run-up heights. For the laser measurements this can be explained by a higher point density, causing a higher accuracy at the upper part of the slope, resulting in a lower bias.

The bias for the camera measurements, with respect to the visual measurements, are mainly caused by the precision of the algorithm to detect the interface of the water and the slope. The run-up height can only be determined up till a certain layer thickness. The underestimation of the algorithm is minimized by the perspective of the camera, showing a projection of the wave run-up on the dike slope. This projection results in higher run-up values, which even lead to run-up heights larger than determined visually. Especially for the upper part of the slope, where the viewing angle of the camera is larger, the projection causes higher run-up values (see Figure 59). This is also confirmed by the results, showing a decrease in bias for increasing run-up height.

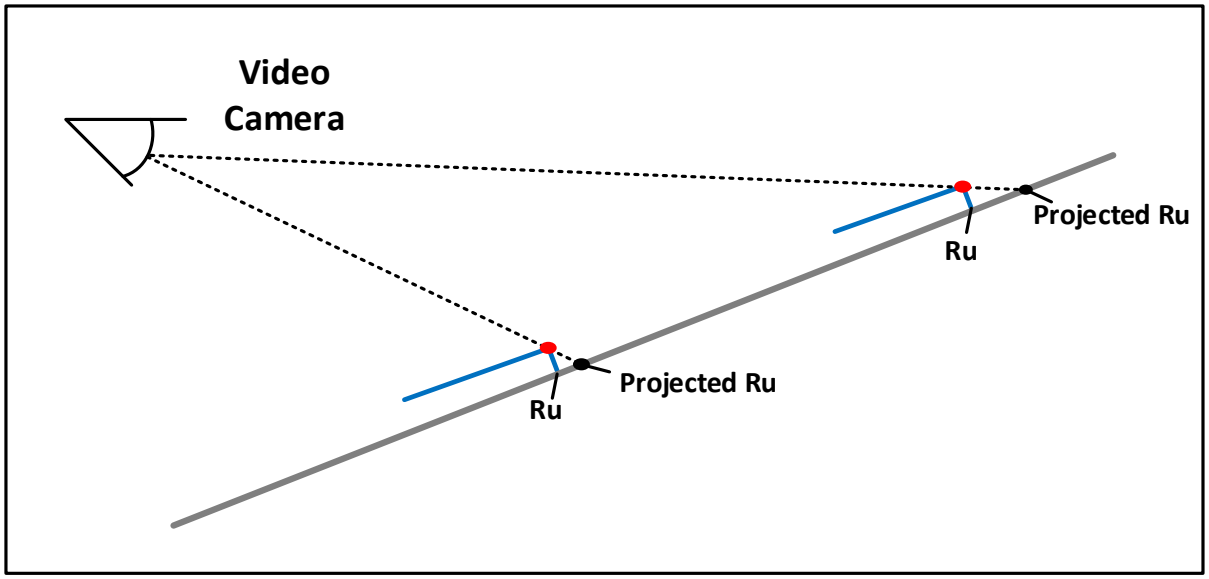

Figure 59 Projection of the run-up by the video camera

6.4 Effect willows

To determine the effect of the 40 m willow forest, tests with and without forest are conducted, eliminating other effects of wave damping. Test results show a significant reduction on the wave run-up height between 10 and 19%. In previous research by Smale et al. (2016) higher significant reductions were found. From modelling a pollard willow forest in SWAN, the maximum effect for a vegetation belt of 20 m was determined at 18% and for a 60 m vegetation belt at 31%. It is remarkable that the test results of a 40 m forest correspond well to the modelled results of a 20 m vegetation belt. This could either be attributed to a higher density in the model compared to the forest in the experiment, or to the model itself. As the model is not validated and a drag coefficient of 1 is used, the real reductions could be lower than determined. From the field experiments executed by Vuik et al. (2016) a reduction in wave height between 25 and 50% was found, for cordgrass and seaweed covered foreshores. In this research, longer foreshores and a higher vegetation density have resulted in higher wave height reduction values than found in the flume experiments with willows.

The test results show that the removal of 50% density reduces the reduction in run-up by approximately 50%, although this is only true for three of the five cases. It is observed that the main difference between the several comparisons is the wave steepness and therefore, the difference possibly could be attributed to the wave steepness. The two cases for which the reduction of the 50% branches is lower, both have a low wave steepness of around 0.02. Indicating that the waves have a relatively long wave length. The wave length for both cases, 22 and 41 m, is larger than halve of the forest length. If waves are longer, the changes in the forest are less felt and could have a smaller impact than for shorter waves. However, it is strange that the 50% density has a small effect on the waves, but the effect of leaves is well noticed. Another possibility could be an error in determining the $R_{u2\%}$ values from the graphs. Interpolation between the data points is used, which could involve some errors. Although these errors are small, the reduction percentages can change a lot. Further analysis of the data is needed to be able to better describe this difference in run-up reduction.

6.5 Effect water depth

An effect of the water depth on the wave run-up is noticed. Further analysis shows that the effect of the foreshore does not differ more than 2% between the mid and high-water level. Here not only breaking, but also some shoaling was observed. This means that the depth induced breaking by the platform is very small and the calculated value of around 20% difference, is mainly due to the willow trees in the flume. The area distribution (given in Appendix C) over the height of the tree shows that the highest surface area is situated at a height of 3 m (mid water level). At mid water level 50% and at high water level 80% of the tree is inundated. For wave damping especially the part around the water line where the waves propagate are important, considering a part of 1 m above and 1 m below the water line. From this follows that around 39% of the total surface area is present to resist the incoming waves at high water level. While at mid water level 52% of the area is present to dampen the waves. Which is a difference in area of 13%. From this can be said that the effect of the water depth on the wave run-up, for more than 50% can be attributed to the difference in area at the two water levels, causing different wave dissipation. However, note that this area distribution is taken for an average tree and does not represent the area distribution for the whole flume, so the real distribution can deviate from this average value.

Previous research conducted in a small-scale flume, shows an increase in relative wave run-up for increasing relative water depth at the toe of the structure (Peiris, 2005). A maximum increase at shallow water compared to deep water, of 25% for surging and about 60% for plunging waves, is found. A possible explanation here, is the difference in wave breaking at the dike. At shallow water, the waves break on the dike, causing less available energy for the run-up. While at deeper water the waves do not break, but surge on the slope of the dike, having more energy, causing a higher run-up. Further experimental and literature research is needed, to find the right explanation for the differences in wave run-up for various water depths.

6.6 Variation run-up over the width

It is found that 70% of the analysed camera measurements have a higher run-up at the right part of the flume. As these experiments are all reference tests, the willows did not have any effect on this. This effect could likely be attributed to the asymmetry of the construction of the foreshore or the dike in the flume. Both are man-made and therefore are subjected to human errors. A slight tilt in the dike slope or foreshore could have caused an asymmetry in the wave reduction and therefore a difference in wave run-up of on average 15 cm over 2.5 m width. The width effect should be measured during more large-scale experiments to get a better understanding of these variations over the width.

6.7 Overtopping discharge

A remarkable aspect that was observed, for two tests with the same steering file and configuration, giving different overtopping discharges. For test T038 and T042, this difference was relatively small. However, for

test T037 and T041 the difference was almost 200%. It is noticed that the two results only deviate for crest freeboards higher than approximately 2 m, showing an odd shape. For the lower crest levels, the results correspond well. Comparing test T041 (reference) with the other tests containing willows, resulted in higher discharges for the tests with willows. Which is very unlikely to happen with a forest of 40 m. For the rest of the comparisons between willows and reference tests this was not the case and the test with willows show, as expected, less overtopping discharge. Therefore, it can be said that the results for the overtopping discharge obtained from test T041, T037, T021 and T029 seem to be not reliable, for crest freeboards larger than 2 m.

Looking at the dike slope, two main things are noticed around a crest freeboard of 2 m. Firstly, at around 2.3 m the concrete dike slope turns into the wooden dike slope. At approximately 1.9 m above the water level, the laser is situated having a zero angle. As a slant angle larger than the recommended 5 to 15 degrees is used, it is very unlikely that direct reflection of the laser light has taken place. Looking more into this specific location on the dike for the tests at high water, shows larger layer thicknesses. Comparing the results with the video camera, show that these large layers of water are caused by wave breaking at the structure, giving a splash of water into the air (see Figure 60 and 61). Even though these splashes are measured as data points, they do not contain a full dense water volume along the vertical. Therefore, the volume of water for those time instances are overestimated. After breaking, these wave volumes run further up the slope. The volumes for the higher run-up values will be lower than the overestimated value and therefore, the determined overtopping volume for an individual wave is overestimated for the higher crest heights. The higher overtopping discharges and the found odd shape of the graph could therefore likely be attributed to these overestimated wave volumes, caused by breaking of the waves at the upper part of the dike. As these kinds of wave breaking especially occur at the upper part of the slope, the results for the lower part of the slope is probably not overestimated. The data must be further analysed to better research the cause and quantity of this overestimation.

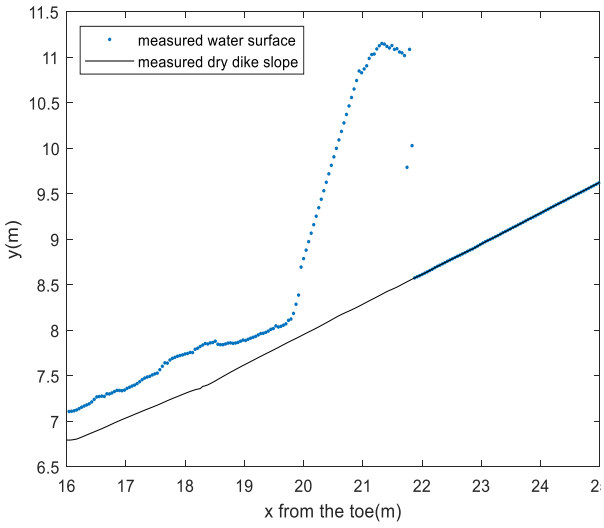

Figure 60 The measured water surface and the dry dike slope for test T041 during wave breaking on the dike.

Figure 61 Wave breaking on the dike measured by laser and by camera, for test T041

For the calculation of the volumes water layer thicknesses smaller than 0.5 cm have been neglected, as these are inside the error margin caused by the deviation of the positioning of the laser scanner. Neglecting these volumes means that the real overtopping volumes are somewhat larger than calculated.

It must be noted that by determining the virtual overtopping discharges an assumption is made, that the overtopping discharge above a certain crest level equals the maximum volume of water of that individual wave run-up. So, the real overtopping discharge could deviate from the real ones. Also, the variation of the run-up over the width could cause higher or lower real volumes. Therefore, validation of this method is needed, measuring the real volumes.

6.8 Reduction in overtopping discharge

The calculated discharges can be compared with the tolerable overtopping discharges for grass covers and people standing on a dike crest, which are between the 0.1 to 5 l/s per m and 10 to 20 l/s per m respectively. However, the values leading to failure can be different. The values are dependent on the wave height and how well the grass cover is maintained. The case with a water level of 3 m and a crest freeboard of 1.5 m, gave an overtopping discharge of around 8 l/s/m which is 3 l/s/m higher than the tolerable discharge for a grass cover. Nevertheless, a 40 m willow forest in front of the dike could reduce the discharge to 2.2 l/s/m, which is now within the tolerable discharges. For the higher water levels and wave heights with a crest freeboard of 3 m, the overtopping discharge could be reduced from 7.6 to 2.6 l/s/m.

7. Conclusions & Recommendations

The main objective of this research was to assess the effectiveness of willow vegetation, in reducing wave loads (wave run-up and wave-overtopping) on a dike, under storm conditions, using novel remote sensing techniques. To reach this objective, large scale flume experiments with a willow forest of 40 m in front of a dike have been conducted in the Delta Flume of Deltares. To determine the wave run-up, two new methods have been used: video imaging processed by a Machine Learning algorithm and a 2D laser scanner measuring the water surface. Also, the wave overtopping has been quantified using a laser scanner, instead of measuring real overtopping volumes with an overtopping tank. In the first part of this chapter the sub-questions are answered and the conclusion to the main research question is drawn. In the second section, recommendations are given for further analysis on this subject and improvement for experiments using video imaging and laser scanning.

7.1 Conclusions

To what extent is terrestrial laser scanning applicable to quantify the run-up and overtopping processes on a dike?

In order to research the hydraulic processes on a dike slope, a laser scanner was placed directed on the slope. The laser was scanning with a frequency of 35 Hz, which resulted in measurements with a high spatial and temporal resolution, even scanning water layers smaller than 1 cm. The measured run-up by laser scanner only deviates with an average of 3% and a maximum of 8.8% to the visual measurements. This concludes that the laser has measured the wave run-up on the dike with a high accuracy. The use of the measured reflection intensity values by the laser, have shown to improve the accuracy of the determined wave run-up, detecting water layers smaller than 1 cm.

Results regarding the virtual overtopping discharges show measured values in the same order of magnitude as calculated using the existing Van der Meer & Bruce formula (2014). This shows that the laser scanner gives reasonable results regarding the overtopping. However, the results also show an overestimation of the overtopping discharges at high water level for higher crest freeboards, making these results less reliable. The laser scanner is a simple substitute in measuring the overtopping volumes and discharges, without measuring real overtopped volumes with an overtopping tank or without having to build a tank into the dike slope. So, this is a more cost-efficient measuring technique, applicable in determining the overtopping volumes on more dikes. However, more research and a thorough validation are required to confirm the accuracy of this method.

To what extent is video imaging applicable to quantify the run-up processes on a dike?

A video camera is placed, recording the wave run-up and run-down on the dike slope. Results show that the use of video imaging in a large-scale flume facility is well applicable, if the following conditions hold. First, the water surface must be visible for the camera, meaning enough light. Second there must be a reference with known length on the footage.

The video-footage was inserted in a Convolutional Neural Network, giving the wave run-up in time over the full width of the flume. At first sight, it is apparent that the wave run-up is very well captured. Results from the video measurements are compared to the visual measurements showing a maximum bias of 9.8%.

From which can be concluded that the run-up is determined very accurately by camera imaging. In contrary, the wave run-down is not captured as well. Therefore, it is better not to use camera imaging for quantifying the processes during the run-down of the wave. This method also gave new insights into the variation of the wave run-up over the flume width. Notable variation over the 2.5 m in the middle of the flume is determined to be on average 15 cm, with a maximum of 29 cm.

Thus, the camera in combination with Machine Learning is an accurate, simple and low-cost technique to measure the wave run-up on a dike. This technique not only gives the run-up height, but also new insights about the variations of the wave run-up over the dike.

What is the effect of willow vegetation on the wave run-up height?
Flume experiments with a dike and a 40 m willow foreshore, are conducted under different low and high hydraulic conditions. To determine the effect of the willow forest, tests with and without forest are conducted, eliminating other effects of wave damping. Results show a significant reduction on the wave run-up height between 10 and 19%, for different wave conditions and water levels. Even when the willows are almost fully inundated, they cause a lower, but still significant reduction in wave run-up. It also follows that the difference between the reduction in run-up, for willows in summer (with leaves) and winter state (no leaves), are on average only 5%. Even when 50 % of the branch density of the willows is taken away, a reduction in run-up between 5 and 13% remains. Willows are therefore an effective measure to lower the run-up on a dike and further research is needed, so willows can be implemented in a design and the effect can be considered in the assessment of dikes in the Netherlands.

What is the effect of willow vegetation on the wave-overtopping?
The wave-overtopping volumes and discharges have been measured by integrating the area between the water surface and the dike slope, measured by the laser scanner. A comparison of values obtained from experiments with and without willows, results in an average reduction of the wave-overtopping discharge between 40 and 80%, for water depths of 3 m. For the higher water levels, a decrease in discharge is calculated between 24 and 66%. The willow forest reduced the overtopping discharges for certain crest levels, so that the discharges do not exceed the tolerable overtopping discharge anymore. This reduction could be beneficial for the erosion of grass covers on a dike.

For both the wave run-up and the wave overtopping, an influence factor is found for a pollard willow forest of 40 m, containing 100% density. The influence factor, γ_{willow} is valued between 0.8 and 0.9 and is valid for the following conditions:

3.0 m	≤	h	≤	4.5 m
0.43 m	≤	H_{m0}	≤	1.47 m
2.7 s	≤	$T_{m-1,0}$	≤	6.0 s
0.27	≤	tan(α)	≤	0.33

7.2 Recommendations

Concerning the performance of the flume experiments, a couple of recommendations are made:

- For the analysis of the experiments it is of great importance to have executed reference tests for quantifying the effect of the willows, as some reference tests were missing. Therefore, it is strongly recommended to conduct enough reference tests, so the effect of the influence can be analysed, and a good comparison can be made.

- To say more about the effect of willows on the wave loads on the dike, it is recommended to research the effect of the forest length and the tree height. Research must be conducted on how dense a forest must be to give enough wave damping, so the dike height can be maintained. Therefore, tests with different forest lengths and tree heights should be executed. Also, other types of trees, such as mangroves, should be tested.

- Analysis show that the wave run-up is possibly dependent on the water level and it is therefore strongly recommended to research this. Several experiments should be conducted, with different water levels containing the least variables affecting the wave run-up, so no willows, foreshore etcetera. It is strongly recommended to measure at several places, to make sure that all factors affecting the wave run-up, are detected.

- To analyse the wave impact forces caused by wave breaking on the dike, implementation of pressure sensors over the full length of the dike slope is recommended. Here it can be analysed how the willows affect the impact forces on the slope of the dike.

- For the improvement of the used design formulas (TAW/EurOtop), it is recommended to conduct more tests measuring the wave run-up and wave overtopping on a dike at full-scale.

- Fundamental understanding of erosion of the dike cover are important to assess and maintain the safety of the dikes. Therefore, it is recommended to analyse the effect of different slope covers (e.g. grass) and dike transitions on the wave processes on a dike. It is also essential to check the effect on the different thresholds used in the filtering process of the data, where possibly higher thresholds on the layer thickness will be needed.

- In the field, wind is causing large set-ups, increasing the run-up on the dike. Therefore, the effect of wind on the run-up should be distinguished by measuring the wind velocities during each experiment.

- In this research uprooting of the willows is not part of the scope. However, this could be of interest when researching the effect of the flexibility of the willows in relation to the wave damping.

Recommendations for the measuring equipment are presented below.

Laser scanner

- To validate the determined virtual overtopping volumes measured by the laser and to research the accuracy of the measurements, it is recommended to measure the real volumes for different crest heights. This can be done by placing a large tank at the end of the slope or next to the laser line in the slope.

- For future experiments it is recommended to place an accelerometer on the laser scanner. This can measure the displacements of the laser. It is also strongly recommended to install the laser scanner so that these deviations are minimum. This will save time during the postprocessing and the extensive calibration of the data.

- For further analysis, the velocities obtained from the laser scanner can be analysed and compared with the velocities obtained from the camera measurements.

- Using a laser scanner in real storms is not feasible, as a large amount of data is produced. Therefore, an alternative method should be found so the laser can be used in practice, producing less data.

- It is necessary to make sure that the laser scanner is positioned so that it measures in a straight line on the slope. As one or more changes in dike slope, can make the distortion from the equilibrium position only larger. Prior to and after executing the tests, the scanning line on the slope must be checked.

- For the use of the laser scanner in the field, the application of different filters for the laser should be explored.

Camera measurements

- It is recommended to extract and analyse the run-up velocities from the camera measurements. These velocities can be compared with the velocities obtained from the laser scanner.

- For the application of deep learning on the camera measurements, it is recommended to adjust the deep learning process, so that it is trained on more representative and diverse time stacks. To make the method more robust, error messages should be implemented indicating unexpected results (e.g. uncaptured wave run-up).

- To capture the full wave run-up on the slope it is recommended to set the Field of View of the camera so that the full range is measured during the tests. So, both the large wave run-up and the wave run-up below the still water level are captured by the video, to get a good computation of the run-up.

- To analyse the effect of the projection of the camera in further studies, two cameras can be applied instead of one.

8. References

Badrinarayanan, V., Handa, A., & Cipolla, R. (2016). "SegNet: A Deep Convolutional Encoder-Decoder Architecture for Image Segmentation" arXiv preprint arXiv:1511.00561v3.

Battjes, J. (1974). Surf similarity. 14th Conference on Coastal Engineering. Copenhagen: Coastal Engineering. 466-480

Battjes, J. A. (1974). Computation of set-up, longshore currents, run-up and overtopping due to wind-generated waves. Doctoral dissertation, TU Delft, Delft, The Netherlands

Battjes, J. A., Groenendijk, H.W. (2000). Wave height distributions on shallow foreshores, Coastal Engineering, 40(3), 161-182, Retrieved from: https://doi.org/10.1016/S0378-3839(00)00007-7.

Deltaprogramma. (2018). Hoogwaterbeschermingsprogramma.
Retrieved from: https://deltaprogramma2018.deltacommissaris.nl/viewer/paragraph/1/2-deltaprogramma-/chapter/1-deltaplan-waterveiligheid/paragraph/1-hoogwaterbeschermingsprogramma

EurOtop. 2018. Manual on wave overtopping of sea defences and related structures. An overtopping manual largely based on European research, but for worldwide application. Van der Meer, J.W., Allsop, N.W.H., Bruce, T., De Rouck, J., Kortenhaus, A., Pullen, T., Schüttrumpf, H., Troch, P. and Zanuttigh, B., www.overtopping-manual.com.

Hofland, B., Diamantidou, E., van Steeg, P., & Meys, P. (2015). Wave runup and wave overtopping measurements using a laser scanner. Coastal Engineering. 106. 20–29. Retrieved from: https://doi.org/10.1016/j.coastaleng.2015.09.003

Hofland, B., I. Wenneker and M. van Gent (2013), Description of the new Delta Flume, Proc. Coastlines, Marine

Holman, R. A. (1986). Extreme value statistics for wave run-up on a natural beach. Coastal Engineering. 9(6). 527–544. Retrieved from: https://doi.org/10.1016/0378-3839(86)90002-5

Hughes, S. A., Thornton, C. I., Van der Meer, J. W., & Scholl, B. N. (2012). Improvements in Describing Wave Overtopping Processes. Coastal Engineering Proceedings. 1(33). Retrieved from: https://doi.org/10.9753/icce.v33.waves.35

Kalloe, S. A. (2019). “Wave damping potential of woody riparian vegetation” comparing terrestrial laser scanning with manual measurements. M.Sc. Thesis, TU Delft, Delft, The Netherlands

Peiris, D., & Wijetunga, J. (2005). Influence of Relative Water Depth on Wave Run-up Over Costal Structures; Smooth Slopes. Engineer, 38(3), 7-13.

Schüttrumpf, H. (2001). Wellenüberlaufströmung bei Seedeichen – Experimentelle und Theoretische Untersuchungen. TU Braunschweig, Leichtweiss Institu.

Schüttrumpf, H., Kortenhaus, A., Bruce, T., & Franco, L. (2009). Wave Run-Up and Wave Overtopping at Armored Rubble Slopes and Mounds. Handbook of Coastal and Ocean Engineering. 10.1142/9789812819307_0015.

SICK. (2011). LMS5xx Laser Measurement sensors operating instructions. Retrieved from https://cdn.SICK.com/media/docs/4/14/514/Operating_instructions_LMS5xx_LASER_MEASUREMENT_SENS.

Smale, A. J., & Borsboom, M. J. A. (2016). Vegetatie als maatregel voor benodigde reductie kruinhoogte. Deltares report 1220539-001-ZWS-0004, Version 2, November 2016

Stockdon, H. F., Holman, R. A., Howd, P. A., & Sallenger, A. H. (2006). Empirical parameterization of setup, swash, and runup. Coastal Engineering. 53(7). 573–588. Retrieved from: https://doi.org/10.1016/j.coastaleng.2005.12.005

TAW. (2002). Technical Report – Wave run-up and wave overtopping at dikes. Technical Advisory Committee for Flood Defence in the Netherlands (TAW). Delft.

Vuik,V., Jonkman, S.N., Borsje, W. B., Suzuki. T. (2016). Nature-based flood protection: The efficiency of vegetated foreshores for reducing wave loads on coastal dikes. Coastal Engineering. 116, 42-56, Retrieved from: https://doi.org/10.1016/j.coastaleng.2016.06.001.

Wolters, G., Van Wesenbeeck, B., (2018). WOODY- Large scale physical model tests of wave attenuation by willow trees. Deltares report 11202659-005-HYE-0001, Version 1, November 2018

9. Appendices

Appendix A - Test set-up previous research

The test set-up of the measurements conducted at the Heeseltsche Uiterwaarden are given (Stam, 2018).

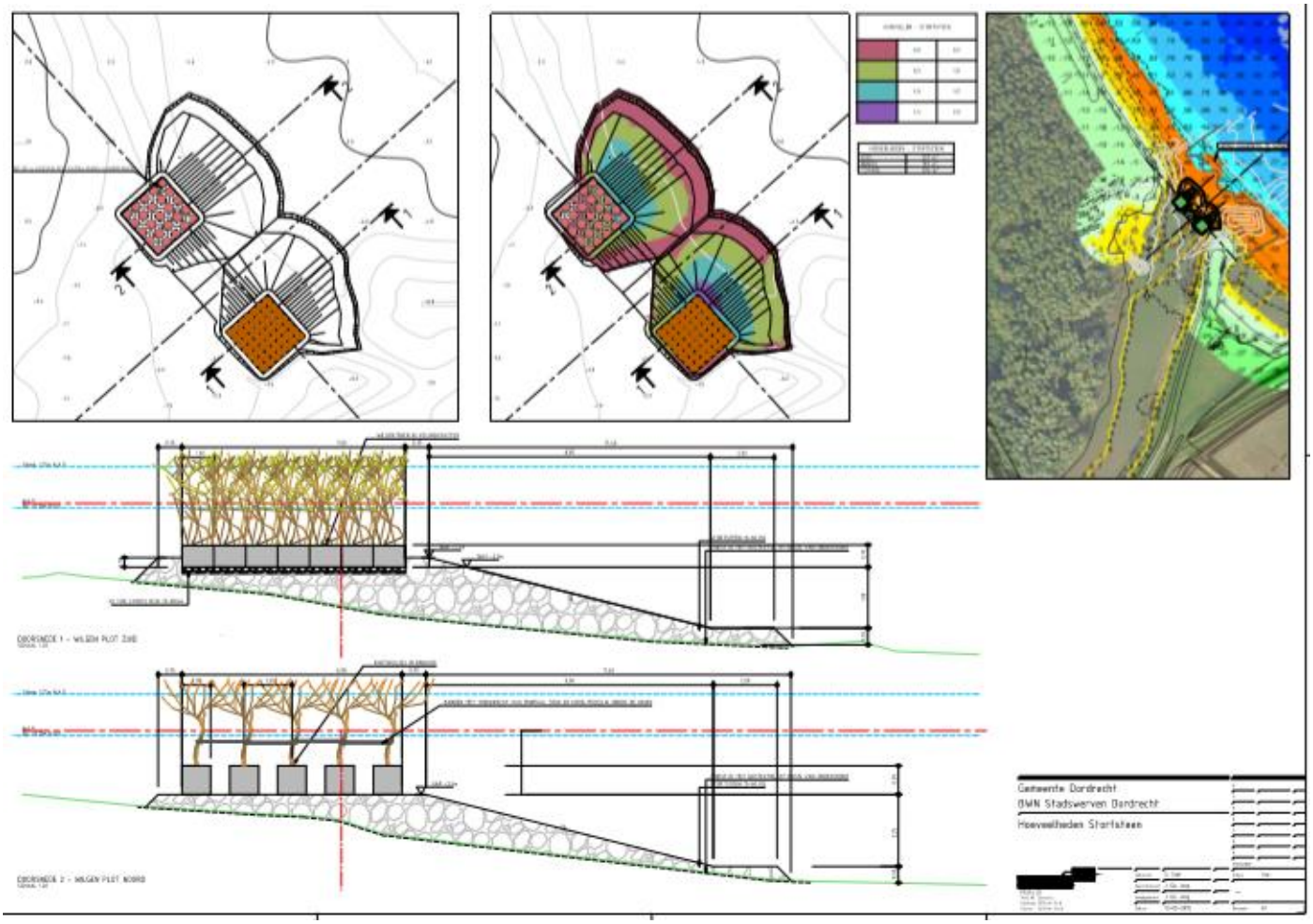

Figure A.62 Test set-up of the willows at the Heeseltsche Uiterwaarden (Stam, 2018)

Appendix B - Configuration willows

In the following figures the four different configurations of the trees in the flume are shown.

Figure B.1 Willows with leaves

Figure B.2 Willows with leaves from above

Figure B.3 Willows without leaves, 100% density

Figure B.4 The configuration in the flume during the reference tests, only a small part of the stem of the willows is left

Figure B.5 Willows 50% density

Appendix C – Biomass distribution

In the following table and graph the distribution of the frontal area of an average tree is given.

Table C.1 Frontal area of average tree with height of 5.3 m (Kalloe, 2019)

Height (m)	Norm height	Frontal area (%)
0 - 1	0	3
1 - 2	0.2	17
2 - 3	0.4	30
3 - 4	0.6	22
4 - 5	0.8	17
>5	1	11

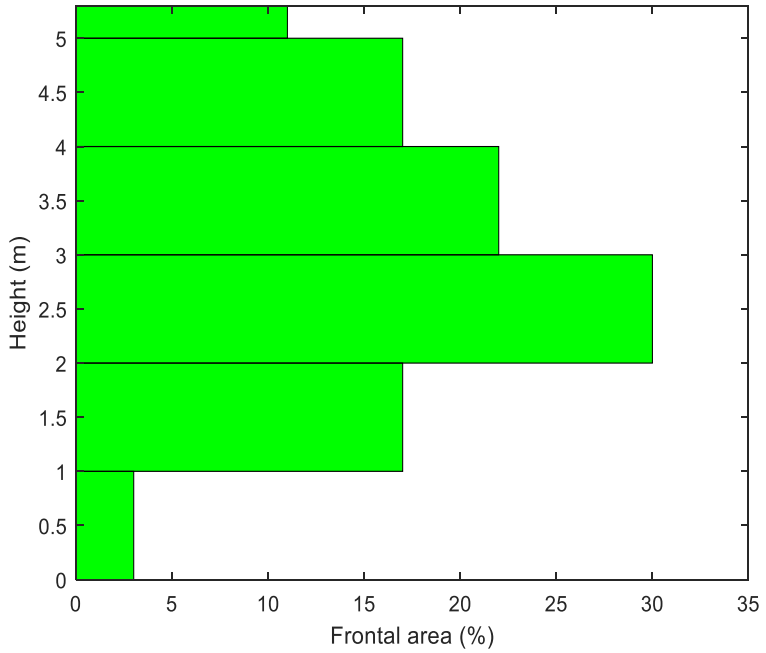

Figure C.1 Distribution of the frontal area over the height, taken for an average tree (Kalloe, 2019)

Appendix D – Coordinates lines on dike

In the following table the coordinates of the drawn lines from 0-65 on the slope of the dike are given. Here the z-coordinates are with respect to the bottom of the flume and the x-coordinate with respect to the wave board.

Table D.1 Coordinates lines on the dike slope

Number of line	Z [m]	X [m]
0	2,37	172,8
1	2,50	173,3
2	2,64	173,8
3	2,77	174,3
4	2,91	174,7
5	3,04	175,1
6	3,17	175,6
7	3,31	176,1
8	3,44	176,6
9	3,58	177,1
10	3,71	177,5
11	3,84	178,0
12	3,98	178,5
13	4,11	179,0
14	4,24	179,5
15	4,38	180,0
16	4,51	180,5
17	4,65	180,9
18	4,78	181,4
19	4,91	181,9
20	5,05	182,4
21	5,18	182,9
22	5,32	183,3
23	5,45	183,9
24	5,58	184,4
25	5,72	184,9
26	5,85	185,3
27	5,99	185,7
28	6,12	186,2
29	6,25	186,7
30	6,39	187,2
31	6,52	187,7
32	6,65	188,2
33	6,79	188,7

34	6,92	189,1
35	7,06	189,6
36	7,19	190,1
37	7,32	190,6
38	7,48	191,0
39	7,64	191,5
40	7,79	192,0
41	7,95	192,4
42	8,10	193,0
43	8,26	193,4
44	8,42	193,9
45	8,57	194,4
46	8,73	194,9
47	8,88	195,3
48	9,04	195,8
49	9,20	196,3
50	9,35	196,7
51	9,51	197,2
52	9,67	197,7
53	9,82	198,1
54	9,98	198,6
55	10,13	199,1
56	10,29	199,5
57	10,45	200,0
58	10,60	200,5
59	10,76	200,9
60	10,91	201,4
61	11,07	201,9
62	11,23	202,3
63	11,38	202,8
64	11,54	203,3
65	11,69	203,8

Appendix E – Comparison tests

In this appendix the tests with the same steering files are shown, with their wave conditions and configurations. ***The wave conditions given, are the conditions measured at the start of the foreshore (in front of the forest) at WHM 6.***

Table E.1 Comparison tests with same steering file. ****T041 and T042 are repetition tests executed without protection nets.***

Number	Wave conditions			Configuration in the flume			
	h [m]	Hm0	Tm-1,0	100% density with leaves	100 % density without leaves	50% density	Reference test
1.	3.00	0.48	2.75	T005	T013	T023	T033
2.	3.00	0.99	3.95	T006			T034
3.	3.00	0.65	3.60		T014	T024	
4.	3.00	0.50	3.80	T007	T015	T025	T035
5.	3.00	1.03	5.10	T008	T016	T026	T036
6.	4.50	0.45	2.80	T009	T017		
7.	4.50	0.94	3.83	T010	T018	T027	
8.	4.50	0.48	3.80	T011	T019		
9.	4.50	1.01	5.40	T012	T020	T028	
10.	4.50	1.43	4.70		T021	T029	T037 / T041*
11.	4.50	1.48	6.00		T022	T030	T038/ T042 *
12.	0.60	0.17	1.90	T001			T031
13.	0.60	0.20	2.70	T002			T032
14.	0.70	0.20	2.10	T003			T039
15.	0.70	0.23	2.90	T004			T040

Appendix F - Instrumentation

The coordinates of the measuring instruments in the flume are given.

Table F.1 Coordinates of the different instrumentation in the flume (Deltares, 2018)

Instrument	x	Y	z
WHM 1	40.5	0	1.5-9.5
WHM 2	43.5	0	1.5-9.5
WHM 3	49.5	0	1.5-9.5
WHM 6	96.5	0	1.5-9.5
RADAC 2	157.70	2.5	11.8
SICK laser scanner	193	0.3	13.3

Appendix G – Hydraulic conditions

Here the hydraulic conditions in front and behind the willow forest are given.

Table G.1 Hydraulic conditions of the tests in front of the forest. Based on measured incident values (WHM 6, located on the foreshore in front of the forest). The measured values of the WHM6 are corrected using the RADAC 1 measurements

Test-ID	Configuration	h (m)	H_{m0} (m)	T_p (s)	$T_{m-1,0}$ (s)
T001	Leaves	0.6	0.17	1.8	1.9
T002	Leaves	0.6	0.20	2.56	2.7
T003	Leaves	0.7	0.20	2.06	2.1
T004	Leaves	0.7	0.23	2.82	2.9
T005	Leaves	3.0	0.49	2.80	2.8
T006	Leaves	3.0	1.01	4.19	3.9
T007	Leaves	3.0	0.52	4.18	3.8
T008	Leaves	3.0	1.07	5.62	5.1
T009	Leaves	4.5	0.46	2.74	2.8
T010	Leaves	4.5	0.96	4.19	3.8
T011	Leaves	4.5	0.49	4.19	3.8
T012	Leaves	4.5	1.03	5.67	5.4
T013	Without leaves	3.0	0.46	2.75	2.7
T014	Without leaves	3.0	0.95	3.49	3.6
T015	Without leaves	3.0	0.49	4.18	3.8
T016	Without leaves	3.0	0.99	5.65	5.1
T017	Without leaves	4.5	0.43	2.75	2.8
T018	Without leaves	4.5	0.91	4.20	3.9
T019	Without leaves	4.5	0.46	4.19	3.8
T020	Without leaves	4.5	0.98	5.71	5.4
T021	Without leaves	4.5	1.41	4.40	4.7
T022	Without leaves	4.5	1.47	5.97	6.0
T023	Without leaves, 50 % branch density	3.0	0.49	2.75	2.8
T024	Without leaves, 50 % branch density	3.0	0.98	3.49	3.6
T025	Without leaves, 50 % branch density	3.0	0.50	4.19	3.8
T026	Without leaves, 50 % branch density	3.0	1.03	5.62	5.1
T027	Without leaves, 50 % branch density	4.5	0.94	4.20	3.9
T028	Without leaves, 50 % branch density	4.5	1.01	5.66	5.3
T029	Without leaves, 50 % branch density	4.5	1.45	4.39	4.7
T030	Without leaves, 50 % branch density	4.5	1.51	5.97	6.0
T031	Calibration, without willows	0.6	0.17	1.83	1.9
T032	Calibration, without willows	0.6	0.20	2.56	2.7
T033	Calibration, without willows	3.0	0.46	2.75	2.7
T034	Calibration, without willows	3.0	0.97	4.20	4.0
T035	Calibration, without willows	3.0	0.50	4.19	3.8
T036	Calibration, without willows	3.0	1.02	5.63	5.1
T037	Calibration, without willows	4.5	1.44	4.40	4.8
T038	Calibration, without willows	4.5	1.47	5.98	6.0
T039	Calibration, without willows	0.7	0.20	2.06	2.1
T040	Calibration, without willows	0.7	0.23	2.82	2.9
T041	Calibration, without willows	4.5	1.38	4.40	4.7
T042	Calibration, without willows	4.5	1.42	5.98	6.0

Table G.2 Hydraulic conditions behind the forest/in front of the dike. Incoming wave conditions from RADAC 2

Test-ID	Configuration	h [m]	H_{m0} [m]	T_p [s]	$T_{m-1.0}$ [s]
T001	*Leaves*	*0.6*	0.14	4.18	3.87
T002	*Leaves*	*0.6*	0.17	5.76	5.44
T003	*Leaves*	*0.7*	0.18	2.77	2.76
T004	*Leaves*	*0.7*	0.23	3.62	3.68
T005	*Leaves*	*3.0*	0.37	4.18	3.76
T006	*Leaves*	*3.0*	0.68	4.21	3.99
T007	*Leaves*	*3.0*	0.36	4.18	3.79
T008	*Leaves*	*3.0*	0.75	5.95	5.59
T009	*Leaves*	*4.5*	0.35	2.79	2.80
T010	*Leaves*	*4.5*	0.77	4.18	3.88
T011	*Leaves*	*4.5*	0.40	4.18	3.87
T012	*Leaves*	*4.5*	0.80	5.76	5.44
T013	*Without leaves*	*3.0*	0.33	2.77	2.76
T014	*Without leaves*	*3.0*	0.72	3.62	3.68
T015	*Without leaves*	*3.0*	0.37	4.18	3.76
T016	*Without leaves*	*3.0*	0.77	5.93	5.53
T017	*Without leaves*	*4.5*	0.38	2.79	2.75
T018	*Without leaves*	*4.5*	0.80	4.18	3.85
T019	*Without leaves*	*4.5*	0.41	4.18	3.85
T020	*Without leaves*	*4.5*	0.82	5.79	5.47
T021	*Without leaves*	*4.5*	1.26	4.42	4.78
T022	*Without leaves*	*4.5*	1.36	6.15	6.10
T023	*Without leaves, 50 % branch density*	*3.0*	0.36	2.78	2.73
T024	*Without leaves, 50 % branch density*	*3.0*	0.77	3.62	3.66
T025	*Without leaves, 50 % branch density*	*3.0*	0.39	4.17	3.71
T026	*Without leaves, 50 % branch density*	*3.0*	0.83	5.93	5.54
T027	*Without leaves, 50 % branch density*	*4.5*	0.83	4.17	3.86
T028	*Without leaves, 50 % branch density*	*4.5*	0.85	5.76	5.43
T029	*Without leaves, 50 % branch density*	*4.5*	1.30	4.42	4.77
T030	*Without leaves, 50 % branch density*	*4.5*	1.41	6.14	6.08
T031	*Calibration, without willows*	*0.6*	0.15	1.83	1.74
T032	*Calibration, without willows*	*0.6*	0.17	2.93	2.85
T033	*Calibration, without willows*	*3.0*	0.40	2.76	2.71
T034	*Calibration, without willows*	*3.0*	0.87	4.20	3.94
T035	*Calibration, without willows*	*3.0*	0.44	4.17	3.72
T036	*Calibration, without willows*	*3.0*	0.96	5.88	5.43
T037	*Calibration, without willows*	*4.5*	1.39	4.45	4.83
T038	*Calibration, without willows*	*4.5*	1.50	6.13	6.09
T039	*Calibration, without willows*	*0.7*	0.18	1.99	2.00
T040	*Calibration, without willows*	*0.7*	0.20	3.19	3.09
T041	*Calibration, without willows*	*4.5*	1.36	4.44	4.80
T042	*Calibration, without willows*	*4.5*	1.50	6.14	6.12

Appendix H – Laser measuring line

The line over which the laser measures is determined during the calibration test, by placing an object on the slope until it disappears on the scan, from there the distance till the wall is measured. This has been evaluated for different lines on the slope

Table H.1 The line over which the laser scans, measured during the calibration

# Line	Distance to the wall (where scanner is situated) [m]
65	3.02
60	2.88
50	2.60
40	2.33
37 *	2.22
30	1.95
20	1.57
10	1.19
1	0.85

* At line 37 the slope angle changes from 1:3.6 at the lower part of the dike to 1:3 at the upper part of the dike.

Figure H.1 Slope of the dike in the delta flume with the painted lines (Source: Deltares, 2018).

Appendix I – PC-Overtopping

To determine the $\xi_{m-1,0}$ the tool PC-overtopping is used. The dike slope contains two different slope angles. Therefore, iteration is needed to find a representative tan(α) for each test.

$$\xi_{m-1.0} = \frac{\tan(\alpha)}{\sqrt{s_{m-1.0}}}. \text{ where } s_{m-1.0} = \frac{H_{m0}}{L_{m-1.0}} \text{ and } L_{m-1.0} = \frac{gT_{m-1.0}^2}{2\pi}$$

The dike profile inserted into the program is shown in Table I.1.

Table I.1 Slope characteristics into Pc-overtopping

Section	X begin	Y begin	X end	Y end	Slope (tan)	Material	Roughness factor
1	172.500	2.330	190.550	7.330	0.277	Own input	1.000
2	190.550	7.330	204.000	11.750	0.329	Own input	1.000

The inserted parameters to obtain results are shown in Table I.2 for test T006. The wave conditions given are the conditions behind the willow forest (WHM 6).

Table I.2 Input parameters

parameter	symbol	value	unit
Significant wave height	Hm0	0.680	[m]
Wave direction	β	0.000	°
Storm duration	tsm	1750.00	[s]
Water level	SWL	5.330	[m]
Average period	Tm	3.990	[s]
Spectral wave period	◉ Tm-1,0	3.990	[s]
Spectral peak period	○ Tp	4.389	[s]

For test T006 the result is given in Figure I.1. The result is obtained after conducting three iterations.

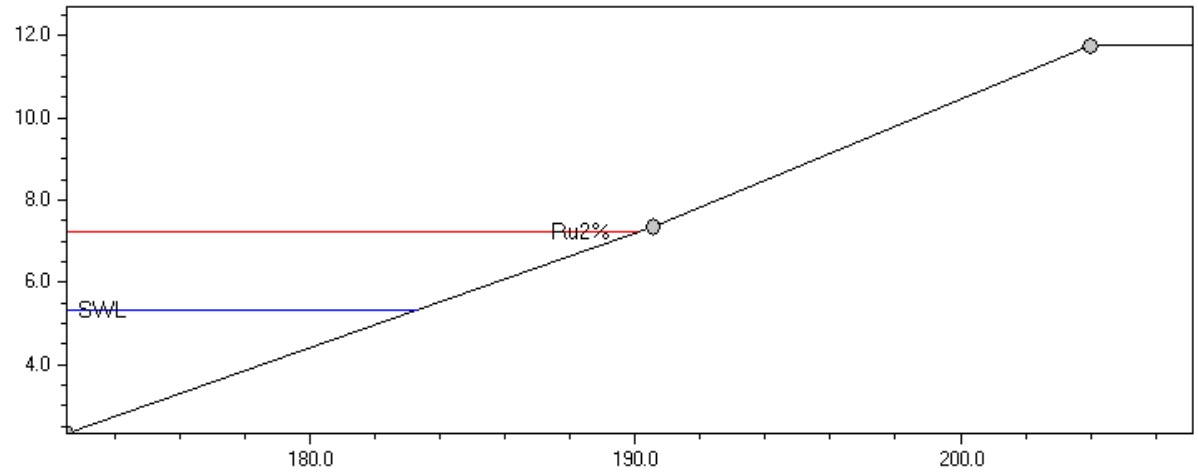

Figure I.1 Calculated run-up for test T006

For the tests in which the $R_{u2\%}$ stays below the slope transition, the representative tan(α) equals 0.278 and for tests in which the $R_{u2\%}$ is above this transition a value of maximum 0.305 is found.

Appendix J – Data processing

The results, obtained by the laser scanner for test T012, for different interpolation distances and layer thickness thresholds are shown in Table J.1.

Table J.1 The 2% exceeded run-up height determined with the laser using different threshold values on the water layer thickness Z. Where pmin is the minimum point distance measured by the laser.

Point distance	$Ru_{2\%\_Z=1cm}$	$Ru_{2\%\_Z=1.5\ cm}$	$Ru_{2\%\_Z=2\ cm}$	$Ru_{2\%\_Z=3\ cm}$	$Ru_{2\%\_RSSI}$
1*pmin	2.8817	2.7917	2.7287	2.6277	
3*pmin	2.8320	2.7800	2.7290	2.6280	
5*pmin	2.8313	2.7743	2.7173	2.6053	3.0876

Appendix K – Visual measurement

This appendix shows the probability of exceedance distributions for the different comparison tests. The wave conditions given are average incident values measured by WHM6 of the tests executed with the same steering file. The range of the TAW 2002 are based on the incoming wave conditions in front of the dike. Also, several plots are shown, comparing tests with different water levels and different wave steepness.

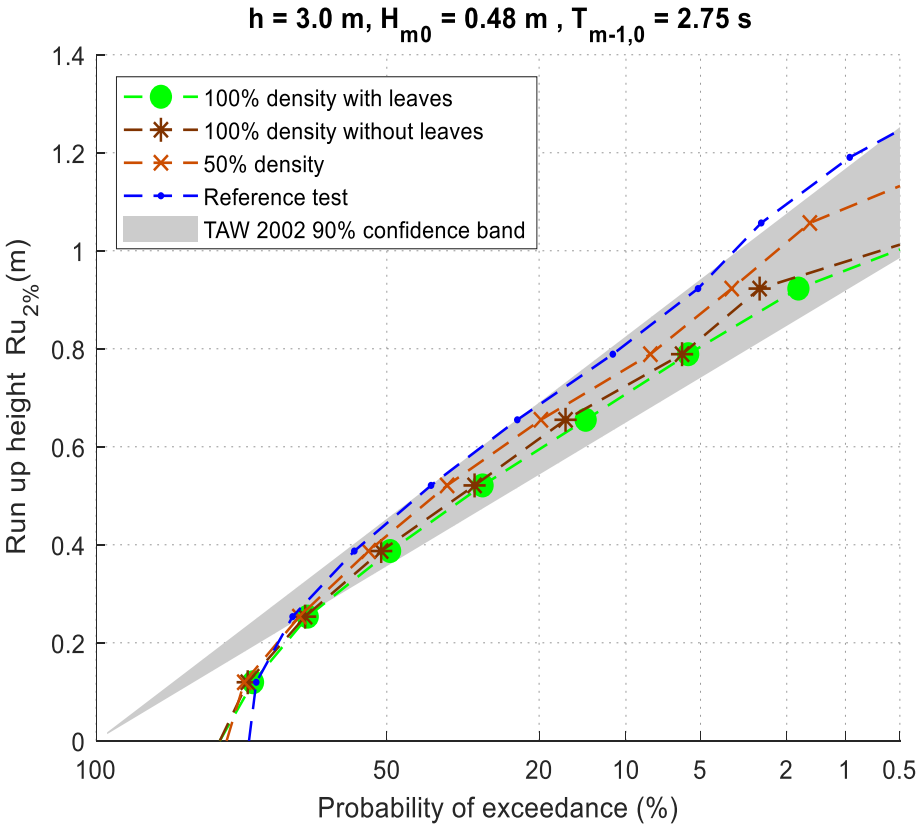

Figure K.1 Comparison 1: T005 - T013 - T023 - T033

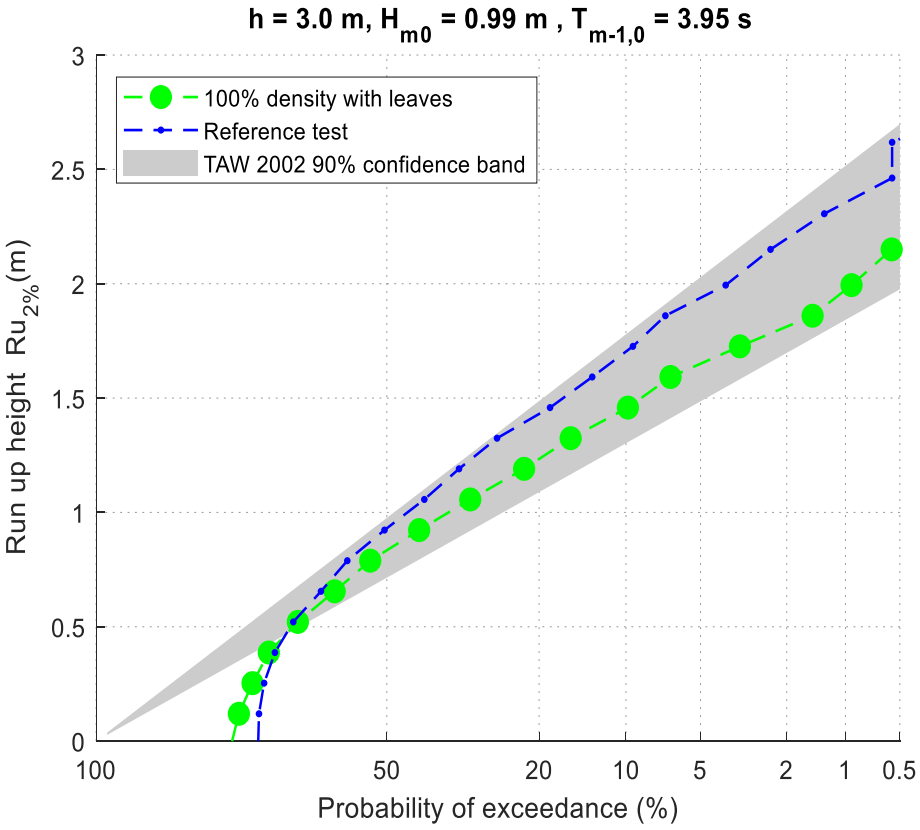

Figure K.2 Comparison 2: T006 - T034

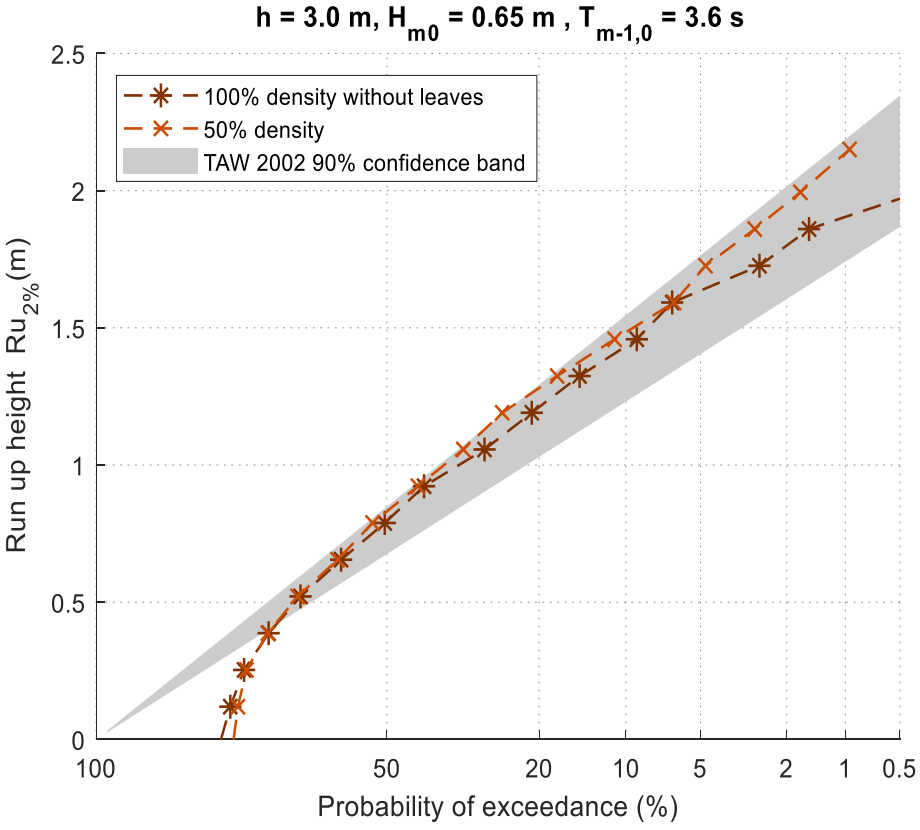

Figure K.3 Comparison 3 : T014 - T024

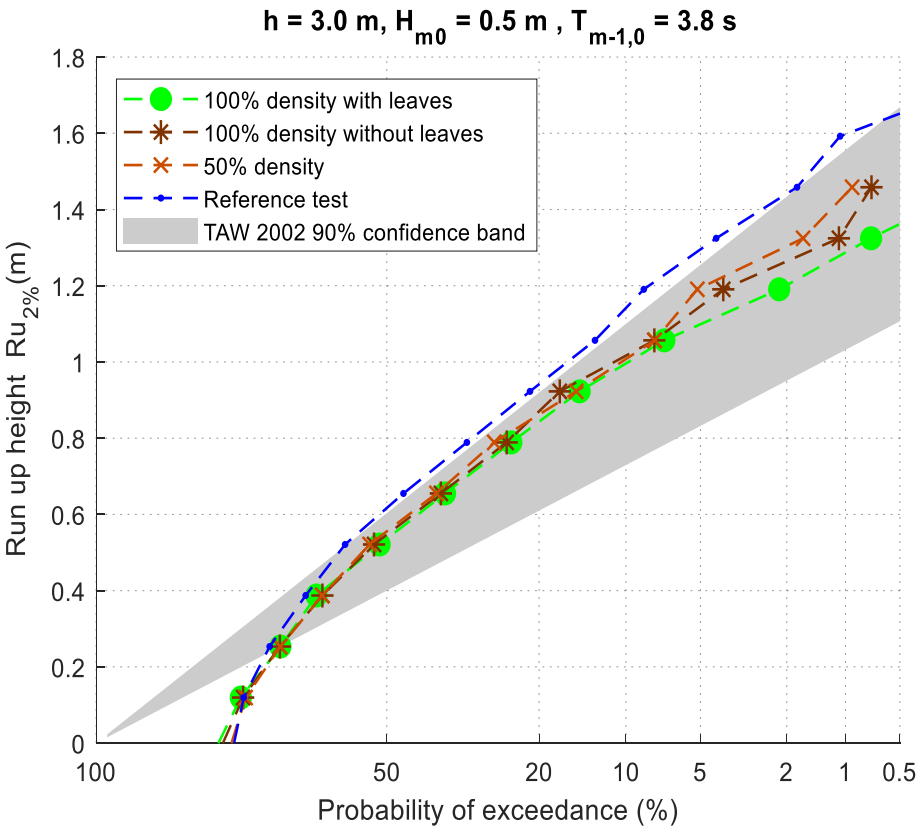

Figure K.4 Comparison 4 : T007 - T015 - T025 - T035

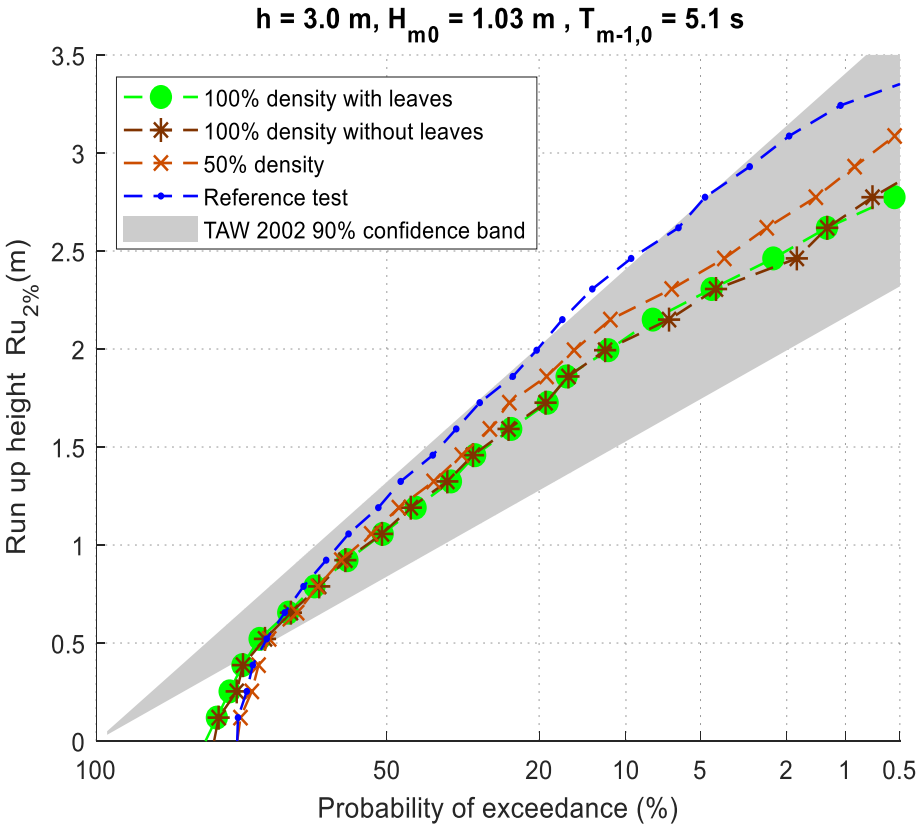

Figure K.5 Comparison 5 : T008 - T016 - T026- T036

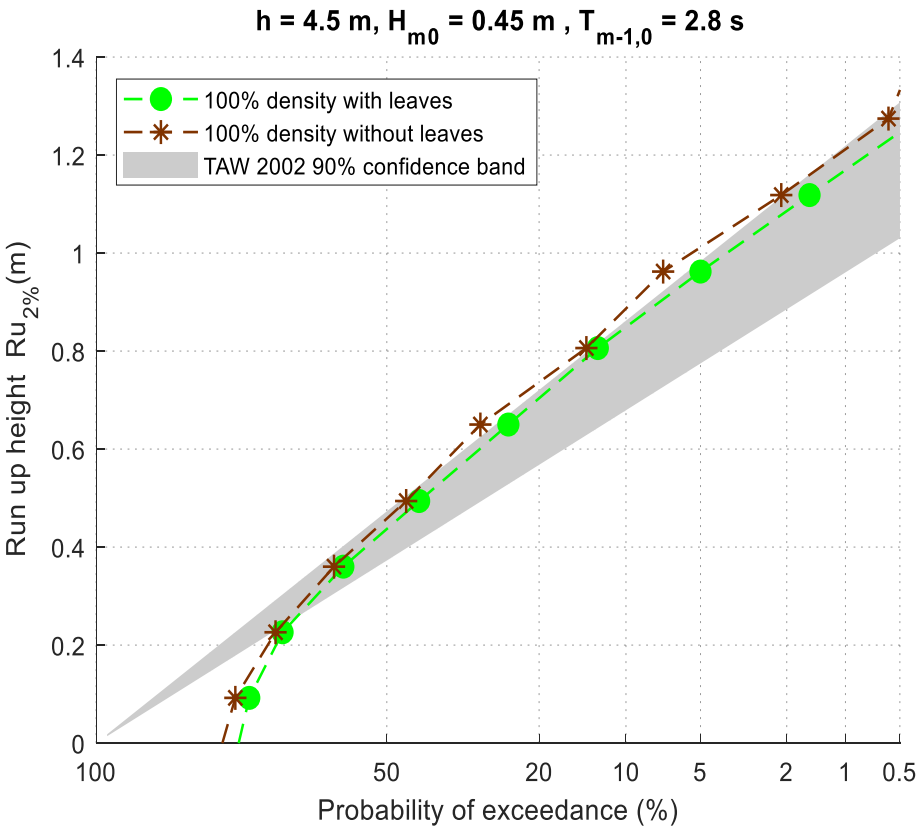

Figure K.6 Comparison 6 : T009 - T017

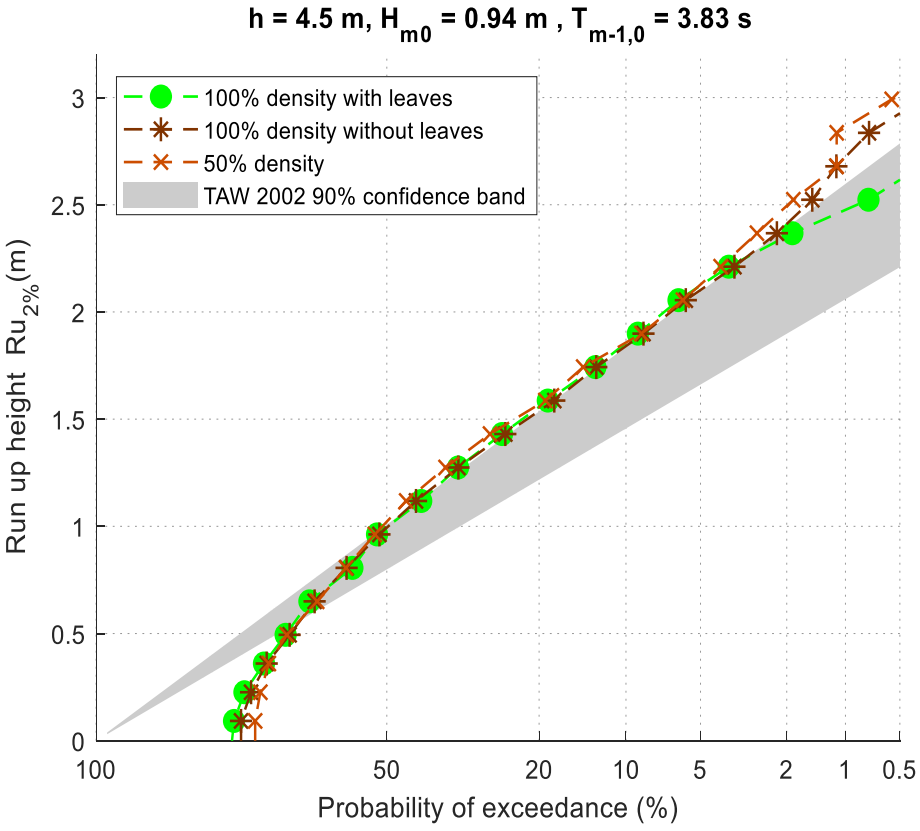

Figure K.7 Comparison 7 : T010 - T018 - T027

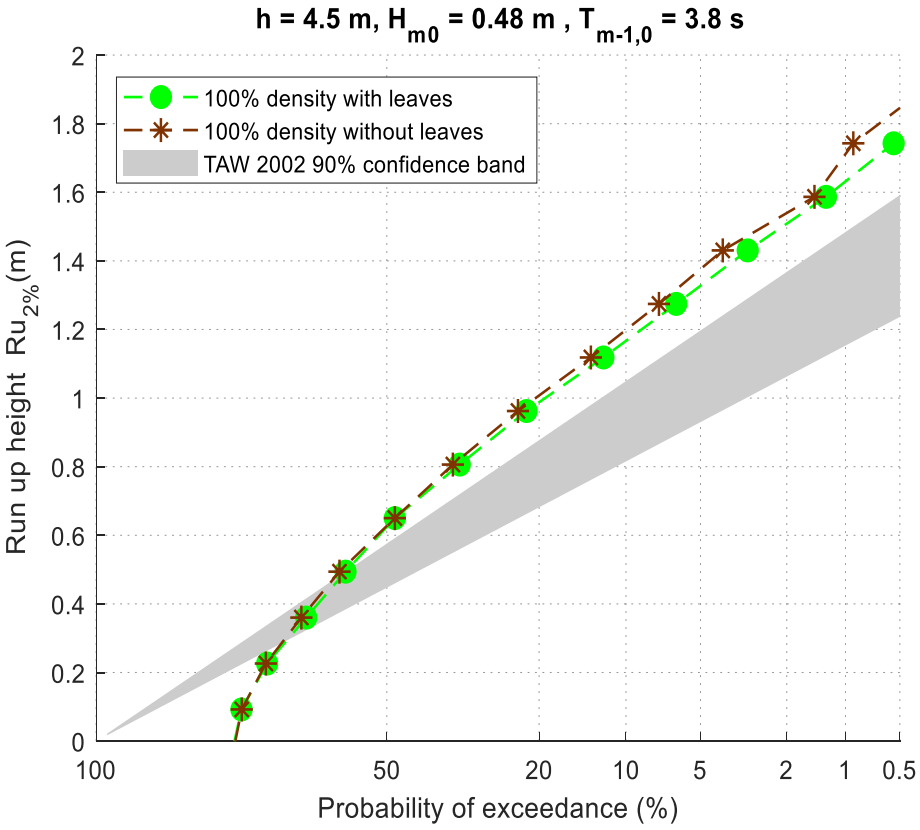

Figure K.8 Comparison 8 : T011 - T019

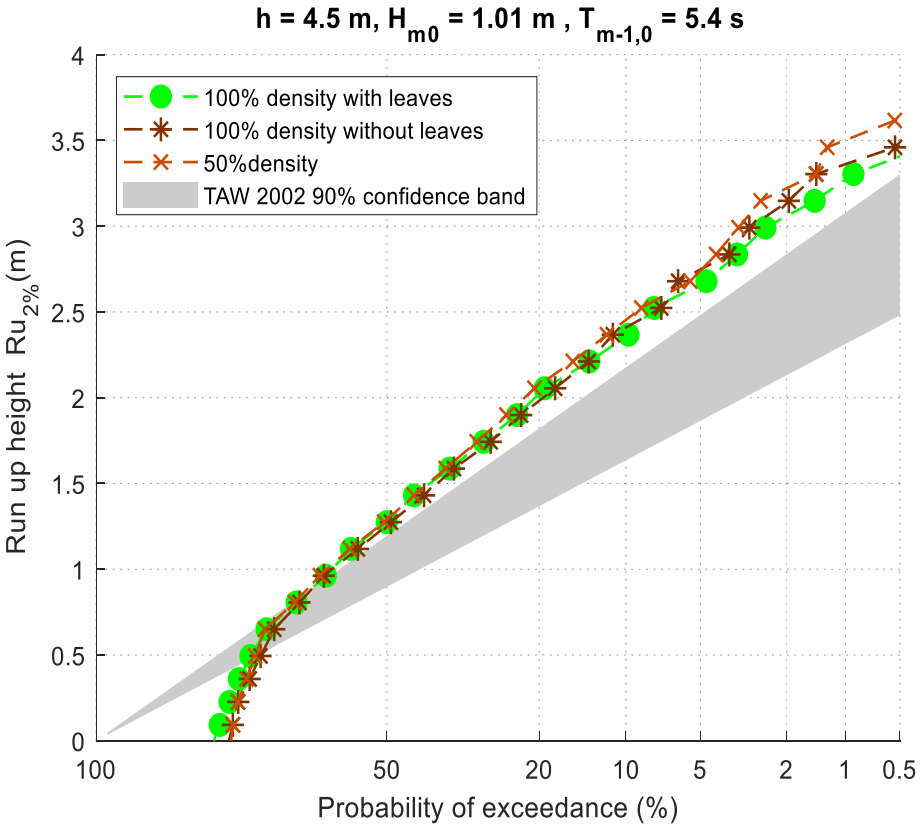

Figure K.9 Comparison 9 : T012 - T020 - T028

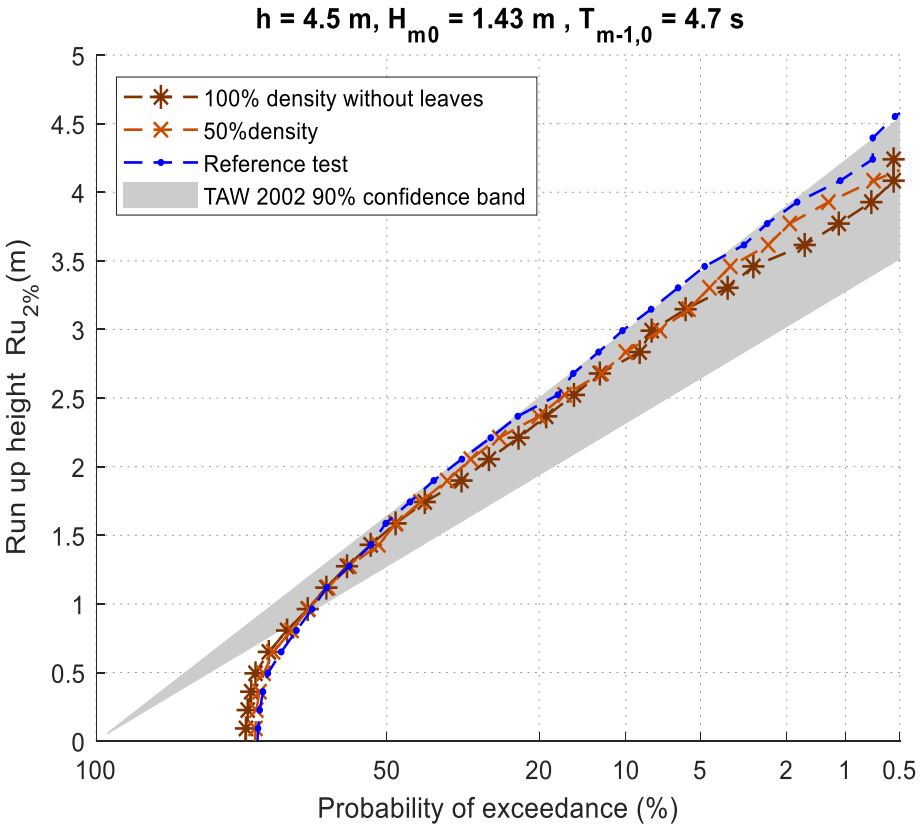

Figure K.10 Comparison 10 : T021 - T029 - T037

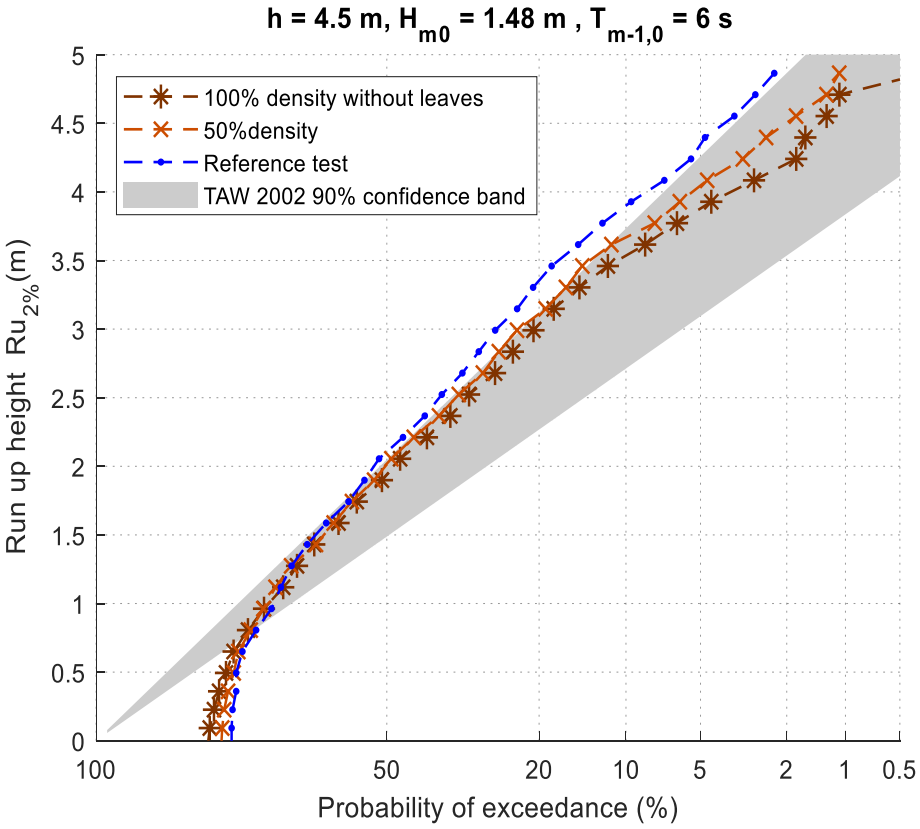

Figure K.11 Comparison 11 : T022 - T030 - T038

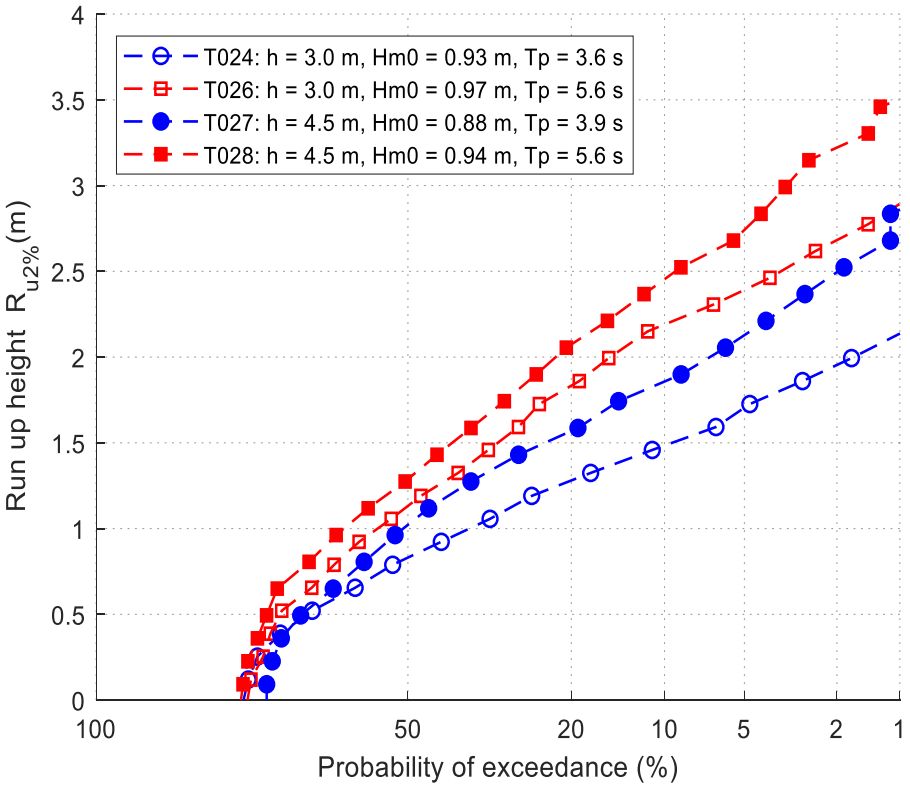

Figure K.12 Comparison run-up height for different tests, willows 50 % density. Wave conditions are at the wave board.

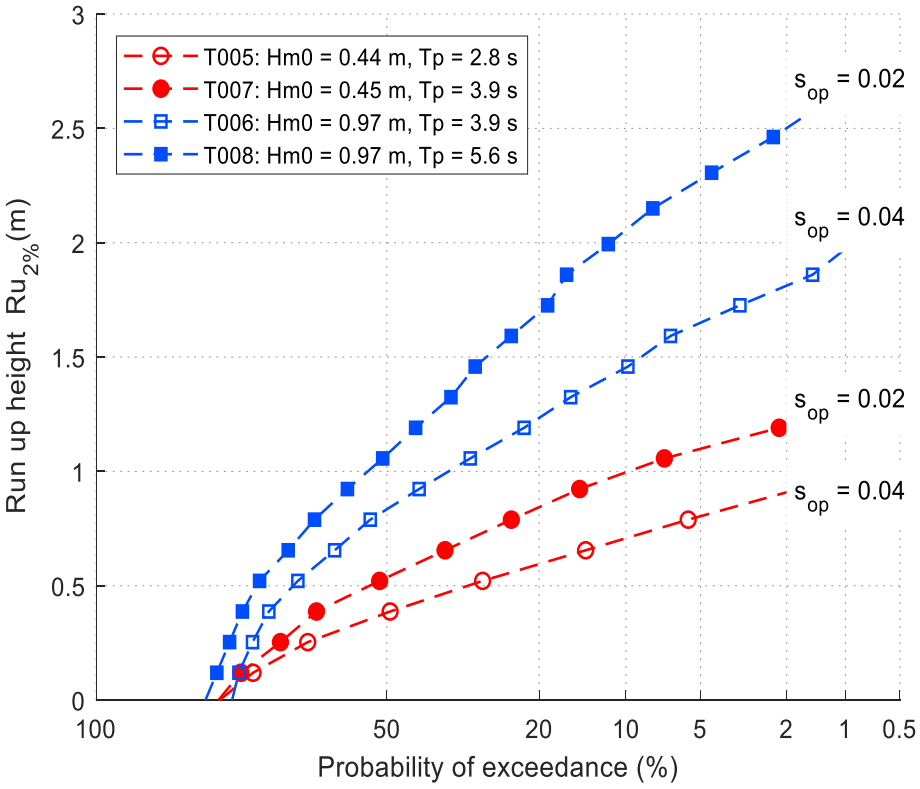

Figure K.13 Comparison tests willows with leaves, mid water level: h = 3.0 m. Wave conditions are at the wave board.

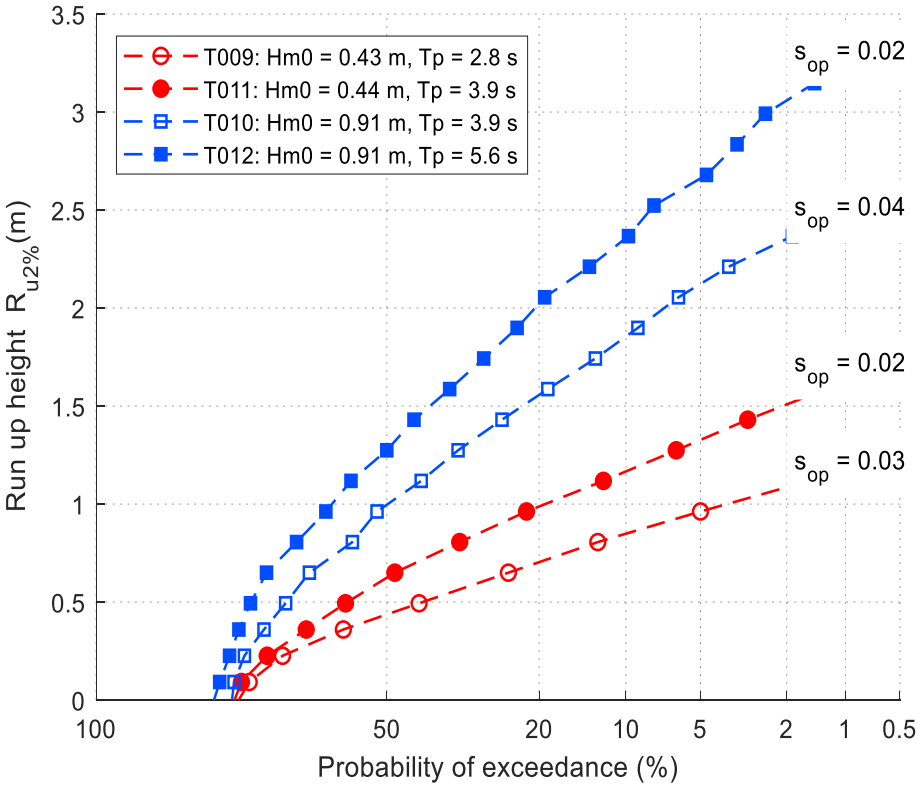

Figure K.14 Comparison tests willows with leaves, high water level: h = 4.5 m. Wave conditions are at the wave board.

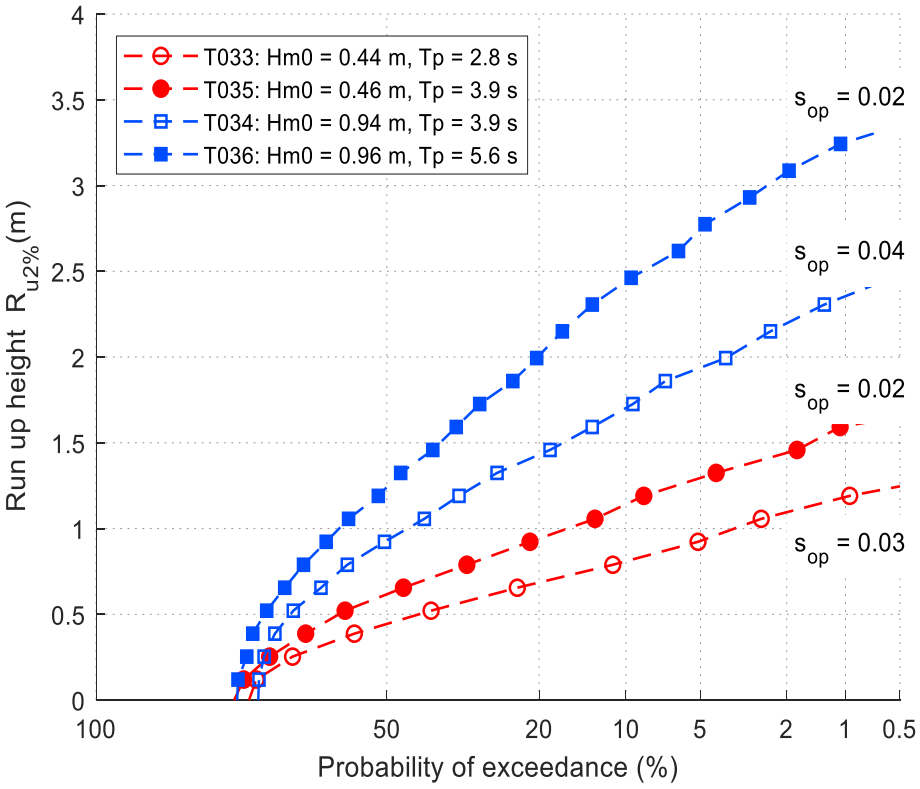

Figure K.15 Comparison reference test for different steepness and wave heights, at mid water level: h = 3.0 m. Wave conditions are at the wave board.

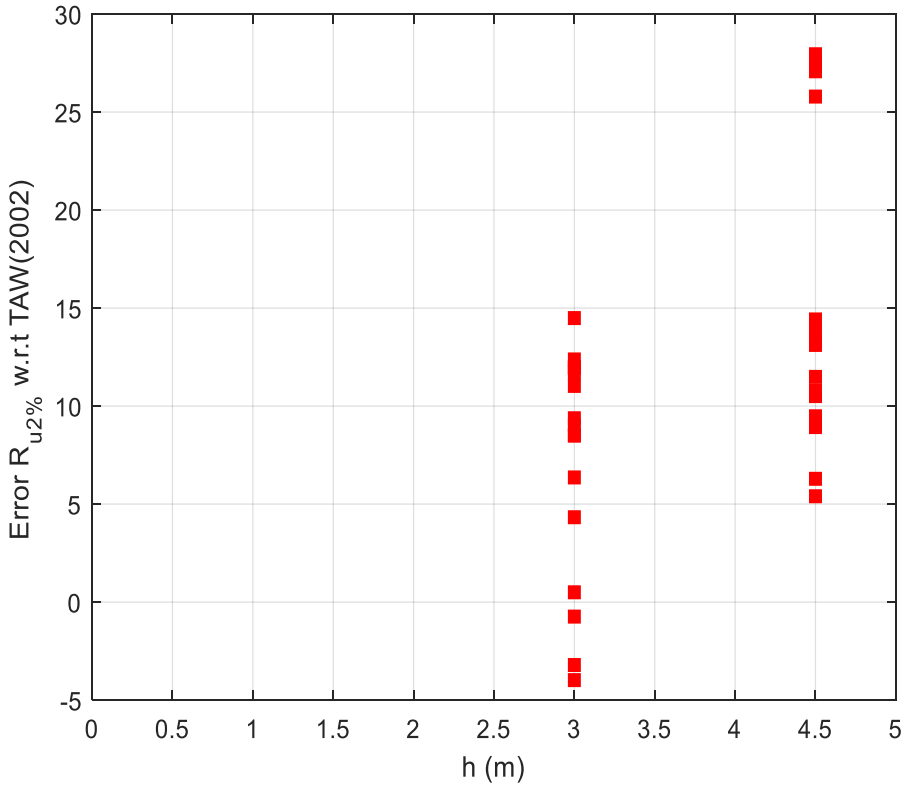

Figure K.16 Difference between the visual measured run-up and the TAW (2002) plotted against the water depth.

Appendix L – Flotsam measurements

During the visual measurements the highest line on the dike reached by debris is listed for each test. The results are given in the Table L.1, together with the highest observed run-up by visual measurement.

Table L.1 Flotsam observations with highest observed run-up during visual measurement

Test-ID	Flotsam observed between	Highest observed run-up
T006	38-39	38
T007	33-34	33
T008	42-43	45
T009	44-45	44
T010	54-55	54
T014	38-39	38
T016	43-44	44
T017	44-45	45
T018	54-55	56
T023	31-32	32
T024	39-40	38
T025	34-35	33
T026	45-46	45
T027	53-54	55
T033	32-33	32
T034	40-41	42
T035	37-38	37

Appendix M - Camera measurements

In this appendix, probability of exceedance distributions determined by the camera measurements are shown. Also, the graphs for the variation of the $R_{u2\%}$ over the width of the flume for the different tests are given.

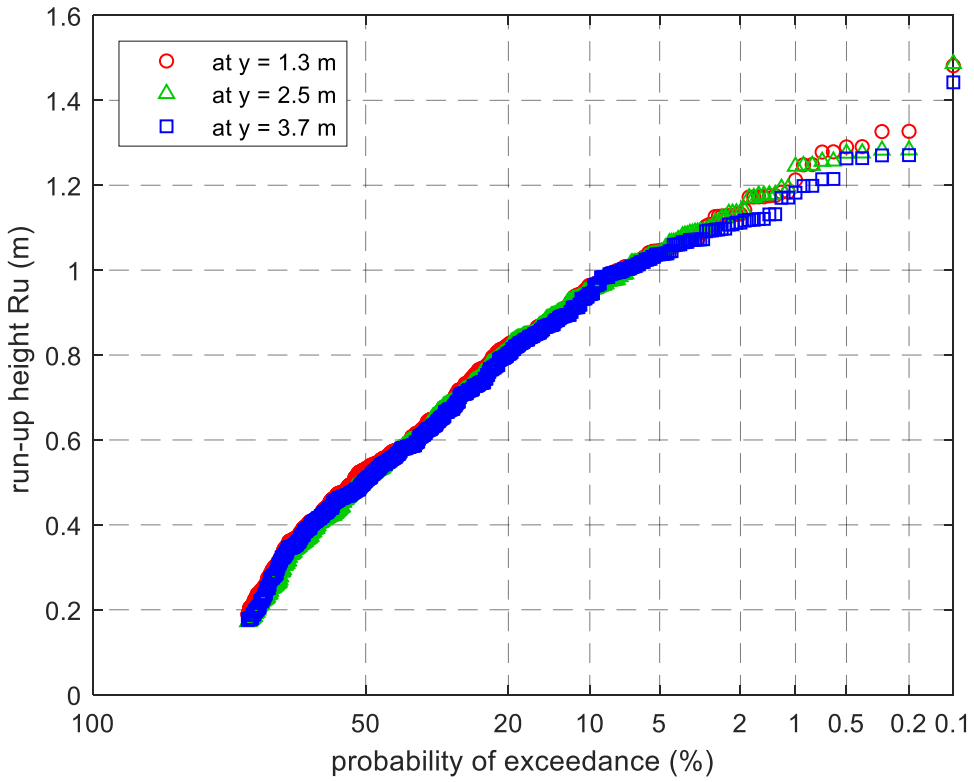

Figure M.1 Probability of exceedance distribution for test T007, with wave conditions in front of the dike: h = 3.0 m, H_{m0} = 0.36 m, $T_{m-1.0}$ = 3.79 s

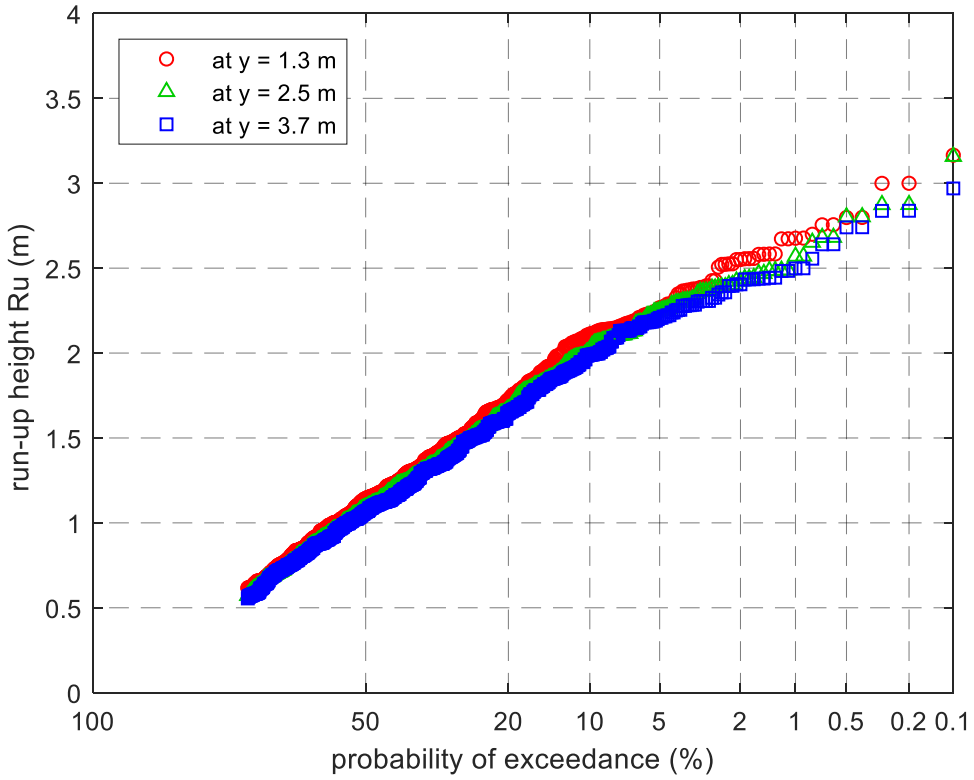

Figure M.2 Probability of exceedance distribution for test T008, with wave conditions in front of the dike: h = 3.0 m, H_{m0} = 0.75 m, $T_{m-1.0}$ = 5.59

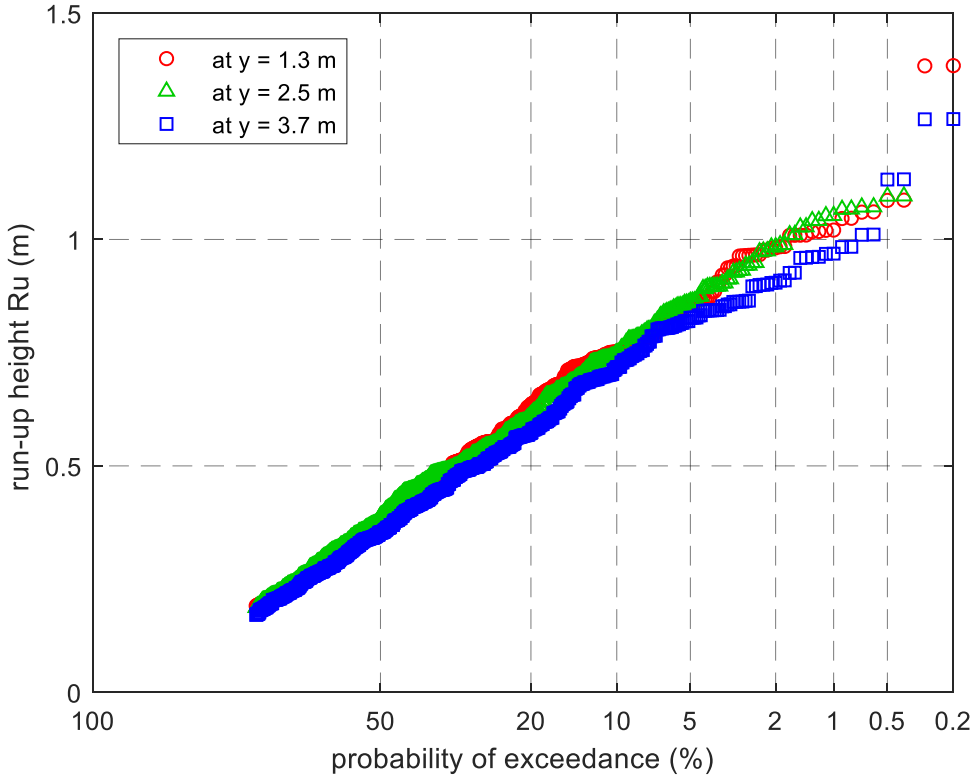

Figure M.3 Probability of exceedance distribution for test T009, with wave conditions in front of the dike: h = 4.5 m, H_{m0} = 0.35 m, $T_{m-1.0}$ = 2.8 s

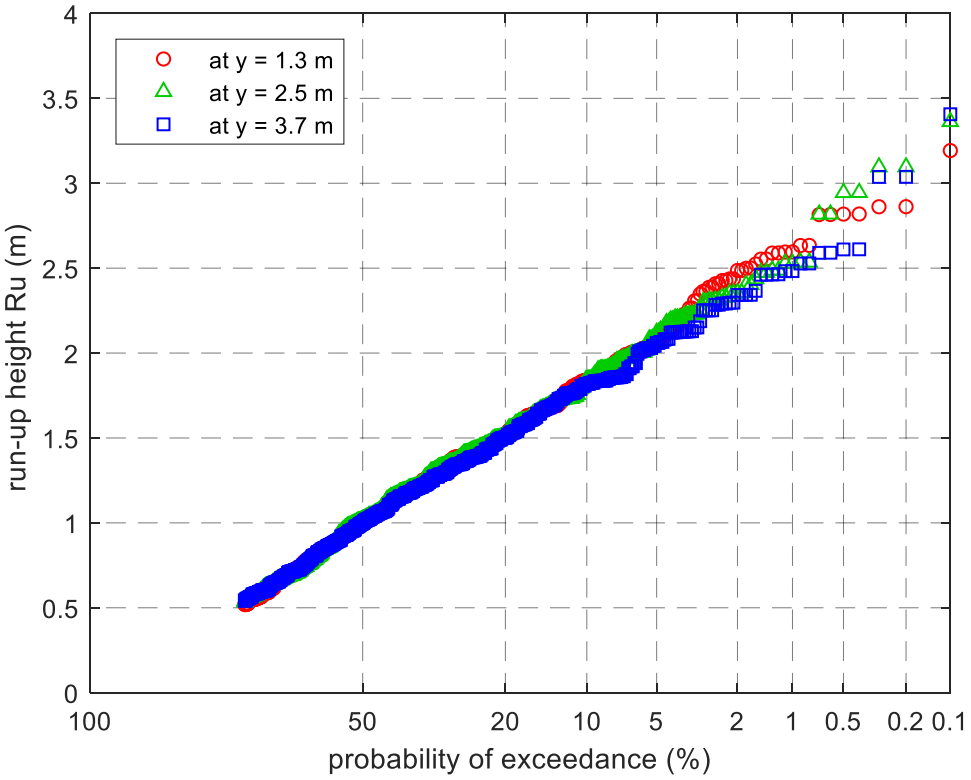

Figure M.4 Probability of exceedance distribution for test T010, with wave conditions in front of the dike: h = 4.5 m, H_{m0} = 0.77 m, $T_{m-1.0}$ = 3.88 s

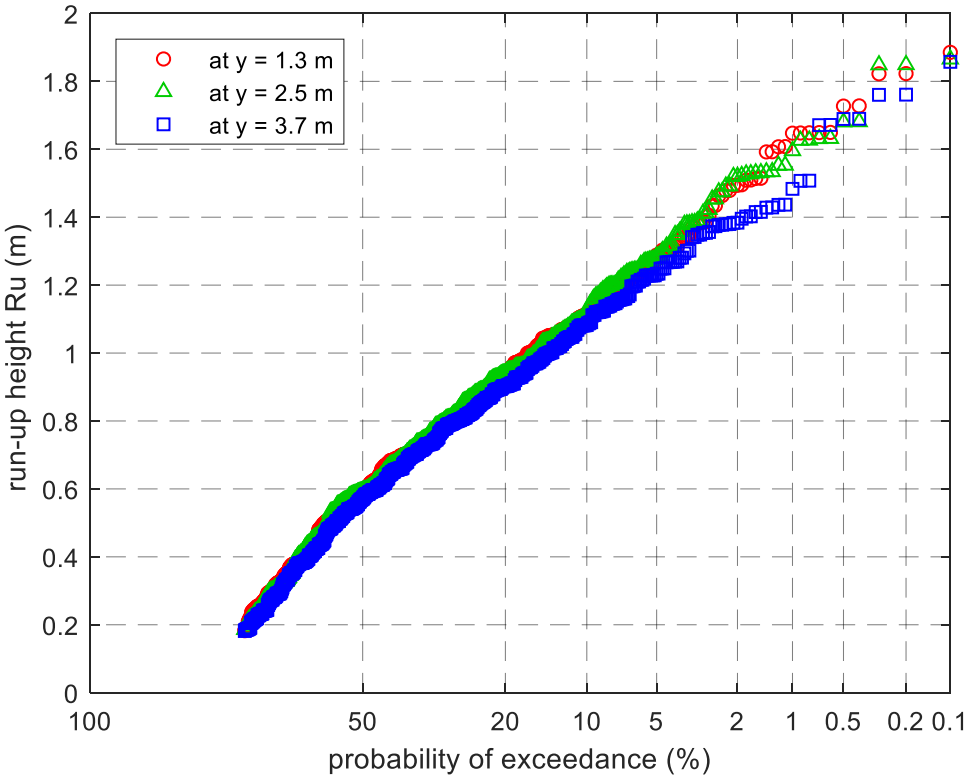

Figure M.5 Probability of exceedance distribution for test T011, with wave conditions in front of the dike: h = 4.5 m, H_{m0} = 0.40 m, $T_{m-1.0}$ = 3.87 s

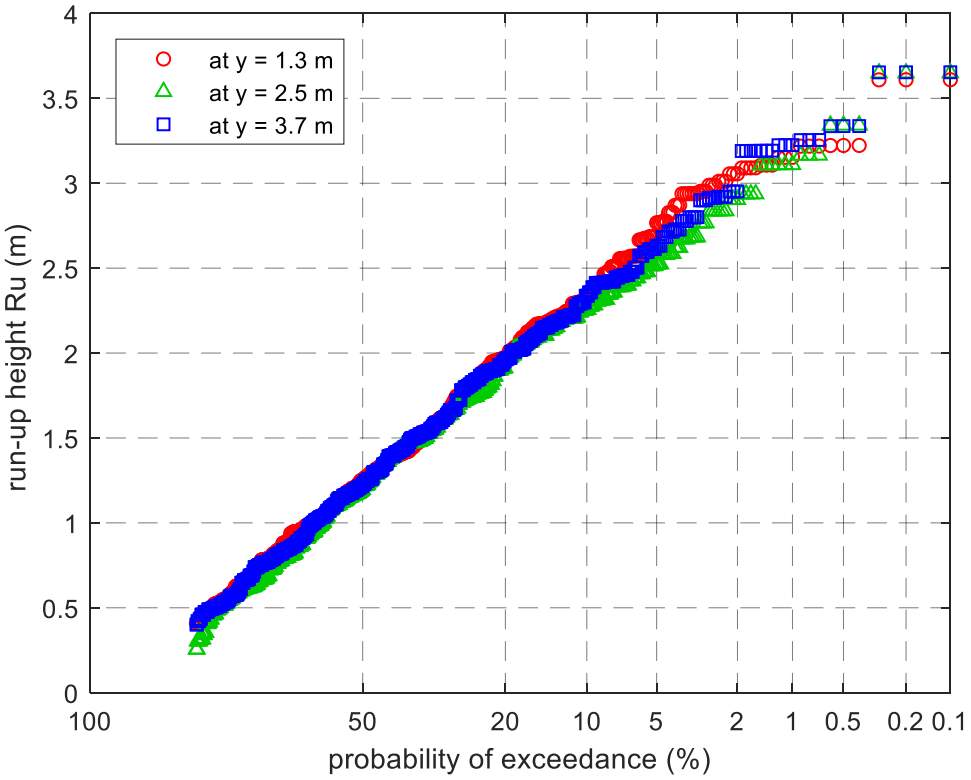

Figure M.6 Probability of exceedance distribution for test T012, with wave conditions in front of the dike: h = 4.5 m, H_{m0} = 0.80 m, $T_{m-1.0}$ = 5.44 s

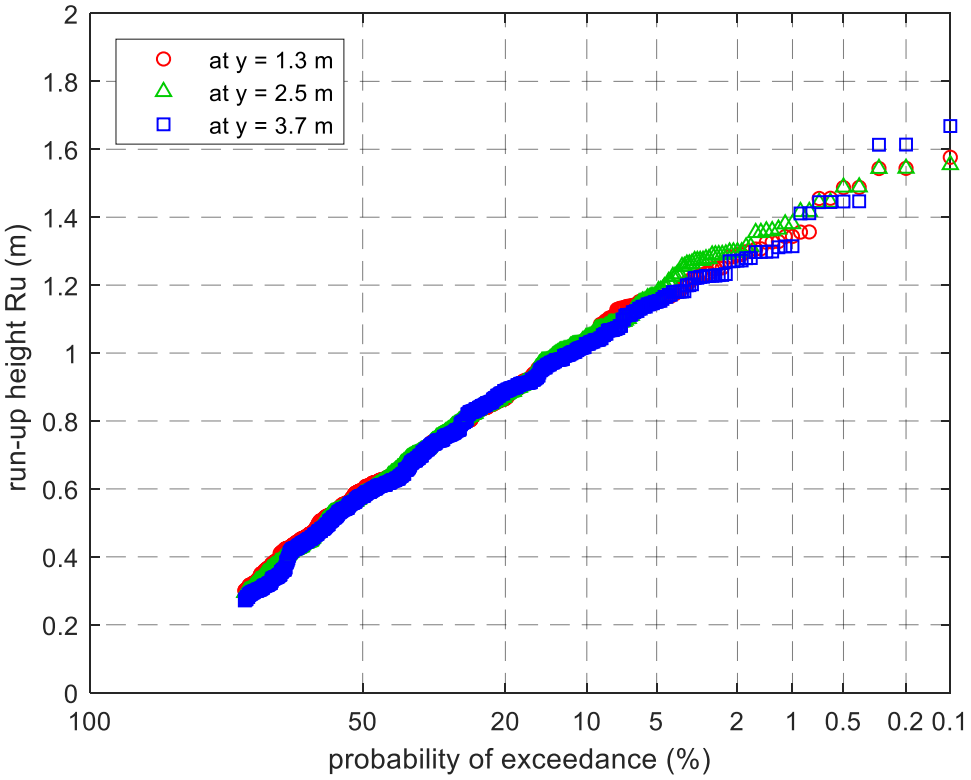

Figure M.7 Probability of exceedance distribution for test T025, with wave conditions in front of the dike: h = 3.0 m, H_{m0} = 0.39 m, $T_{m-1.0}$ = 3.71 s

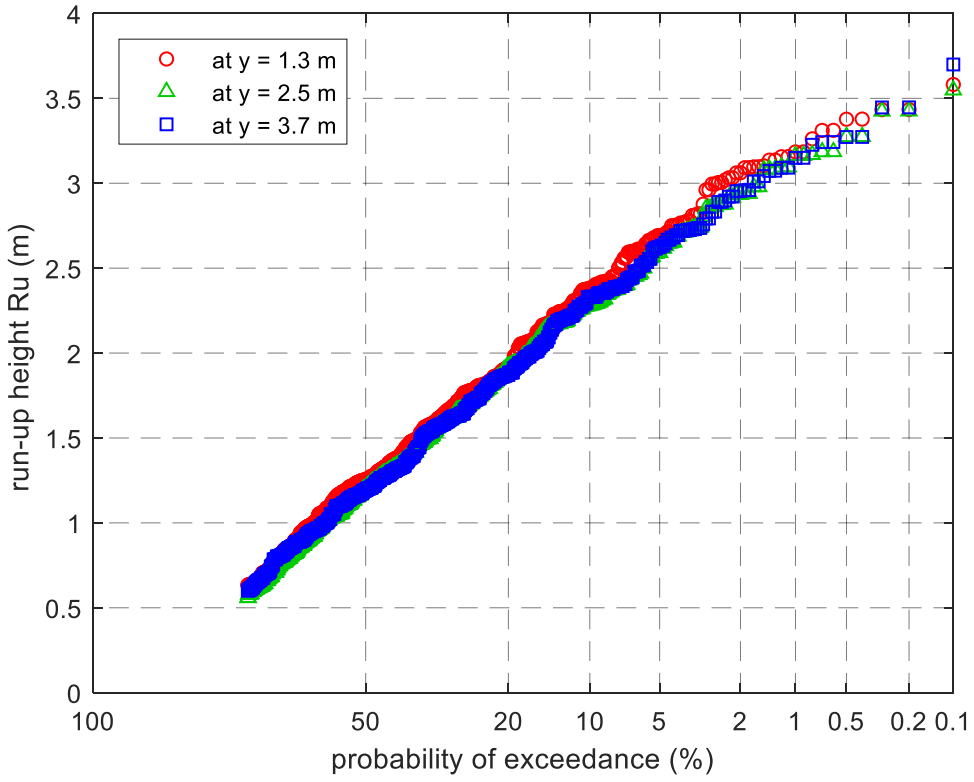

Figure M.8 Probability of exceedance distribution for test T036, with wave conditions in front of the dike: h = 3.0 m, H_{m0} = 0.96 m, $T_{m-1.0}$ = 5.43 s

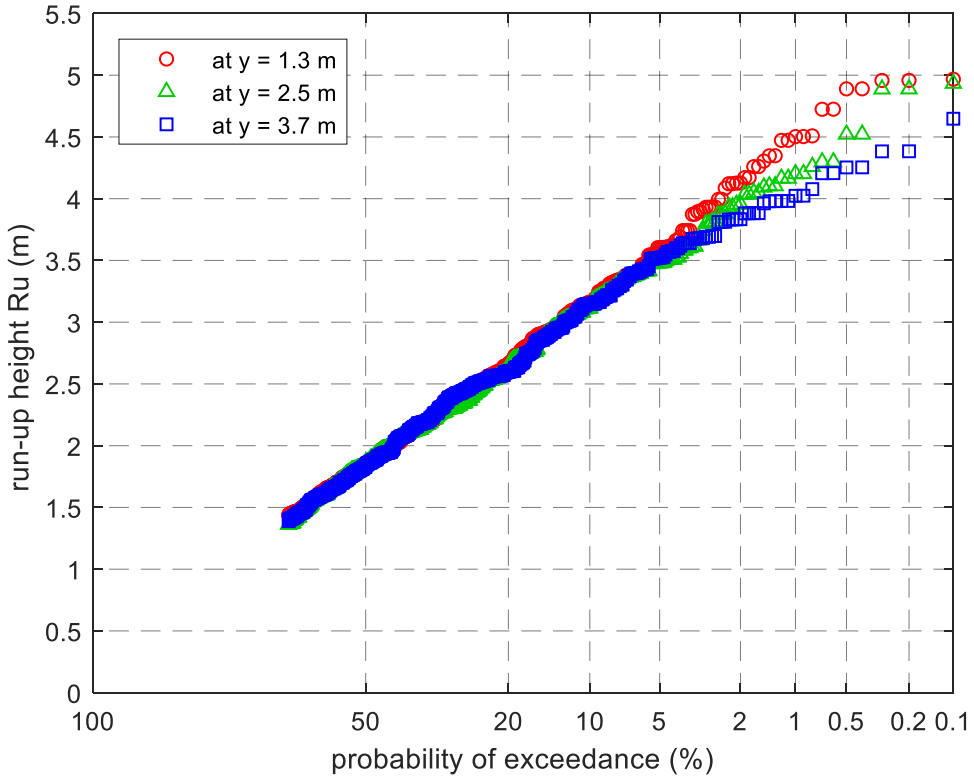

Figure M.9 Probability of exceedance distribution for test T037, with wave conditions in front of the dike: h = 4.5 m, H_{m0} = 1.39 m, $T_{m-1.0}$ = 4.83 s

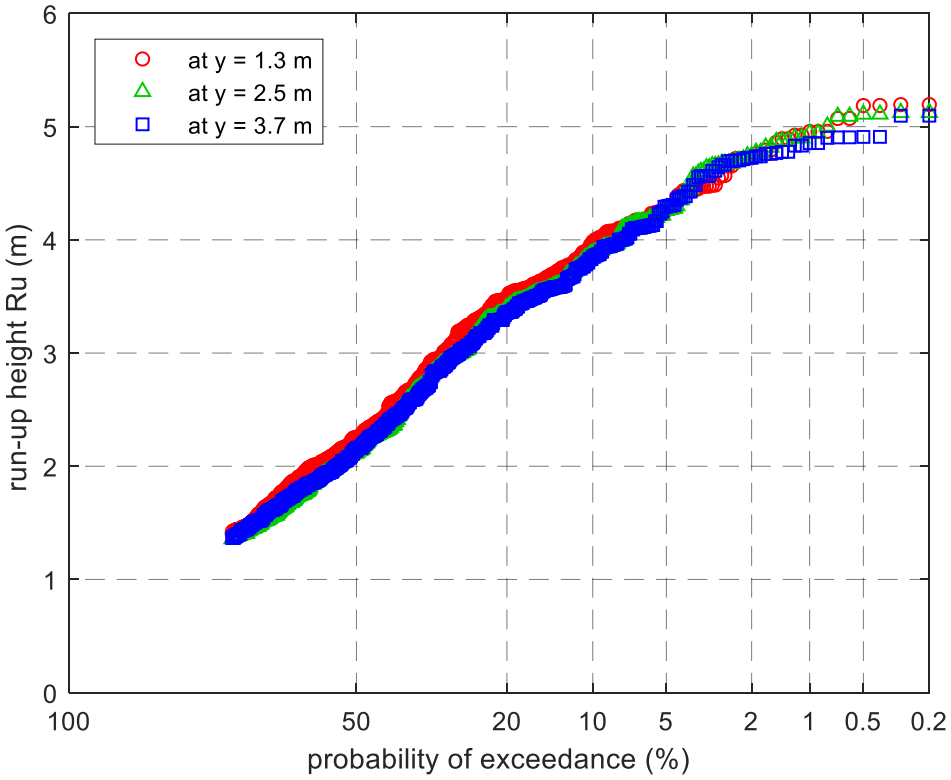

Figure M.10 Probability of exceedance distribution for test T042, with wave conditions in front of the dike: h = 4.5 m, H_{m0} = 1.50 m, $T_{m-1.0}$ = 6.12 s

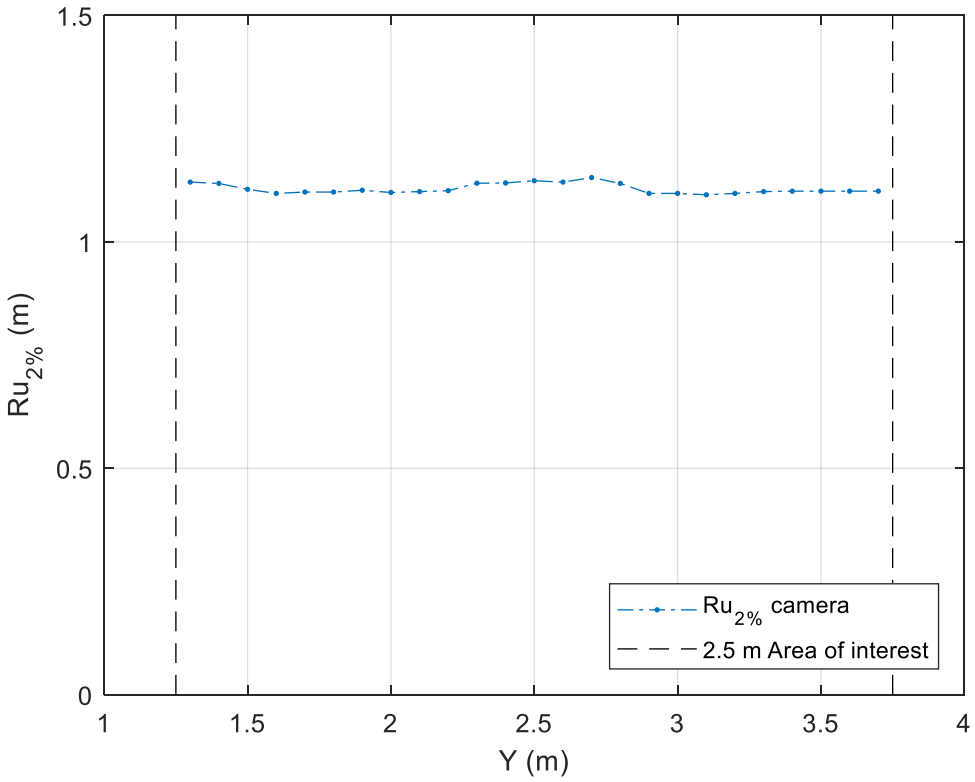

Figure M.11 Variation of the run-up for T007, wave conditions in front of the dike: h = 3.0 m, H_{m0} = 0.36 m, $T_{m-1.0}$ = 3.79 s

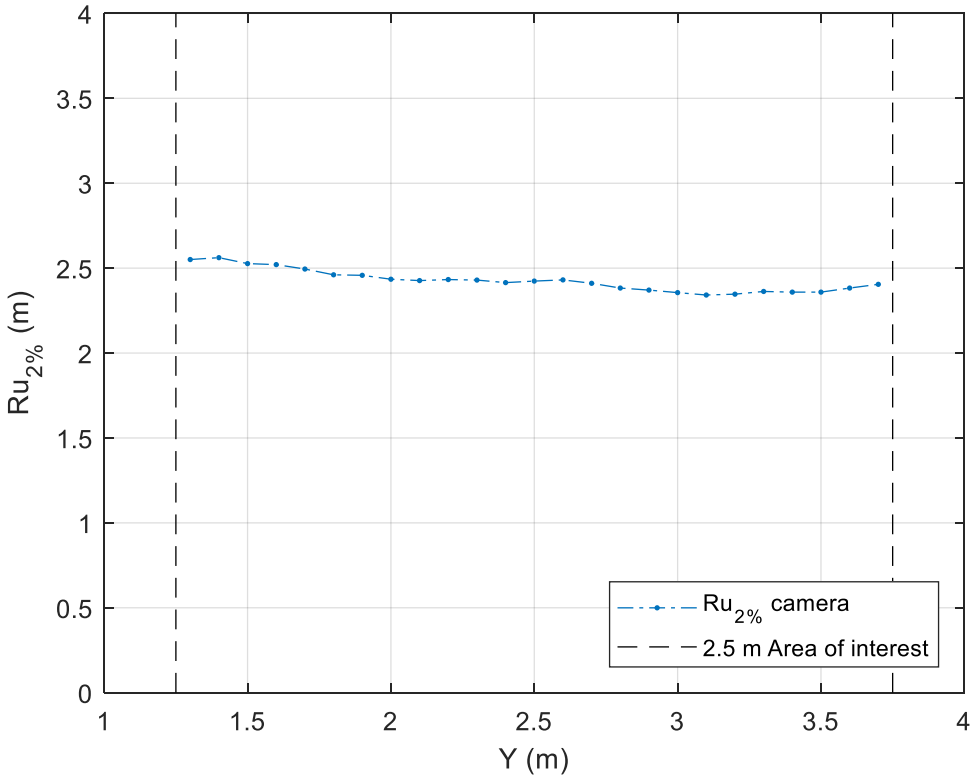

Figure M.12 Variation of the run-up for T008, wave conditions in front of the dike: h = 3.0 m, H_{m0} = 0.75 m, $T_{m-1.0}$ = 5.59 s

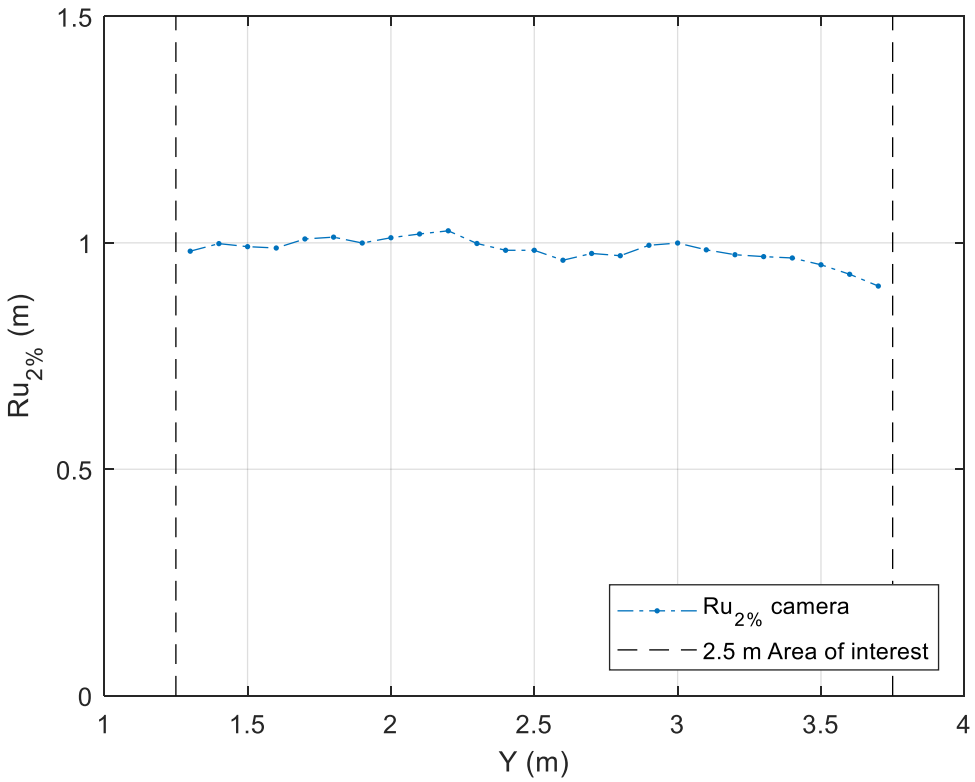

Figure M.13 Variation of the run-up for T009, wave conditions in front of the dike: h = 4.5 m, H_{m0} = 0.35 m, $T_{m-1.0}$ = 2.8 s

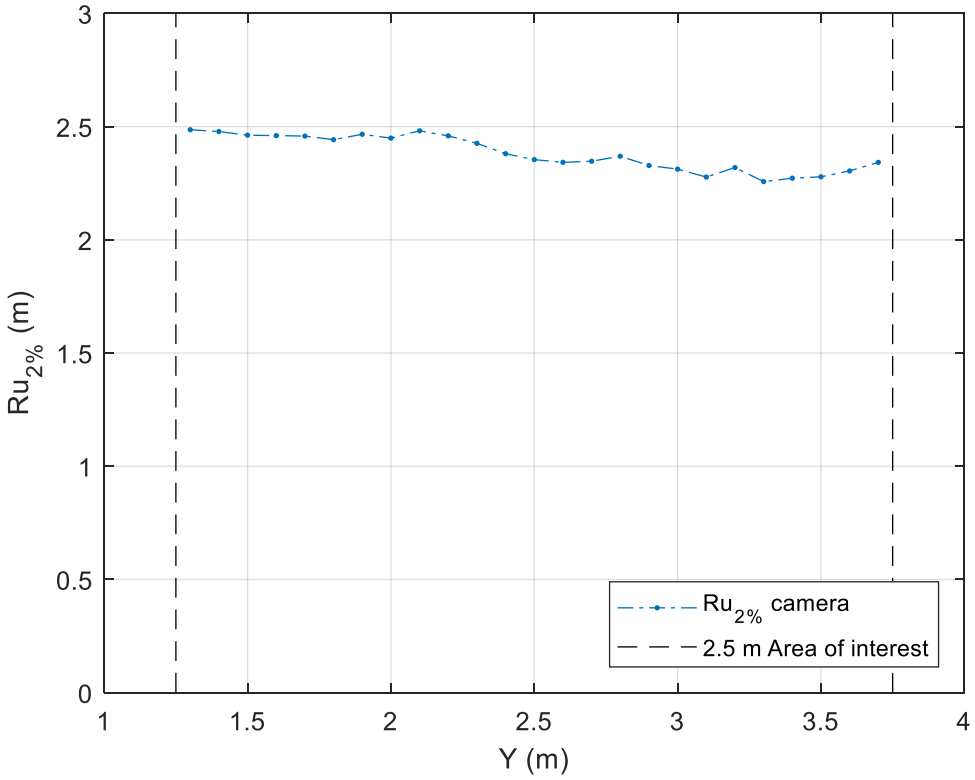

Figure M.14 Variation of the run-up for T010, wave conditions in front of the dike: h = 4.5 m, H_{m0} = 0.77 m, $T_{m-1.0}$ = 3.88 s

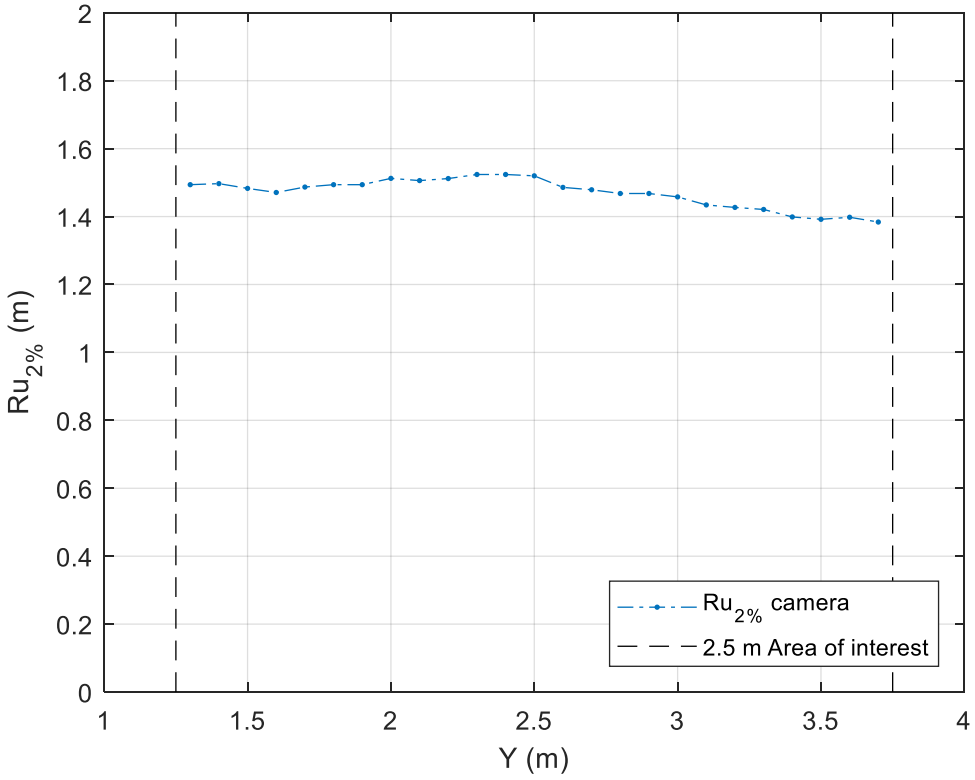

Figure M.15 Variation of the run-up for T011, wave conditions in front of the dike: h = 4.5 m, H_{m0} = 0.40 m, $T_{m-1.0}$ = 3.87 s

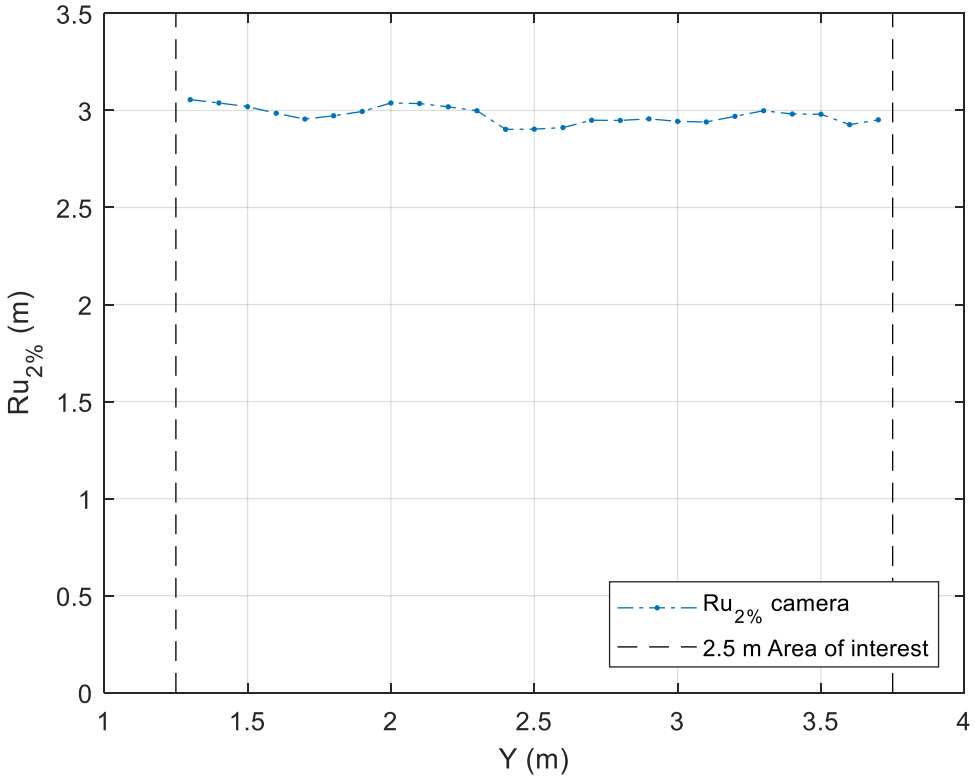

Figure M.16 Variation of the run-up for T012, wave conditions in front of the dike: h = 4.5 m, H_{m0} = 0.80 m, $T_{m-1.0}$ = 5.44 s

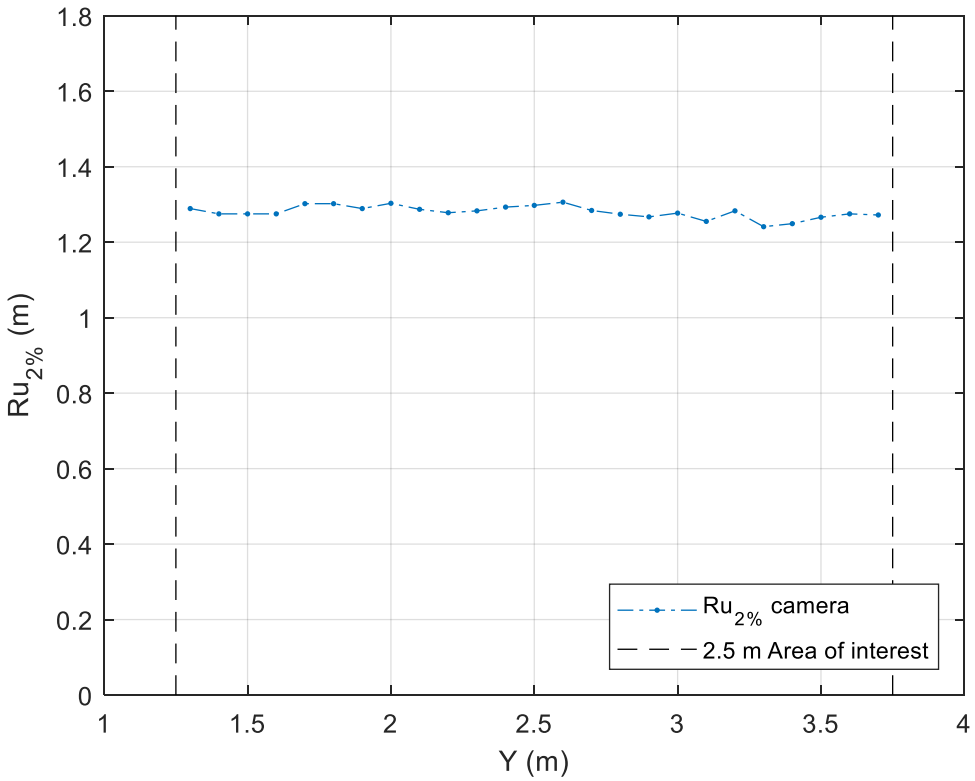

Figure M.17 Variation of the run-up for T025, wave conditions in front of the dike: h = 3.0 m, H_{m0} = 0.39 m, $T_{m-1.0}$ = 3.71 s

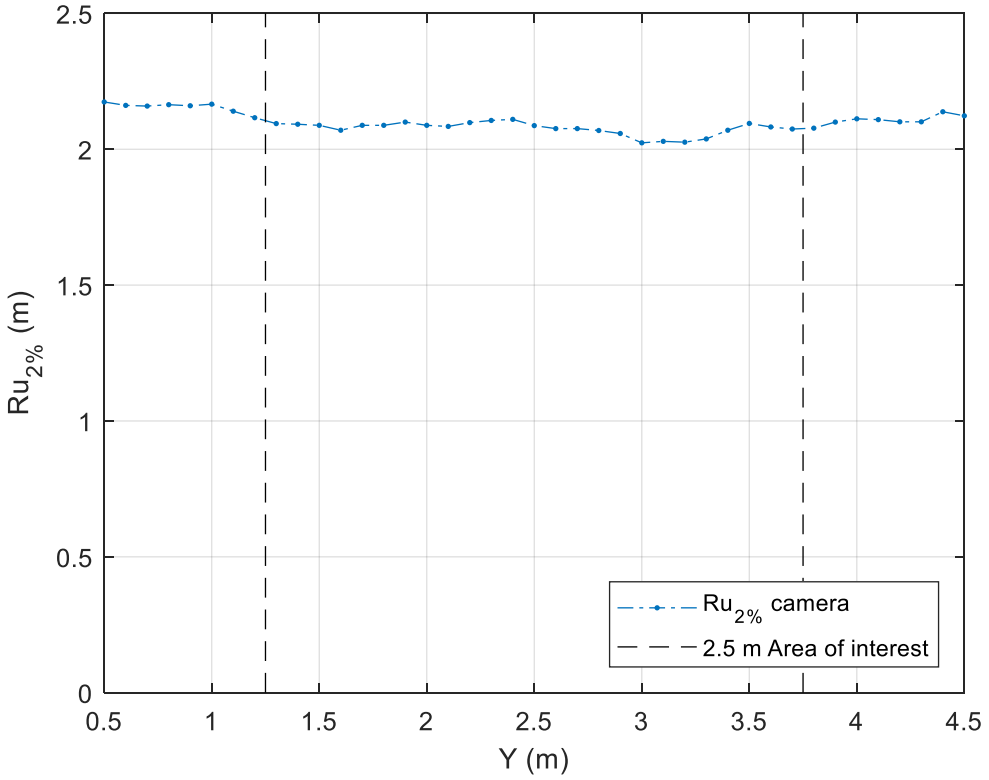

Figure M.18 Variation of the run-up for T034, wave conditions in front of the dike: h = 3.0 m, H_{m0} = 0.87 m, $T_{m-1.0}$ = 3.94 s

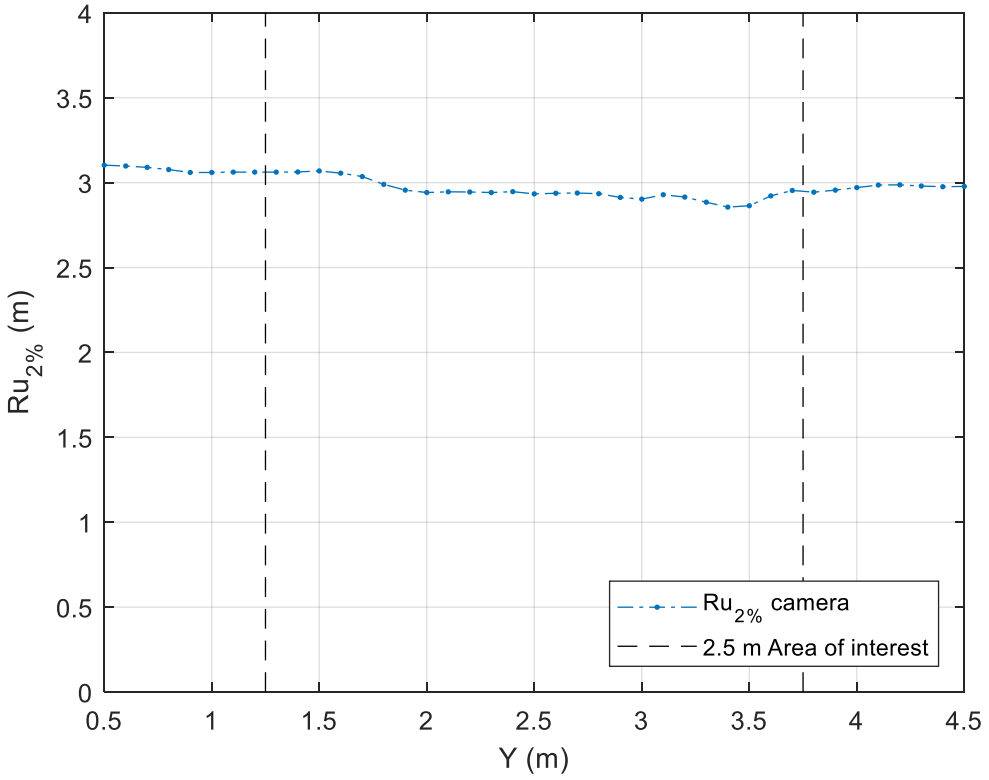

Figure M.19 Variation of the run-up for T036, wave conditions in front of the dike: h = 3.0 m, H_{m0} = 0.96 m, $T_{m-1.0}$ = 5.43 s

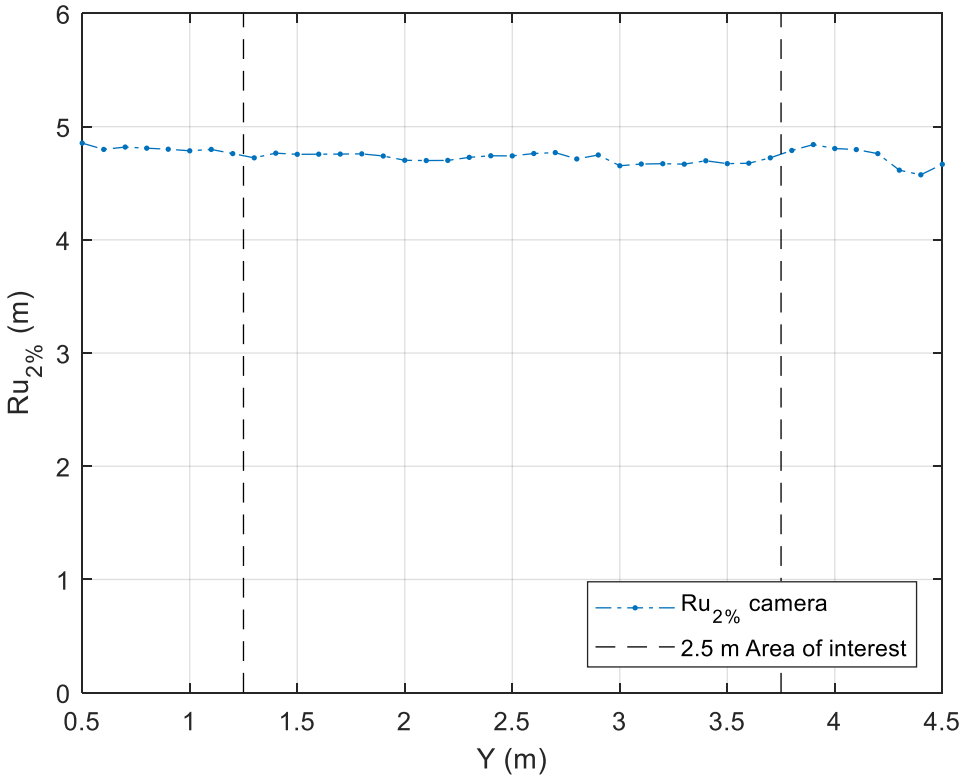

Figure M.20 Variation of the run-up for T042, wave conditions in front of the dike: h = 4.5 m, H_{m0} = 1.50 m, $T_{m-1.0}$ = 6.12 s

Figure M.21 Test T042, overtopping captured by the algorithm

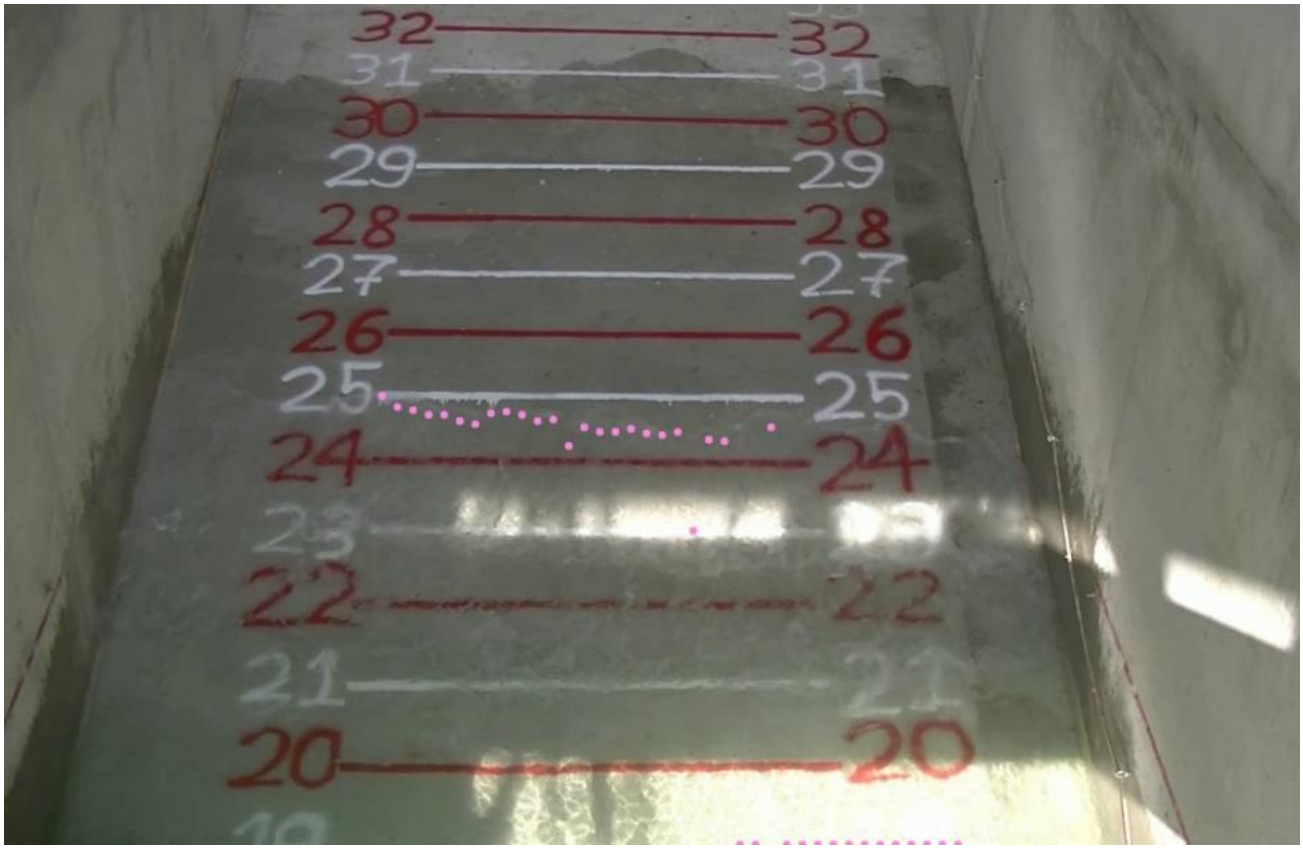

Figure M.22 Test T005, result from CNN, with data points not following the water surface

Appendix N – Results laser run-up

Results of all three measuring methods together with the empirical TAW (2002) formula is shown in this appendix.

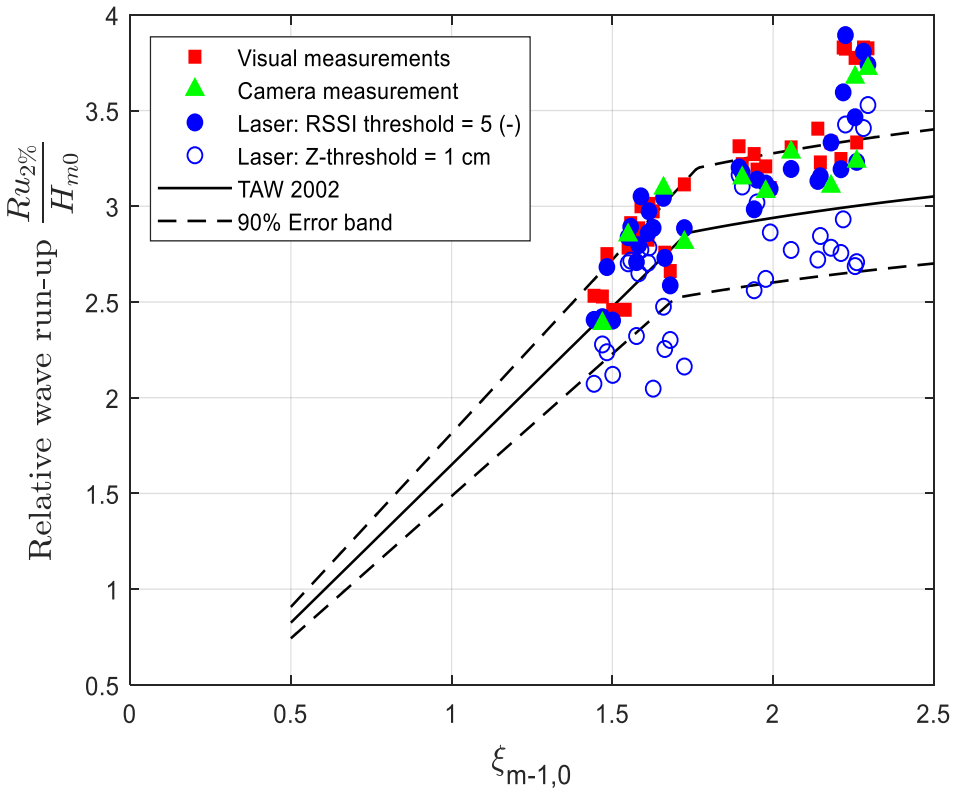

Figure N.1 Result normalized run-up for all three measuring methods compared to the TAW (2002), with the wave conditions taken in front of the dike.

Appendix O – Results laser overtopping

In this section the results of the overtopping discharges measured by the laser scanner are shown for different tests.

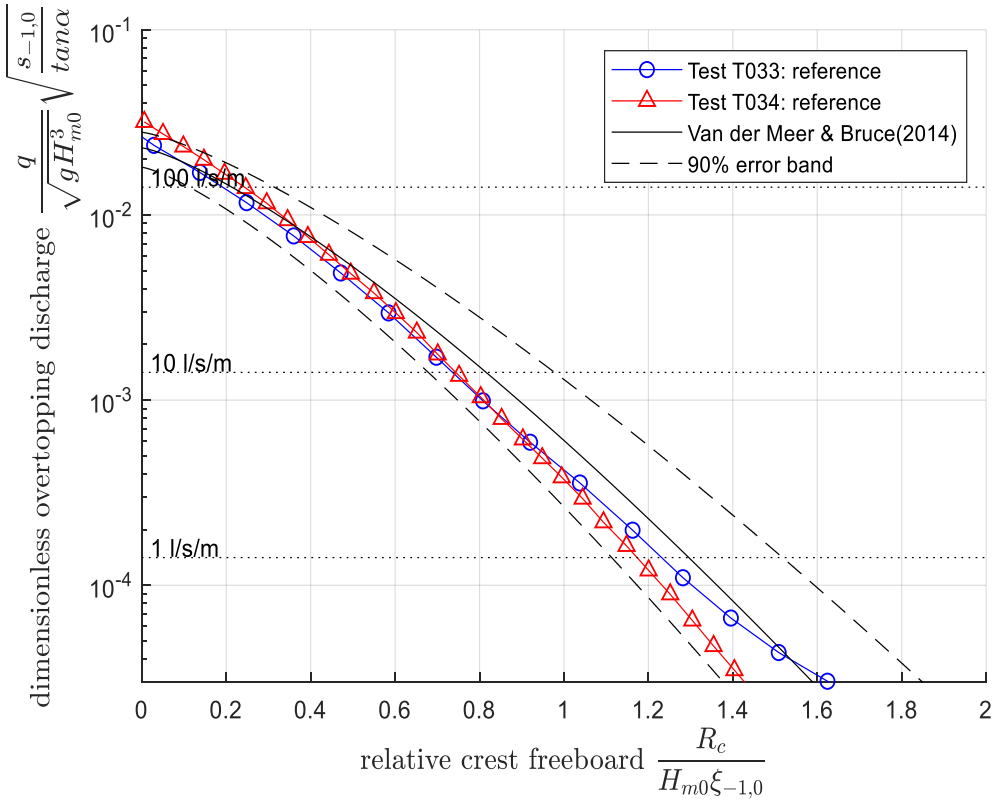

Figure O.1 Dimensionless overtopping discharge for tests T033 and T034 with the following condition at the wave board: T033: h = 3.0 m, H_{m0} = 0.44 m, $T_{m-1.0}$ = 2.6 s, T034: h = 3.0 m, H_{m0} = 0.94 m, $T_{m-1.0}$ = 3.7 s

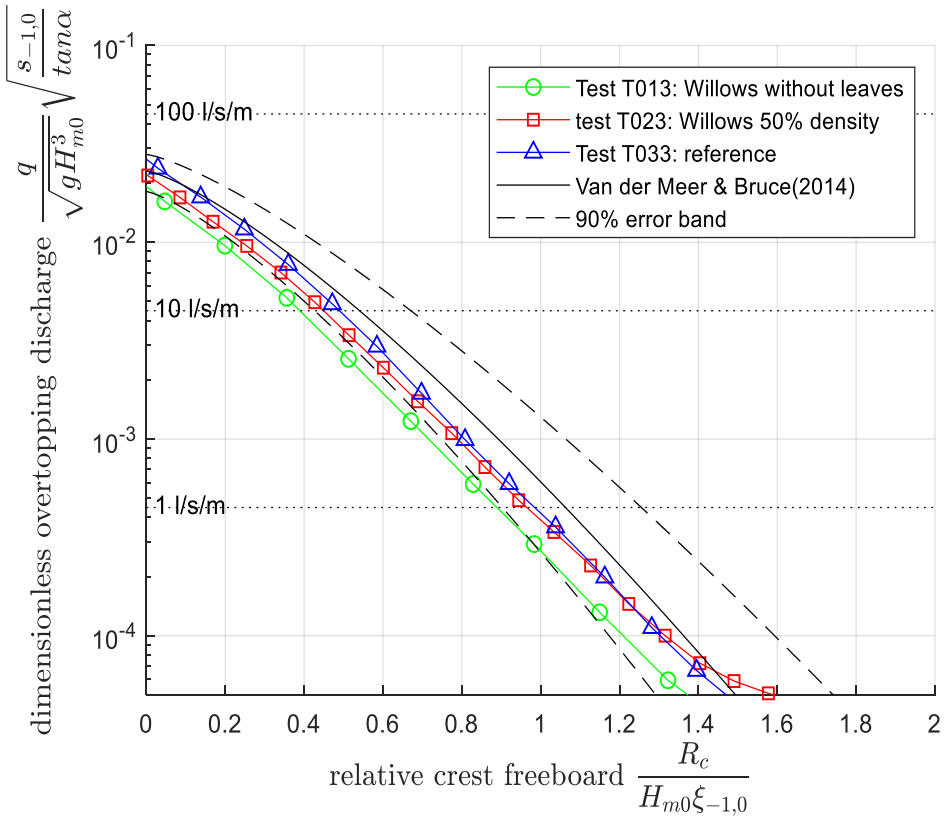

Figure O.2 Dimensionless overtopping discharge with the following incoming conditions at the wave board: h = 3.0 m, H_{m0} = 0.44 m, $T_{m-1.0}$ = 2.6 s

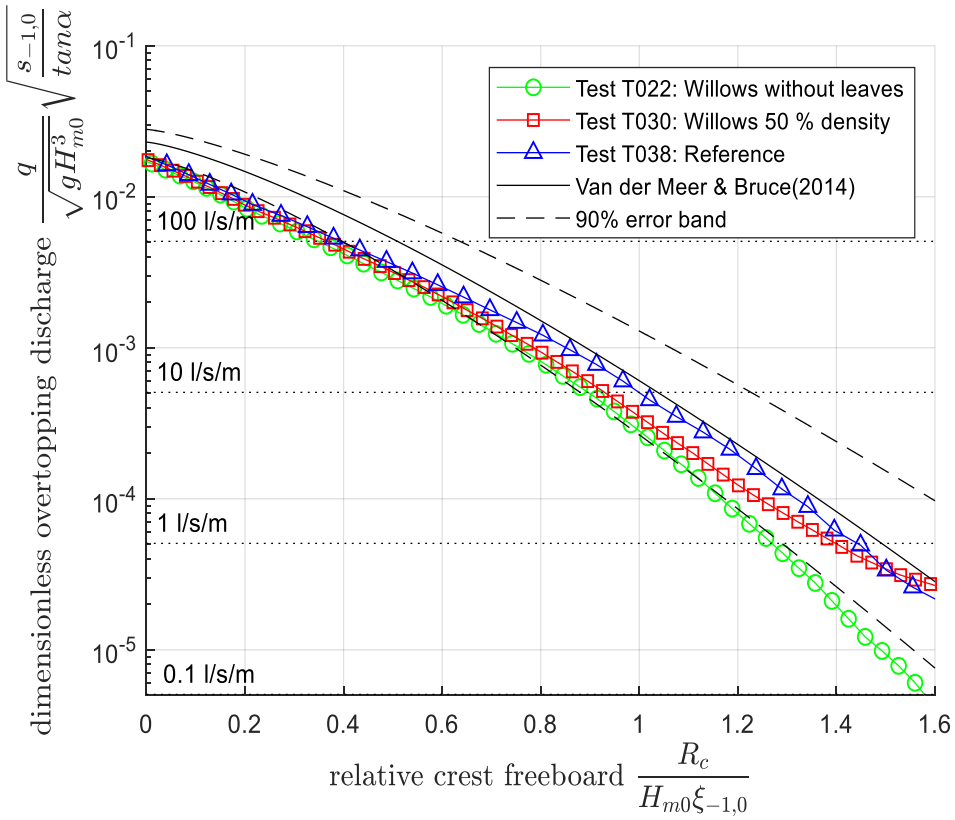

Figure O.3 Dimensionless overtopping discharge with the following incoming conditions at the wave board: h = 4.5 m, H_{m0} = 1.43 m, $T_{m-1.0}$ = 6.3 s.

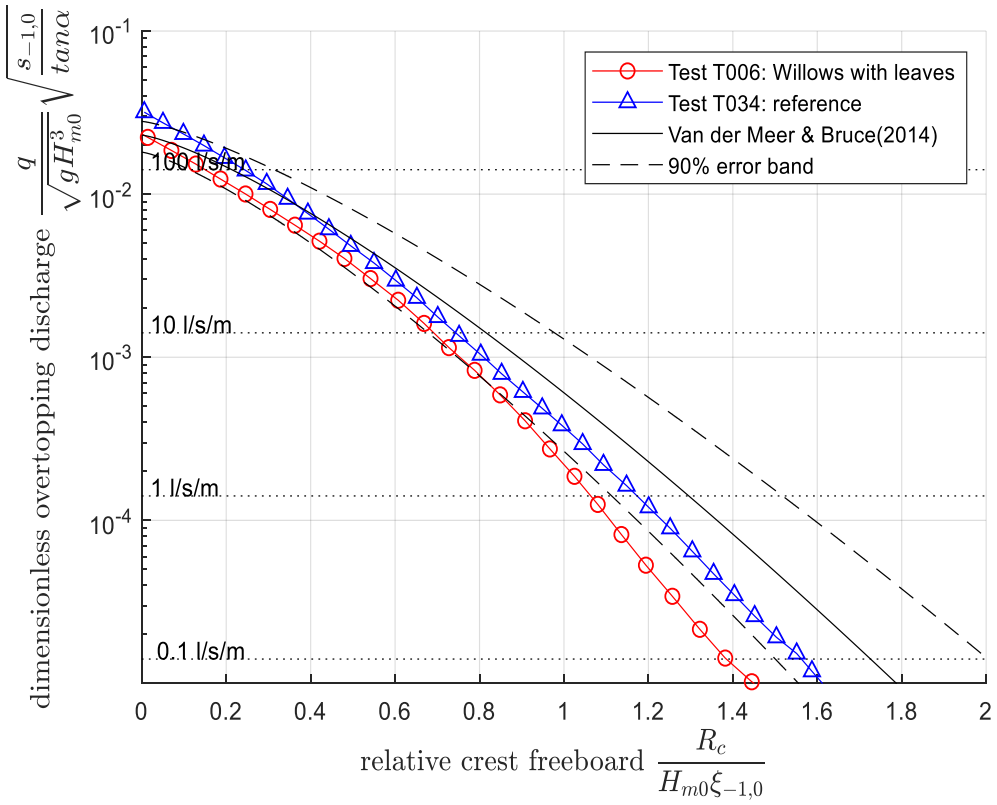

Figure O.4 Dimensionless overtopping discharge with the following incoming conditions at the wave board: h = 3.0 m, H_{m0} = 0.97 m, $T_{m-1.0}$ = 3.7 s

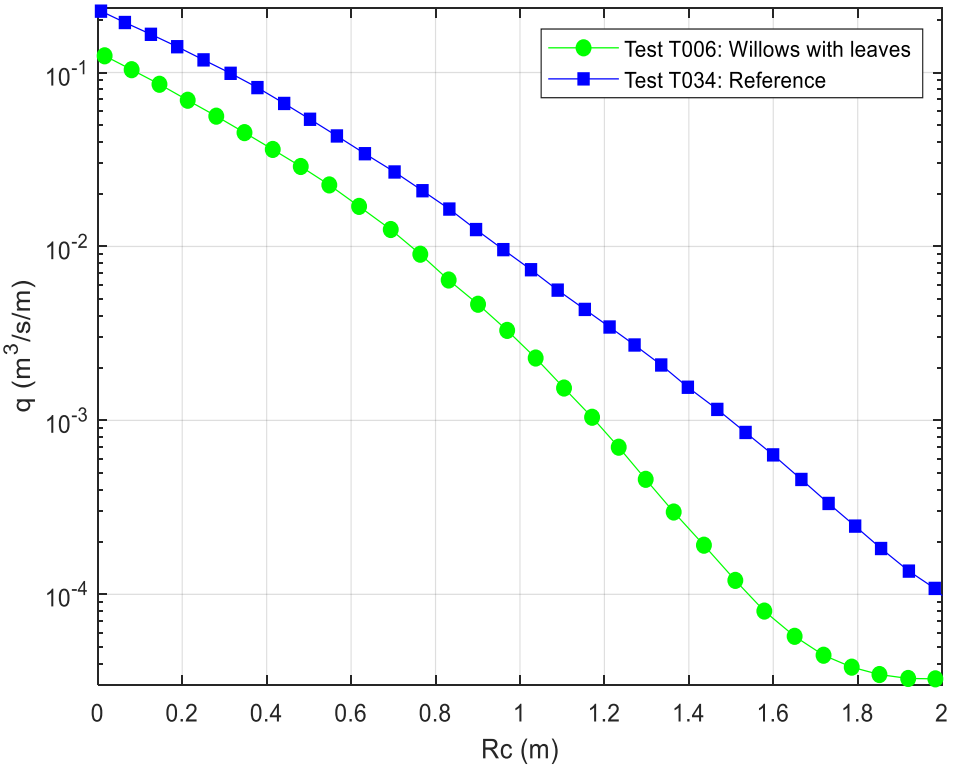

Figure O.5 Overtopping discharge for tests with the same incoming wave conditions at the wave board: h = 3.0 m, H_{m0} = 0.97 m, $T_{m-1.0}$ = 3.7 s

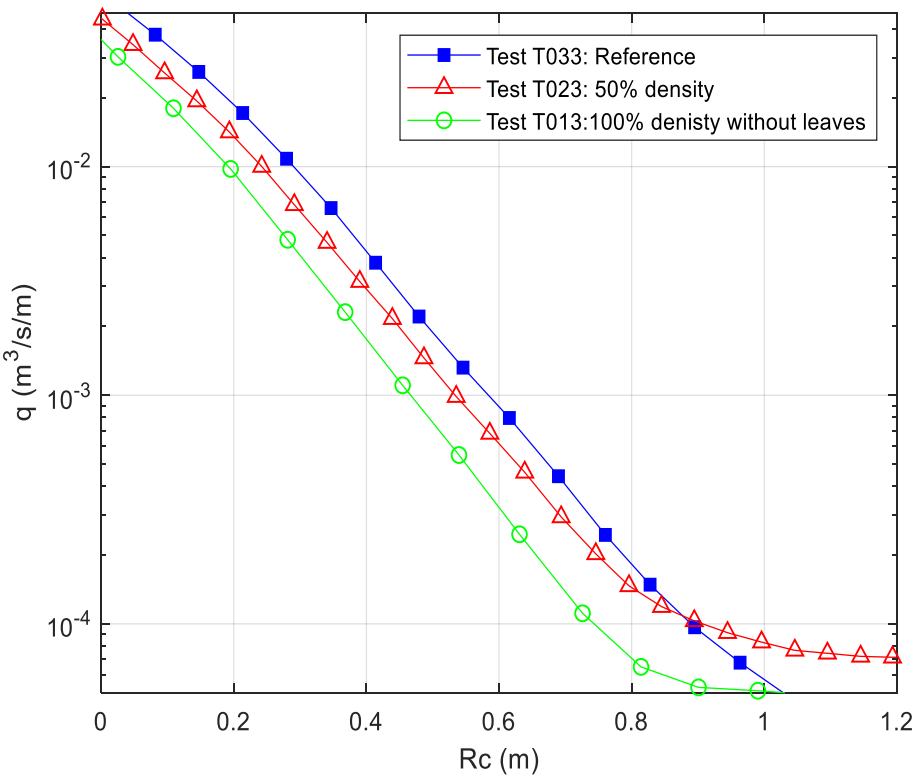

Figure O.6 Overtopping discharge for tests with the same incoming wave conditions at the wave board: h = 3.0 m, H_{m0} = 0.44 m, $T_{m-1.0}$ = 2.6 s

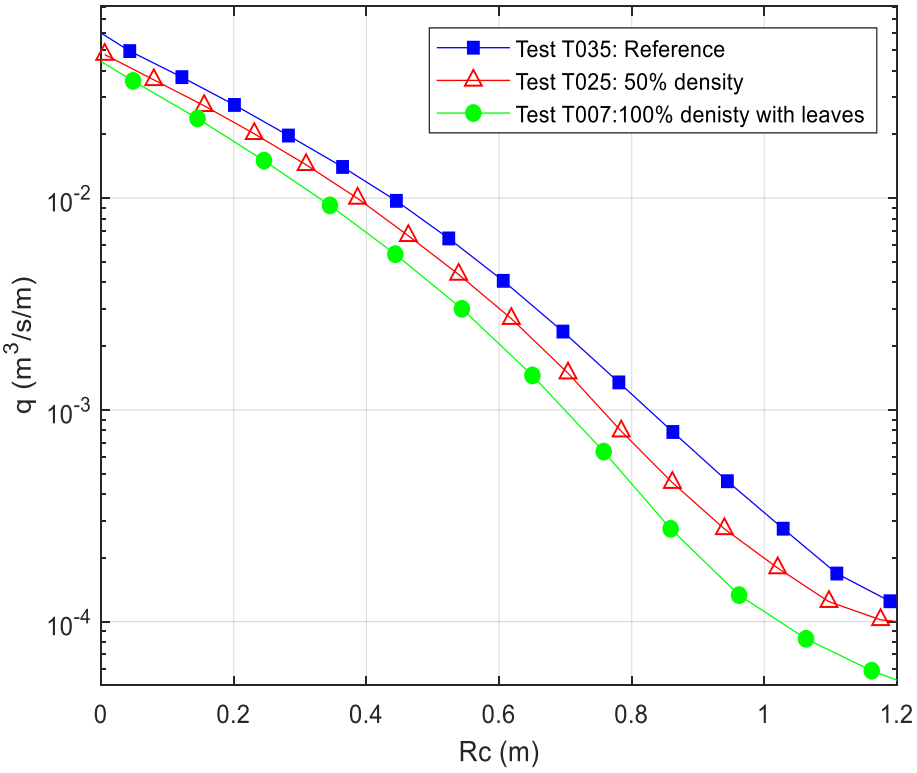

Figure O.7 Overtopping discharge for tests with the same incoming wave conditions at the wave board: h = 3.0 m, H_{m0} = 0.46 m, $T_{m-1.0}$ = 3.7 s

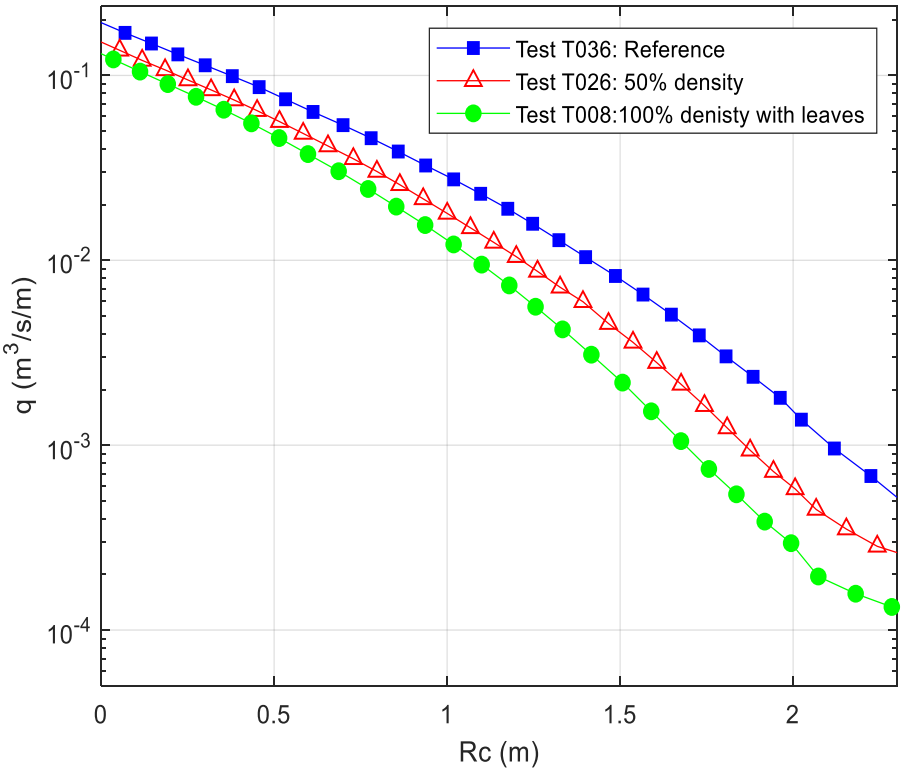

Figure O.8 Overtopping discharge for tests with the same incoming wave conditions at the wave board: h = 3.0 m, H_{m0} = 0.96 m, $T_{m-1.0}$ = 5.1 s

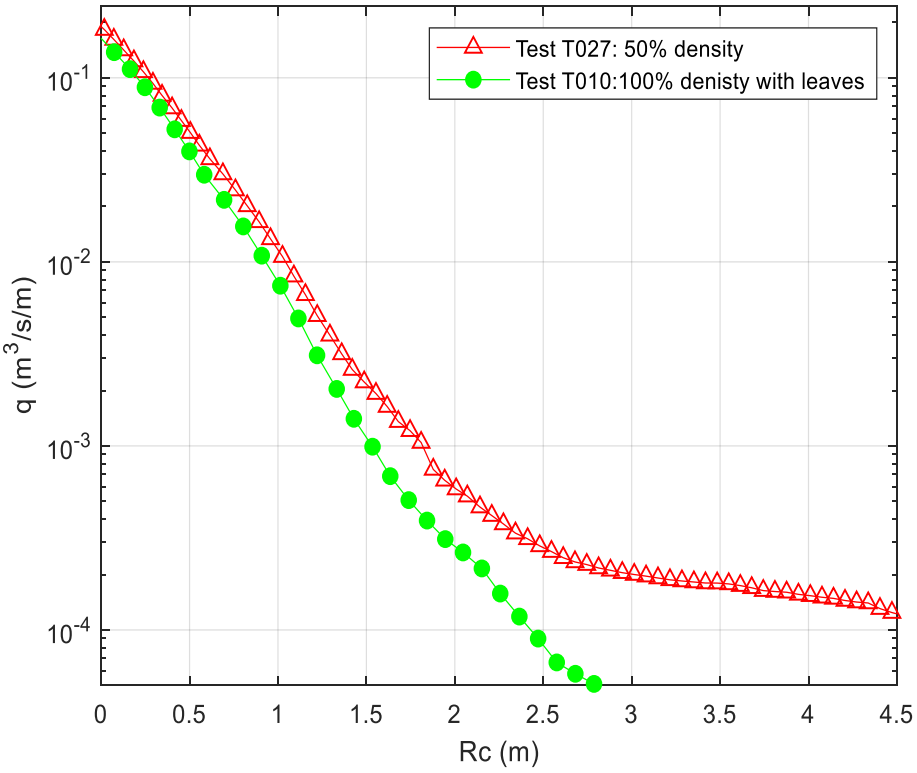

Figure O.9 Overtopping discharge for tests with the same incoming wave conditions at the wave board: h = 4.5 m, H_{m0} = 0.88 m, $T_{m-1.0}$ = 3.7 s

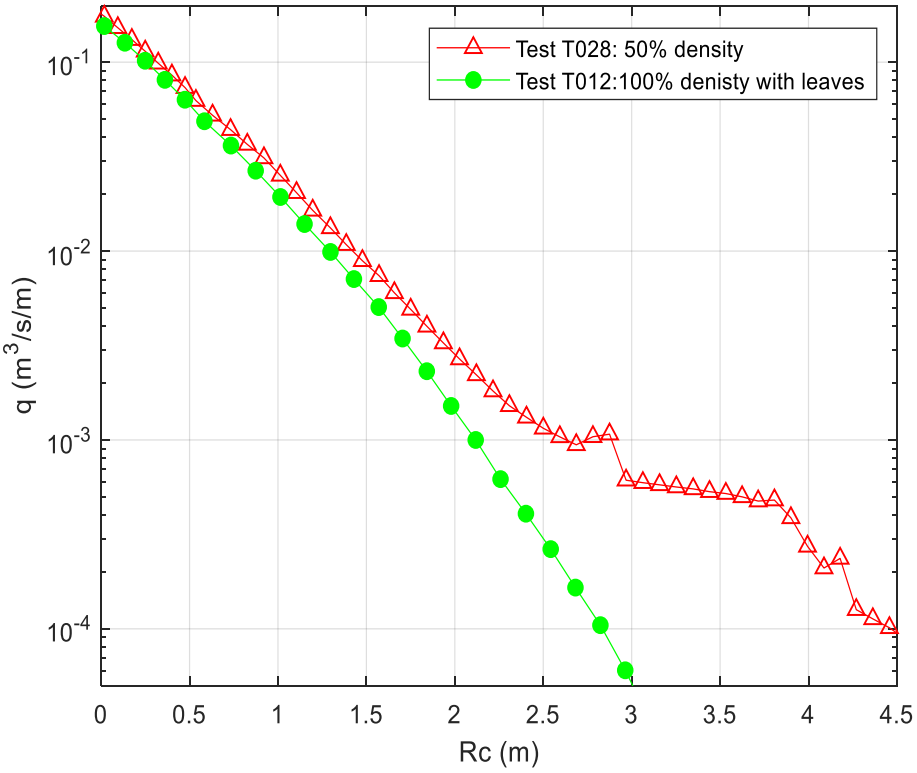

Figure O.10 Overtopping discharge for tests with the same incoming wave conditions at the wave board: h = 4.5 m, H_{m0} = 0.94 m, $T_{m-1.0}$ = 5.2 s

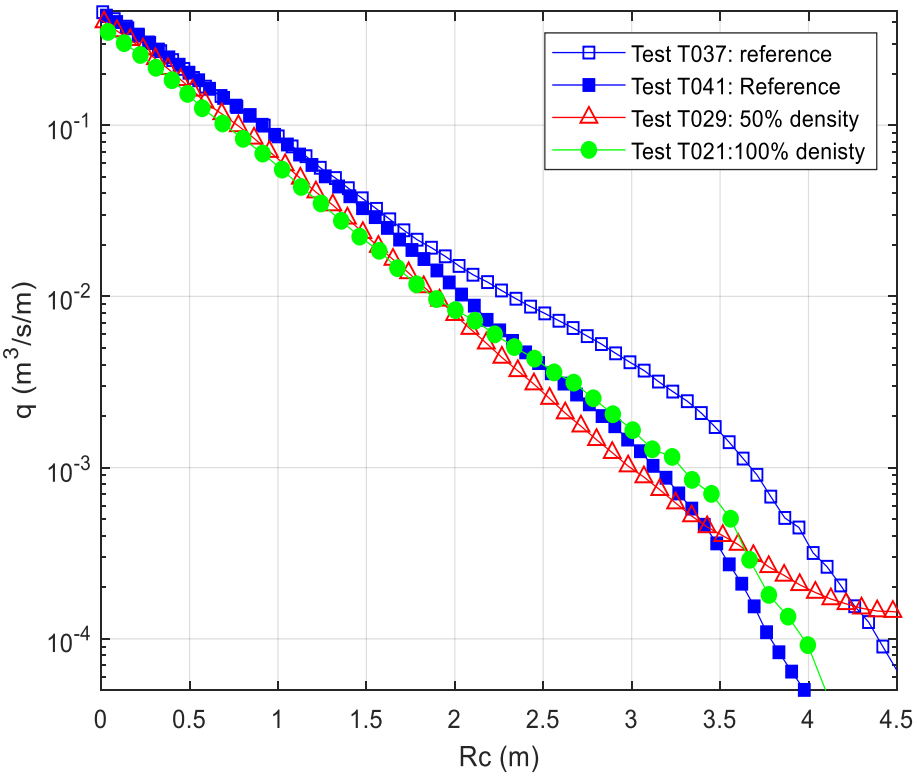

Figure O.11 Overtopping discharge for tests with the same incoming wave conditions at the wave board: h = 4.5 m, H_{m0} = 1.40 m, $T_{m-1.0}$ = 4.5 s. With T041 a repetition of T037.

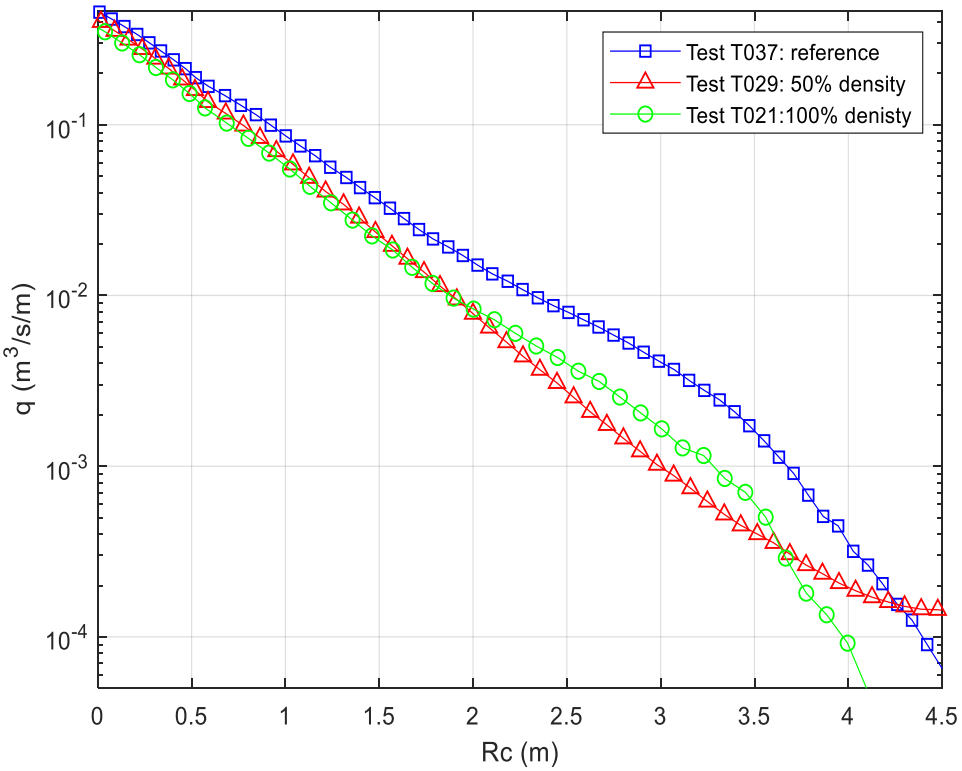

Figure O.12 Overtopping discharge for tests with the same incoming wave conditions at the wave board: h = 4.5 m, H_{m0} = 1.40 m, $T_{m-1.0}$ = 4.5 s.

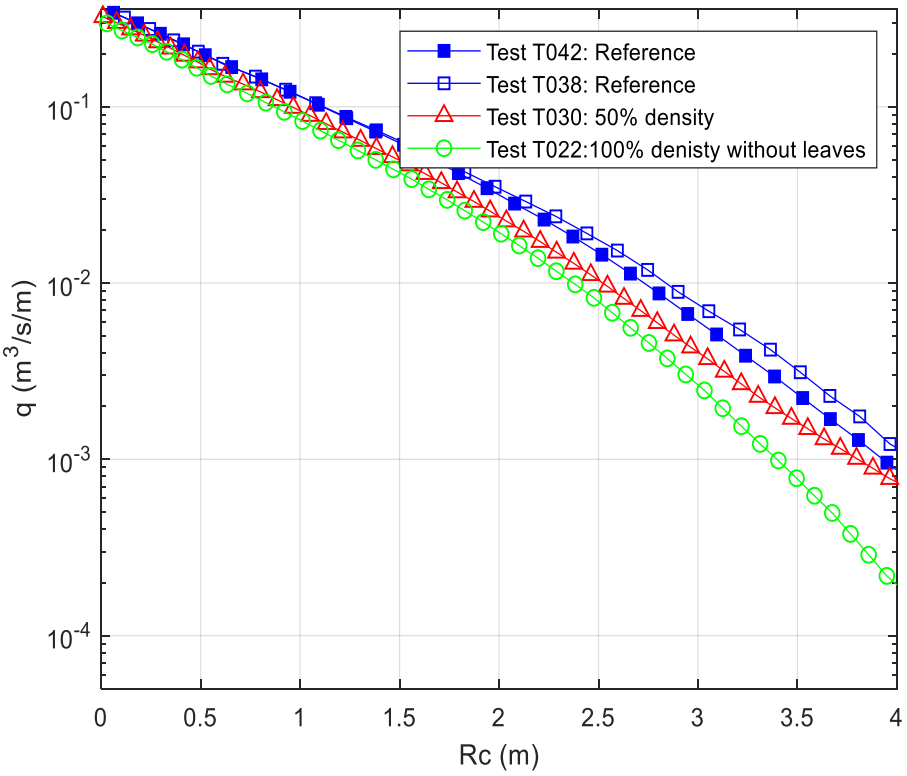

Figure O.13 Overtopping discharge for tests with the same incoming wave conditions at the wave board: h = 4.5 m, H_{m0} = 1.43 m, $T_{m-1.0}$ = 6.3 s. T042 is a repetition of T038.